

**An Integrated Used Fuel Disposition and Generic Repository Model for Fuel
Cycle Analysis**

by

Kathryn D. Huff

A dissertation submitted in partial fulfillment of
the requirements for the degree of

Doctor of Philosophy

(Nuclear Engineering and Engineering Physics)

at the

UNIVERSITY OF WISCONSIN–MADISON

2013

Date of final oral examination: 08/16/2013

The dissertation is approved by the following members of the Final Oral Committee:

Jean M. Bahr, Professor, Geoscience

Michael L. Corradini, Professor, Nuclear Engineering and Engineering Physics

Douglass L. Henderson, Professor, Nuclear Engineering and Engineering Physics

W. Mark Nutt, Nuclear Engineer, Argonne National Laboratory

Paul P.H. Wilson, Professor, Nuclear Engineering and Engineering Physics

Robert J. Witt, Professor, Nuclear Engineering and Engineering Physics

© Copyright by Kathryn D. Huff 2013

All Rights Reserved

For my beloved family - Diane, Harold, Allison, and Joanie. Above all, for Strom.

ACKNOWLEDGMENTS

I am grateful to a number of extraordinary professors and colleagues at the Universities of Wisconsin and Chicago, as well as the national laboratories, who have inspired and encouraged me. My committee members, Dr. Jean M. Bahr, Dr. Michael L. Corradini, Dr. Douglass L. Henderson, Dr. W. Mark Nutt, Dr. Paul P.H. Wilson, and Dr. Robert J. Witt, were especially supportive in this endeavor.

Among them, I am particularly indebted to my advisor, Professor Wilson, for his indispensable technical and practical guidance. He has been a dedicated ally, always generous with analytical perspectives, far-ranging enthusiasm, and deep concern for the professional and personal well being of his students. I am similarly grateful to my laboratory advisor, Dr. Nutt, an outstanding mentor who has provided critical direction and resources for the work at hand. Special gratitude also goes to Professor Bahr, whose expertise and detailed feedback were of exceptional value.

So too, my colleagues Kyle M. Oliver, Matthew J. Gidden and Robert W. Carlsen have been essential in the success of the CYCLUS project as well the growth of my collaborative abilities. I thank Alexander Bara for dedicating a summer to starting the STC database. Additionally, all confidence I have in these results is owed to software practices inspired by my friends among The Hacker Within and Software Carpentry. At the risk of neglecting someone, I must thank Greg Wilson, Animal1, Wolfman, Slayer, Scopz, Nico, BlackBeard, BlondeBeard, and RedBeard. I owe my sanity to Denia Djokić.

This work was carried out in the Computational Nuclear Engineering Research Group (CNERG) of the University of Wisconsin - Madison's Engineering Physics (EP) Department and the Used Fuel Disposition (UFD) Campaign at Argonne National Laboratory (ANL). This work is supported by the U.S. Department of Energy, Basic Energy Sciences, Office of Nuclear Energy, under contract # DE-AC02-06CH11357.

CONTENTS

Contents	iii
List of Tables	x
List of Figures	xii
Abstract	xvii
1 Introduction	1
<i>1.1 Motivation</i>	1
1.1.1 Future Fuel Cycle Options	3
1.1.2 Future Waste Disposal System Options	4
1.1.2.1 Thermal Modeling Needs	5
1.1.2.2 Radionuclide Transport Modeling Needs	7
1.1.3 Domestic Research and Development Program	8
<i>1.2 Methodology</i>	9
1.2.1 Identification of the Modeling Domain	9
1.2.2 Identification of Dominant Physics	10
1.2.3 Abstraction and Implementation	11
<i>1.3 Research Goals</i>	12
2 Literature Review	15
<i>2.1 Repository Capabilities within Systems Analysis Tools</i>	15
2.1.1 Repository Performance Calculations	15
2.1.2 Detail	16
2.1.3 Accessibility	16

2.1.4	Repository Focused Fuel Cycle Analyses	17
2.2	<i>Disposal Environment Concepts</i>	18
2.2.1	Clay Disposal Environments	19
2.2.1.1	Disposal System Components	19
2.2.1.2	Hydrology	20
2.2.1.3	Geochemistry	20
2.2.1.4	Thermal Behavior	20
2.2.2	Granite Disposal Environments	21
2.2.2.1	Disposal System Components	22
2.2.2.2	Hydrology	22
2.2.2.3	Geochemistry	23
2.2.2.4	Thermal Behavior	23
2.2.3	Salt Disposal Environments	24
2.2.3.1	Disposal System Components	25
2.2.3.2	Hydrology	25
2.2.3.3	Geochemistry	25
2.2.3.4	Thermal Behavior	25
2.2.4	Deep Borehole Disposal Environments	26
2.2.4.1	Disposal System Components	26
2.2.4.2	Hydrology	27
2.2.4.3	Geochemistry	28
2.2.4.4	Thermal Behavior	28
2.3	<i>Analytical Models of Radionuclide Transport</i>	28
2.3.1	Waste Form Release Models	29
2.3.1.1	Degradation Rates	29

2.3.1.2	Solubility Limitation	31
2.3.1.3	Flow Assumptions	32
2.3.2	Waste Package Failure Models	33
2.3.2.1	Physical Model	33
2.3.2.2	Degradation Rate Based	34
2.3.2.3	Probabilistic	35
2.3.2.4	Instantaneous	36
2.3.3	Radionuclide Transport Through Secondary Engineered Barriers . .	37
2.3.4	Hydrologic Transport	38
2.4	<i>Analytical Models of Heat Transport</i>	45
2.4.1	Conduction	45
2.4.2	Lumped Parameter Model	47
2.4.3	Specific Temperature Integral	50
2.5	<i>Computational Models of Radionuclide Transport</i>	51
2.5.1	European RED-IMPACT	51
2.5.2	UFD Generic Disposal System Models	51
2.5.2.1	Clay/Shale GDSM	53
2.5.2.2	Granite GDSM	54
2.5.2.3	Salt GDSM	54
2.5.2.4	Deep Borehole GDSM	55
2.5.3	Li Model [63]	56
2.5.4	ANDRA Dossier 2005	57
2.6	<i>Detailed Computational Models of Heat Transport</i>	58
2.6.1	ANL SINDA\G Model	59
2.6.2	LLNL MathCAD Model	61

2.6.3	Yucca Mountain Layout Analyses	63
2.6.4	Other Numerical Methods	65
3	Modeling Paradigm	67
3.1	<i>CYCLUS Simulator Paradigm</i>	67
3.1.1	Dynamic Module Loading	68
3.1.1.1	Encapsulation	69
3.1.1.2	Modularity and Extensibility	70
3.1.2	Market-based Material Transactions	71
3.1.3	Discrete Materials and Facilities	71
3.1.4	Implications for CYDER	73
3.2	<i>CYDER Repository Modeling Paradigm</i>	74
3.2.1	Waste Stream Acceptance	74
3.2.2	Waste Stream Conditioning	75
3.2.3	Waste Form Packaging	75
3.2.4	Package Emplacement	76
3.2.5	Nested Components	76
3.2.5.1	Component Geometry	78
3.2.5.2	Component Material Data	78
3.2.5.3	Component ThermalModel	78
3.2.5.4	Component NuclideModel	79
3.2.6	Output Tables	79
4	Methodology	81
4.1	<i>Radionuclide Mass Transport In CYDER</i>	81
4.1.1	Time Stepping Algorithm	82

4.1.1.1	Phase 1: Initial Conditions	82
4.1.1.2	Phase 2: Interior Mass Balance	83
4.1.1.3	Phase 3: Mass Transfer Calculation	83
4.1.1.4	Phase 4: Exterior Mass Balance	83
4.1.1.5	Phase 5: Interior Mass Balance Update	84
4.1.2	Mass Transfer Modes	84
4.1.2.1	Explicit Advection Dominated Mass Transfer	86
4.1.2.2	Explicit Dispersion Dominated Mass Transfer	88
4.1.2.3	Explicit Coupled Advective Dispersive Mass Transfer	90
4.1.2.4	Explicit Maximum Flow Mass Transfer	91
4.1.2.5	Implicit Mass Transfer	91
4.1.3	Mass Balance Models	92
4.1.3.1	Degradation Rate Radionuclide Mass Balance Model	93
4.1.3.2	Mixed Cell Radionuclide Mass Balance Model	96
4.1.3.3	Lumped Parameter Radionuclide Mass Balance Model	102
4.1.3.4	One Dimensional Permeable Porous Medium Radionuclide Mass Balance Model	105
4.2	<i>Thermal Transport in CYDER</i>	108
4.2.1	Specific Temperature Change Method	108
4.2.2	Supporting Thermal Response Dataset	110
5	Demonstration Cases and Benchmarking	116
5.1	<i>Radionuclide Transport Base Cases</i>	116
5.1.1	Basic Transport and Containment Problem Specification	116
5.1.1.1	Degradation Rate Model	117
5.1.1.2	Mixed Cell Model	123

5.1.1.3	Lumped Parameter Model	127
5.1.1.4	One Dimensional Permeable Porous Medium Model	133
5.2	<i>Radionuclide Transport Validation</i>	135
5.2.1	Case I : Vertical Advective Velocity and Diffusion Coefficient Sensitivity	135
5.2.1.1	Advection vs. Diffusion Sensitivity GDSM Results	135
5.2.1.2	Advection vs. Diffusion Sensitivity CYDER Results	139
5.2.2	Case II : Solubility Sensitivity	140
5.2.3	Case III : Sorption Sensitivity	142
5.2.3.1	Reference Distribution Coefficient Sensitivity	142
5.2.3.2	Reference Sorption Coefficient Sensitivity	144
5.2.4	Case IV : Waste Form Degradation Rate and Inventory Sensitivity .	145
5.2.4.1	Waste Form Degradation Rate and Contaminant Inventory Sensitivity	145
5.3	<i>Thermal Transport Validation</i>	148
5.3.1	Parametric Domain	149
5.3.2	Approach	149
5.3.3	Thermal Conductivity Sensitivity Validation	150
5.3.3.1	LLNL Model Results	150
5.3.3.2	Cyder Results	151
5.3.4	Thermal Diffusivity Sensitivity Validation	155
5.3.4.1	LLNL Model Results	155
5.3.4.2	Cyder Results	156
5.3.5	Waste Package Spacing Sensitivity Validation	158
5.3.5.1	LLNL Model Results	158
5.3.5.2	Cyder Results	160

6	Conclusions	164
	<i>6.1 Contributions</i>	164
	<i>6.2 Suggested Future Work</i>	165
	References	167
A	Radionuclide Transport Sensitivity Analysis	180
	<i>A.1 Approach</i>	180
	<i>A.2 Mean of the Peak Annual Dose</i>	181
	<i>A.3 Sampling Scheme</i>	182
	<i>A.4 Parametric Analyses With The Clay GDSM</i>	184
	A.4.1 Vertical Advective Velocity and Reference Diffusivity	184
	A.4.1.1 Parametric Range	185
	A.4.2 Diffusion Coefficient of Far Field	187
	A.4.2.1 Parametric Range	188
	A.4.3 Solubility Limitation	189
	A.4.3.1 Parametric Range	191
	A.4.4 The Partition Coefficient	191
	A.4.4.1 Parametric Range	192
	A.4.5 Waste Form Degradation Rate	193
	A.4.5.1 Parametric Range	193
	A.4.5.2 Safety Indicators	194
	A.4.6 Waste Package Failure Time	198
	A.4.6.1 Parametric Range	198
B	Thermal Calculation Accuracy Determination	199
	<i>B.1 Description of the Comparisons</i>	200

B.2 Results 200

LIST OF TABLES

2.1	Clay repository features.	19
2.2	Granite repository features.	22
2.3	Salt repository features.	24
2.4	Borehole repository features.	27
2.5	Waste form types.	29
2.6	Current waste package failure models.	34
2.7	International use of radionuclide transport models in various geologic host media.	52
2.8	International repository concepts.	52
2.9	Contaminant transport codes used by ANDRA	58
2.10	Yucca Mountain footprint expansion calculations.	64
2.11	International heat transport modeling methods in various geologic host media.	66
4.1	Thermal reference database parametric space	110
5.1	Degradation rate model no release problem results.	118
5.2	The sensitivity analyses conducted in this work covered a range of thermal and hydrologic parameters in the context of canonical fuel cycle choices.	136
5.3	A thermal reference dataset of Specific Temperature Change (STC) values as a function of each of these parameters was generated by repeated parameterized runs of the LLNL MathCAD model[35, 36].	149
A.1	For an individual one group of 100 realizations was run for each discrete value, P_i , within the range considered for P	182
A.2	The simulation groups for a dual simulation sample each parameter within the range over which it was considered.	183

A.3	Vertical advective velocity and diffusion coefficient simulation groupings. . . .	186
A.4	Diffusion coefficient and mass factor simulation groupings.	188
A.5	Safety indicators for soluble, non-sorbing nuclides.	195
A.6	Safety indicators for solubility limited and sorbing nuclides.	196
A.7	Safety indicators for the actinides and their daughters.	197
B.1	Benchmarking in the single tunnel case showed that the peak heat was calculated to be lower and arrived consistently sooner in the semi-analytic model.	201
B.2	Benchmarking in the multiple tunnel case showed that the peak heat was calculated to be consistently lower in the semi-analytic model and deviated further from the numerical model than did the single tunnel case.	202

LIST OF FIGURES

2.1	A schematic of the SINDAG geometry.	59
2.2	LLNL semi-analytic thermal model geometry	62
3.1	Schematic of the CYCLUS code repository.	68
3.2	Module Interfaces and Encapsulation in CYCLUS.	70
3.3	CYCLUS FacilityModel offer and request interface.	72
3.4	CYDER request-only interface.	73
3.5	Waste stream conditioning in CYDER.	75
3.6	Waste packaging in CYDER.	76
3.7	The gridded CYDER repository emplacement geometry.	77
3.8	An example CYDER output table of component parameters.	80
3.9	An example CYDER output table of contaminant history.	80
4.1	Constituents of a Degradation Rate Control Volume	93
4.2	Constituents of a Mixed Cell Control Volume	97
4.3	A system of volumes can be modeled as lumped parameter models in series.	102
4.4	1D finite advection dispersion solution.	106
4.5	Scaling of and STC curve for ^{242}Cm	111
4.6	Superposition of scaled Cm STC curves	112
4.7	STC method validation against LLNL model	114
4.8	STC method validation against LLNL model, percent error	115
5.1	^{235}U residence. Degradation Rate Waste Form No Release.	119
5.2	Case DRI Waste Form Contaminants.	119
5.3	Case DRI Buffer Contaminants	119

5.4	Case DRI Waste Package Contaminants.	119
5.5	Case DRI Far Field Contaminants.	119
5.6	^{235}U residence. Degradation Rate Waste Package No Release.	120
5.7	Case DRII Waste Form Contaminants.	120
5.8	Case DRII Buffer Contaminants	120
5.9	Case DRII Waste Package Contaminants.	120
5.10	Case DRII Far Field Contaminants.	120
5.11	^{235}U residence. Degradation Rate Buffer No Release.	121
5.12	Case DRIII Waste Form Contaminants.	121
5.13	Case DRIII Buffer Contaminants	121
5.14	Case DRIII Waste Package Contaminants.	121
5.15	Case DRIII Waste Package Contaminants.	121
5.16	^{235}U residence. Degradation Rate Buffer No Release.	122
5.17	Case DRIV Waste Form Contaminants.	122
5.18	Case DRIV Buffer Contaminants	122
5.19	Case DRIV Waste Package Contaminants.	122
5.20	Case DRIV Waste Package Contaminants.	122
5.21	^{235}U residence. Mixed Cell Without Sorption or Solubility Limitation.	124
5.22	Case MCI Waste Form Contaminants.	124
5.23	Case MCI Buffer Contaminants	124
5.24	Case MCI Waste Package Contaminants.	124
5.25	Case MCI Waste Package Contaminants.	124
5.26	^{235}U residence. Mixed Cell Coupled Sorption and Solubility Limitation.	126
5.27	Case MCII Waste Form Contaminants.	126
5.28	Case MCII Buffer Contaminants	126

5.29	Case MCII Waste Package Contaminants.	126
5.30	Case MCII Waste Package Contaminants.	126
5.31	^{235}U residence. Lumped Parameter PFM Waste Package No Release.	128
5.32	Case LPPFMII Waste Form Contaminants.	128
5.33	Case LPPFMII Buffer Contaminants	128
5.34	Case LPPFMII Waste Package Contaminants.	128
5.35	Case LPPFMII Far Field Contaminants.	128
5.36	^{235}U residence. Lumped Parameter Waste Package No Release.	129
5.37	Case LPEMII Waste Form Contaminants.	129
5.38	Case LPEMII Buffer Contaminants	129
5.39	Case LPEMII Waste Package Contaminants.	129
5.40	Case LPEMII Far Field Contaminants.	129
5.41	^{235}U residence. Lumped Parameter DM Waste Package No Release.	130
5.42	Case LPDMII Waste Form Contaminants.	130
5.43	Case LPDMII Buffer Contaminants	130
5.44	Case LPDMII Waste Package Contaminants.	130
5.45	Case LPDMII Far Field Contaminants.	130
5.46	Lumped Parameter Dispersion Model Transit Time Sensitivity	131
5.47	Lumped Parameter Exponential Model Transit Time Sensitivity	132
5.48	Lumped Parameter Piston Flow Model Transit Time Sensitivity	132
5.49	One Dimensional PPM Model.	134
5.50	Case ODI Waste Form Contaminants.	134
5.51	Case ODI Buffer Contaminants	134
5.52	Case ODI Waste Package Contaminants.	134
5.53	Case ODI Waste Package Contaminants.	134

5.54	^{129}I reference diffusivity sensitivity.	137
5.55	^{129}I vertical advective velocity sensitivity.	137
5.56	^{36}Cl reference diffusivity sensitivity.	137
5.57	^{36}Cl vertical advective velocity sensitivity.	137
5.58	^{99}Tc reference diffusivity sensitivity.	137
5.59	^{99}Tc vertical advective velocity sensitivity.	137
5.60	^{237}Np reference diffusivity sensitivity.	138
5.61	^{237}Np vertical advective velocity sensitivity.	138
5.62	^{79}Se reference diffusivity sensitivity.	138
5.63	^{79}Se vertical advective velocity sensitivity.	138
5.64	Advection vs. Diffusion Sensitivity in CYDER	139
5.65	Solubility factor sensitivity in GDSM Clay model	140
5.66	Solubility limit sensitivity in GDSM Clay model	141
5.67	Solubility Sensitivity in the Mixed Cell Model	142
5.68	K_d factor sensitivity	143
5.69	K_d sensitivity	144
5.70	K_d sensitivity in the Mixed Cell Model	145
5.71	^{129}I waste form degradation rate sensitivity.	146
5.72	^{129}I mass factor sensitivity.	146
5.73	^{36}Cl waste form degradation rate sensitivity.	146
5.74	^{36}Cl mass factor sensitivity.	146
5.75	^{99}Tc waste form degradation rate sensitivity.	147
5.76	^{99}Tc mass factor sensitivity.	147
5.77	^{237}Np waste form degradation rate sensitivity.	147
5.78	^{237}Np mass factor sensitivity.	147

5.79 Sensitivity demonstration of the degradation rate in CYDER for an arbitrary isotope.	148
5.80 K_{th} Sensitivity in LLNL Model	151
5.81 K_{th} Sensitivity in Cyder	152
5.82 K_{th} vs. r_{lim} Sensitivity in Cyder	153
5.83 K_{th} vs. Waste Package Spacing Sensitivity in Cyder	154
5.84 K_{th} Sensitivity to α_{th}	155
5.85 α_{th} Sensitivity in Cyder	156
5.86 α_{th} vs. K_{th} Sensitivity in Cyder	157
5.87 α_{th} vs. r_{lim} Sensitivity in Cyder	158
5.88 Thermal Sensitivity to K_{th} and s	159
5.89 Thermal Sensitivity to r_{lim} and s	160
5.90 Spacing Sensitivity in Cyder	161
5.91 r_{lim} Sensitivity in Cyder	162
5.92 Thermal Sensitivity to s and r_{lim} Sensitivity in CYDER	163

ABSTRACT

As the United States and other nuclear nations consider alternative fuel cycles and waste disposal options simultaneously, an integrated fuel cycle and generic disposal system analysis tool grows increasingly necessary for informing spent nuclear fuel management policy. The long term performance characteristics of deep geologic disposal concepts are affected by heat and radionuclide release characteristics sensitive to disposal system choices as well as variable spent fuel compositions associated with alternative fuel cycles. Computational tools capable of simulating the dynamic, heterogeneous spent fuel isotopics resulting from alternative nuclear fuel cycles and fuel cycle transition scenarios are, however, lacking in disposal system modeling options. This work has resulted in CYDER, a generic repository software library appropriate for system analysis of potential future fuel cycle deployment scenarios. By emphasizing modularity and speed, CYDER is capable of representing the dominant physics of candidate geologic host media, repository designs, and engineering components. Robust and flexible integration with the CYCLUS fuel cycle simulator enables this analysis in the context of fuel cycle options.

1 INTRODUCTION

The scope of this work includes development and validation of CYDER, a software library for generic modeling of various long-term disposal system concepts for nuclear material. CYDER is integrated with the CYCLUS computational fuel cycle systems analysis platform in order to inform repository performance metrics with respect to candidate fuel cycle options. By abstraction of more detailed models, this work captures the dominant physics of radionuclide and heat transport phenomena affecting repository performance in various geologic media and as a function of arbitrary spent fuel composition.

1.1 Motivation

The development of sustainable nuclear fuel cycles is a key challenge as the use of nuclear power expands domestically and internationally. Accordingly, the United States and other nations are considering a number of nuclear fuel cycle and geologic disposal options simultaneously [29, 61]. These decisions are technologically coupled by repository capacity. That is, radionuclide containment performance of a geologic repository is, in part, a function of spent fuel and high level waste composition, which varies among fuel cycle options. For this reason, integration of a generic disposal model and a fuel cycle systems analysis framework is necessary to illuminate performance distinctions of candidate repository host media, designs, and engineering components in the context of fuel cycle options. In answer to this need, CYDER integrates with the CYCLUS computational fuel cycle systems analysis platform [48, 102].

To support analysis of numerous combinatoric fuel cycle possibilities, a top-level simulation tool capable of modular substitution of various fuel cycle facility, repository, and engineered barrier components is needed. The modularity of natural and engineered

barrier representations resulting from this work will assist in informing an array of current technology choices, identifying important coupled parameters contributing to key waste disposal metrics, and highlighting the most promising waste disposal combinations with respect to metrics chosen by the user.

System level fuel cycle simulation tools must facilitate efficient sensitivity and uncertainty analyses and simulation of a wide range of fuel cycle alternatives. Therefore, a generic repository model appropriate for systems analysis must emphasize speed in accordance with use cases requiring repeated simulations. Simultaneously, it must provide modeling options at a level of detail that successfully captures significant aspects of the underlying physics. Often termed abstraction, the process of simplifying calculations while maintaining the salient features of the underlying physics was used to develop thermal and radionuclide transport models in this work.

Parameters of particular interest in fuel cycle systems analysis have historically been those related to the front end of the fuel cycle. However, parameters representing decisions concerning the back end of the fuel cycle are of increasing interest as repositories are being considered internationally and as the United States further investigates repository alternatives to the Yucca Mountain Repository Site (YMR). Choices such as geologic media, engineered barriers, appropriate loading strategies and schedules are all independent parameters up for debate. Due to the coupled nature of repository capacity and performance, these parameters are coupled with decisions about the fuel cycle.

Thus, coupled parameters require full synthesis with a systems analysis code that dynamically and appropriately determines the isotopic mass flows into the repository, their appropriate conditioning, densities, and other physical properties.

1.1.1 Future Fuel Cycle Options

As the United States and other nations seek to develop technologies and strategies to support a sustainable future for nuclear energy, various fuel cycle strategies and corresponding disposal system options are being considered. For example, the domestic fuel cycle option space under current consideration is described in terms of three distinct fuel cycle categories with the monikers Once Through, Full Recycle, and Modified Open. Each category presents unique disposal system design challenges. Systems analyses for evaluating these options must be undertaken in order to inform a national decision to deploy a comprehensive fuel cycle system by 2050 [28].

The Once-Through Cycle category includes fuel cycles similar to the fuel cycle currently deployed in the United States, utilizing light water reactors and direct disposal of spent nuclear fuel in a geologic repository. Such fuel cycles neglect reprocessing and present excavation, siting, and packaging challenges associated with high volumes of minimally treated spent fuel streams. In a business as usual scenario, conventional power reactors comprise the majority of nuclear energy production. Calculations from the Electric Power Research Institute corroborated by the United States (US) Department of Energy (DOE) in 2008 indicate that without an increase in the statutory capacity limit of the YMR, continuation of the current Once Through fuel cycle will generate a volume of spent fuel that will necessitate the siting of an additional federal geologic repository to accommodate spent fuel [27, 57].

A Full Recycle option, on the other hand, requires the research, development, and deployment of partitioning, transmutation, and advanced reactor technology for the reprocessing of used nuclear fuel. In this scheme, conventional once-through reactors will be phased out in favor of advanced transmutation technologies. All fuel in the Full Recycle strategy will be reprocessed using an accelerator driven system or by cycling through an

advanced fast reactor. Such fuel may undergo partitioning, the losses from which will require waste treatment and ultimate disposal in a repository. Thus, a repository under the Full Recycle scenario must support a waste stream composition that is highly variable during transition periods as well as myriad waste forms and packaging associated with isolation of differing waste streams.

Finally, the Modified Open Cycle category of options includes a variety of fuel cycle options that fall between once through and fully closed. This category of includes advanced fuel cycles such as deep burn and small modular reactors as well as partial recycle options. Partitioning and reprocessing strategies, however, will be limited to simplified chemical separations and volatilization. This scheme presents a dual challenge in which spent fuel volumes and composition will both vary dramatically among various possibilities within this scheme [28] .

Clearly, the waste streams resulting from potential fuel cycles present an array of corresponding waste disposition, packaging, and engineered barrier system options. Differing spent fuel composition, partitioning, transmutation, and chemical processing decisions upstream in the fuel cycle may demand differing natural and engineered barrier requirements during disposal. The capability to model thermal and radionuclide transport phenomena of arbitrary isotopic compositions is therefore required. This work has produced a disposal system simulator that meets this need.

1.1.2 Future Waste Disposal System Options

In addition to reconsideration of fuel cycle policy, the option space of potential geologic repository host media includes a number of concepts, most notably granite, clay/shale, salt, and deep borehole concepts [61, 71].

In accordance with various fuel cycle options, corresponding waste form, waste package,

and other engineered barrier systems are being considered. Specifically, current considerations include ceramic (e.g. Uranium Oxide), glass (e.g. borosilicate glasses), and metallic (e.g. hydride fuels) waste forms. Waste packages may be copper, steel, or other alloys. Similarly, buffer and backfill materials vary from the crushed salt recommended for a salt repository [40] to bentonite or concrete in other geologic settings [8]. For this reason, CYDER was designed to be capable of modular substitution of engineered barrier components and data in order to analyze the broad, relevant option space.

The physical, hydrologic, and geochemical mechanisms that dominate radionuclide and heat transport vary among the geologic and engineered containment barriers in the disposal system option space. Therefore, to support the system level simulation effort and quantification of associated disposal metrics, a disposal system model must capture the salient physics of these geologic options. Furthermore, in the same way that system level modularity facilitates analysis, so too does modular linkage between subcomponent process modules. The subcomponent models and repository environmental model in this work therefore provide a cohesively integrated disposal system simulator.

1.1.2.1 Thermal Modeling Needs

The decay heat from nuclear material generates a significant heat source within a repository. This decay heat varies among fuel cycles, is transported differently in different geologic media [35], and affects the resilience of engineered barrier choices [8]. Since repository loading capacity is constrained by the resistance of such barriers to degradation, allowable decay heat burden varies among repository concepts. In order to distinguish among the performance of fuel cycle, geologic media, and Engineered Barrier System (EBS) choices, an accordingly capable thermal model has been included in the repository model.

First, to distinguish among the repository decay heat burdens associated with various

fuel cycles, the repository analysis model must capture the decay heat behavior of dominant heat contributors. In particular, partitioning and transmutation of heat generating radionuclides within some fuel cycles will alter the isotopic composition of materials sent to the repository [89], and the dominant heat contributing isotopes will therefore vary. Isotopes of plutonium, americium, curium, and their decay daughters dominate long term decay heat contribution within directly deposited nuclear fuels. Other high heat contributing radionuclides that may dominate shorter term decay heat include fission products such as isotopes of cesium and strontium [77].

Second, the capability to model thermal evolution in each component is also necessary since the repository capacity may be constrained by thermal limits in EBSs components. Such thermal limits have their technical basis in the temperature dependence of isolation integrity of the waste forms, waste packages, and buffer materials. Alteration, corrosion, degradation, and dissolution behaviors are often a function of heat, in addition to redox conditions, and constrain loading density within the engineered barriers.

In addition, the capability to model far field thermal evolution is necessary in order to capture differences in thermal loading sensitivity among host rock choices. Thermal limits in the geologic environment can be based on the mechanical integrity of the rock as well as mineralogical, hydrologic, and geochemical phenomena. The isolating characteristics of a geologic environment are most sensitive to hydrologic and geochemical effects of thermal loading. Thus, heat load constraints are typically chosen to control hydrologic and geochemical response to thermal loading. Thermal limits are a design consequence driven by regulations that seek to passively steward the repository's hydrologic and geochemical integrity against radionuclide release. Such constraints affect the repository waste package spacing and repository footprint among other parameters.

Finally, since some material and hydrologic phenomena affecting radionuclide transport

are thermally coupled, future advanced implementation goals include dynamically informing those parameters with the thermal modeling capability developed here. Those temperature coupled phenomena include corrosion processes, dissolution rates, diffusion, solubility, and partition coefficients. It is expected that only a coarse time resolution will be necessary to capture that coupling, since time evolution of repository heat is such that thermal coupling can typically be treated as quasi-static for long time scales [8].

1.1.2.2 Radionuclide Transport Modeling Needs

Domestically, the Environmental Protection Agency (EPA) has defined a limit on human exposure associated with the deep geologic disposal of spent fuel and high level nuclear waste. Such regulations establish important limitations on capacity, design, and loading techniques for repository concepts under consideration. Repository concepts developed in this work must therefore quantify radionuclide transport through the geologic environment in order to calculate contaminant releases that inform performance metrics.

In particular, the radionuclides in need of containment vary among fuel cycles and travel differently through various geologic environments and engineered barrier choices. Thus, in order to distinguish among the performance of fuel cycle, geologic media, and EBS options, a hydrologic radionuclide contaminant transport modeling capability has been included in the repository model. These capabilities focused on hydrologic, geochemical, and mechanical modeling behaviors identified as especially important to repository performance by sensitivity analyses conducted with a detailed geologic repository performance tool.

Furthermore, to support varying modeling simplifications and assumptions common in performance assessment, modeling capabilities are necessary at varying levels of detail. Accordingly, four interchangeable radionuclide transport models have been implemented. The simplest of these captures only the simplest mechanical modeling needs while the

most detailed additionally captures geochemical and hydrologic behaviors.

1.1.3 Domestic Research and Development Program

By interfacing directly with the DOE-NE Fuel Cycle Technology (FCT) program, this work contributes directly to current fuel cycle analysis and disposal research underway domestically. The FCT program has three groups of relevance to this effort: these are the Used Fuel Disposition (UFD), the Separations and Waste Forms (SWF), and Fuel Cycle Options (FCO) (previously Systems Analysis) campaigns. The UFD campaign is conducting the Research Development and Demonstration (RD&D) related to the storage, transportation, and disposal of radioactive wastes generated under both the current and potential advanced fuel cycles. The SWF campaign is conducting Research and Development (R&D) on potential advanced separations technologies including associated waste forms that could be used to effectively isolate the wastes that would be generated in advanced fuel cycles. The SWF and UFD campaigns are developing the fundamental tools and information base regarding the performance of waste forms and geologic disposal systems. The FCO campaign is developing the overall fuel cycle simulation tools and interfaces with the other FCT campaigns, including UFD.

This effort has interfaced with those campaigns to develop the higher level dominant physics representations for use in fuel cycle system analysis tools. Specifically, this work has leveraged conceptual framework development and primary data collection underway within UFD. It has also benefited from University-laboratory collaboration via work by Radel, Wilson, Bauer et. al. to model repository behavior as a function of the contents of the waste [83].

1.2 Methodology

In this work, concise dominant physics thermal and radionuclide transport models were developed by comparison of analytical models with more detailed repository modeling tools. The result of this work is a software library capable of assessing a broad combinatoric domain of potential engineered barriers, repository design concepts, and geologic settings in the context of fuel cycle alternatives. Within this software library, a suite of basic capabilities have been demonstrated and validated and a few advanced features are operational.

1.2.1 Identification of the Modeling Domain

An appropriate modeling domain was identified according to a review of current domestic and international candidate repository concepts, analytic models, and computational performance assessment techniques.

Specifically, in order to capture the current domestic option space, three candidate geologic settings and four corresponding repository concepts under consideration by the UFD campaign were selected for modeling in this work. The three geologic environments selected were clay, granite and salt. The four concepts included three enclosed, saturated, 500m deep horizontal plane concepts in each of the three geologic settings and a fourth 5km deep borehole concept conceived in crystalline basement rock.

Analytic models and detailed computational tools for repository analysis were investigated and categorized within the literature review. Of these, candidate computational tools appropriate for performing abstraction and regression analyses were identified. Specifically, a suite of Generic Disposal System Model (GDSM) tools developed by DOE UFD campaign was selected to inform radionuclide transport model abstraction[24] and two thermal analysis tools, also developed by the UFD campaign, were selected to inform the

thermal abstraction process [35, 45, 46].

1.2.2 Identification of Dominant Physics

Sensitivity analyses characterized the importance of physical mechanisms of repository performance within the materials and media under consideration with respect to thermal and radionuclide transport.

Sensitivity analysis concerning thermal parameters was undertaken with available detailed models. These models, a 2D finite element thermal performance assessment model [45, 46] and a semi-analytic model [35] were used to characterize the parametric dependence of thermal loading in a specific geologic environment. In the conductive thermal transport regime found in enclosed saturated repository concepts, the primary parameters distinguishing clay, salt, and granite geologic settings included thermal conductivity, thermal diffusivity, waste package spacing, and near field thermal limits. The results of these analyses provided the database powering CYDER's thermal capability. A benchmarking effort between these models was conducted (see Appendix B) and informed the level of detail with which repository capacity and thermal evolution are modeled in this work.

Sensitivity analysis utilizing a UFD GDSM tool built on the GoldSim simulation framework informed performance sensitivity to engineered barrier system failure parameters as well as hydrologic and geochemical radionuclide transport phenomena. In saturated geologic settings, key parameters included dominant transport mechanism (diffusive or advective), isotopic spent fuel inventory and composition, engineered barrier failure, and redox state (insofar as it affected sorption behavior and solubility limitation).

Particular hydrologic modeling needs identified in Appendix section A.4.1 include the need to capture differing behavior in advectively dominated and diffusively dominated

transport regimes. As advection and diffusion parameters vary among geologic media, and performance is sensitive to the dominant mode of transport, this distinction is necessary when modeling the far field in particular.

Particular geochemical modeling needs identified in Appendix sections A.4.3 and A.4.4 include the need for solubility and sorption behaviors which vary greatly among host rock options and were identified to, in some cases, significantly affect contaminant transport behaviors.

Particular mechanical modeling needs identified in Appendix sections A.4.5 and A.4.6 include the need for EBS degradation based failure modeling. Waste package and waste form degradation and failure were shown in those sensitivity analyses to be important in geologic settings where transport is dominated by a fast advective pathway.

1.2.3 Abstraction and Implementation

Iterative abstraction between analytic models and sensitivity analysis results produced concise models that capture performance among candidate geologic media as a function of radionuclide inventory and heat generation over long time scales. Supporting data are derived primarily from the UFD campaign GDSMs and data, as well as European efforts such as the RED-IMPACT assessment and Agence Nationale pour la gestion des Déchets Radioactifs, the French National Agency for Radioactive Waste Management (ANDRA) Dossier efforts [8, 24, 61] .

These concise models are a combination of two components: semi-analytic mathematical models that represent a simplified description of the most important physical phenomena, and semi-empirical models that reproduce the results of detailed models. By combining the complexity of the analytic models and regression against numerical experiments, variations were limited between two models for the same system. Different approaches have been

compared in this work, with final modeling choices balancing the accuracy and efficiency of the possible implementations.

In addition, the concise models are capable of roughly adjusting release pathways according to the characteristics of the natural system (both the host geologic setting and the site in general) and the engineered system (such as package loading arrangements, tunnel spacing, and engineered barriers).

The full abstraction process was iterated to achieve a balance between calculation speed and simulation detail. Model improvements during this stage sought a level of detail appropriate for informative comparison of subcomponents, but with sufficient speed to enable systems analysis. By varying input parameters and comparing with corresponding results from detailed tools, the behavior of each model on its parametric domain was explored.

In the CYDER library, the resulting concise models support performance estimation within components of a robust disposal system simulation module. It was designed as a dynamically loadable module appropriate to represent a facility within the CYCLUS fuel cycle simulator. Furthermore, the robust architecture implemented within the repository module allows for interchangeable loading of components and model in support of simulations at various levels of fidelity.

1.3 Research Goals

The purpose of this work was to design a fast, flexible code for medium fidelity calculation of generic repository performance in the context of fuel cycle analysis. In addition to implementing fundamental modeling capabilities, CYDER has been designed to accommodate the development of advanced capabilities in the future.

Cyder has emphasized repository concept generality, dominant physics models of

radionuclide and thermal transport, and dynamic integration with a fuel cycle simulation platform.

To identify the key conceptual components and modeling methods for geologic radioactive waste disposal, a literature review, Chapter 2, presents background material that organizes and reports upon previous relevant work. First it summarizes the state of the art of repository modeling integration within current systems analysis tools. It then describes current domestic and international disposal system option space. Next, the literature review focuses upon current analytical and computational modeling of radionuclide and heat transport through various waste forms, engineered barrier systems, and geologic media of interest. It also addresses previous efforts in generic geologic environment repository modeling in order to categorize and characterize detailed computational models of radionuclide and heat transport considered for abstraction and validation efforts.

To support repository concept generality and dynamic integration, CYDER was designed with a modular paradigm as a part of the CYCLUS fuel cycle simulation platform. Chapter 3 details the computational paradigm of the CYCLUS systems analysis platform and CYDER repository model which constitute this work. It describes the CYCLUS fuel cycle simulation context which drives fundamental CYDER design decisions as well as the modular paradigm emphasized in both CYCLUS and CYDER.

Chapter 4 describes radionuclide transport and heat transport models that resulted from an abstraction process between analytic models and the results of detailed tools. These models, used to represent engineered barrier and geologic disposal system components, are defined by their interfaces and their relationships as interconnected modules, distinctly defined, but coupled. This modular implementation allows exchange of technological options for comparison as well as exchange of models for the same technological option with varying levels of detail.

As a demonstration of the capabilities implemented in CYDER, Chapter 5 presents the results of simulation cases conducted to demonstrate radionuclide transport and thermal capacity model performance. It also describes verification and validation procedures which benchmarked CYDER behavior against analytic solutions and more detailed models.

Finally, in Chapter 6, contributions to the field and suggested future work are summarized.

2 LITERATURE REVIEW

The following literature review first addresses current integration of repository modeling within systems analysis, followed by a discussion of the disposal system concepts and geologic host media under consideration domestically and internationally. Finally, a review of analytical and computational models of radionuclide and thermal transport follows.

2.1 Repository Capabilities within Systems

Analysis Tools

Several computational fuel cycle simulation tools have been developed to inform calculations of fuel cycle metrics. This literature review focused on seven : Nuclear Waste Assessment System for Technical Evaluation (NUWASTE) [2], Dynamic Analysis of Nuclear Energy System Strategies (DANESS) [93], Nuclear Fuel Cycle Simulator (NFCSim) [85], ORION [37], Commelini-Sicard (COSI) [15], the Verifiable Fuel Cycle Simulation Model (VISION) [15, 81, 101, 103], and Code for Advanced Fuel Cycles Assessment (CAFCA) [38].

2.1.1 Repository Performance Calculations

Most current tools treat the waste disposal phase of fuel cycle analysis statically in post processing by reporting values such as mass, volumes, radiotoxicity, or heat production of accumulated spent nuclear fuel (SNF) and high level waste (HLW). Such tools (e.g., NUWASTE [2], DANESS [93], NFCSim [85], and ORION [37]) fail to address the impact of those waste streams on the performance of the geologic disposal system [101]. Two tools, COSI [15] and VISION [15, 81, 101, 103], dynamically perform heat based capacity calculations. However, those calculations are applicable only for specific repository concepts

and cannot inform sensitivity to alternate geologic disposal system characteristics.

2.1.2 Detail

A few sophisticated fuel cycle tools (e.g., NUWASTE [2], NFCSim [85], and COSI [15]) have emphasized discrete material tracking and have demonstrated the improved flexibility of that strategy over more traditional flow sheet calculations. A few (e.g., NUWASTE [2] and COSI [15]) utilize discrete material tracking to provide per-package metrics including heat generation and radiotoxicity.

The number of isotopes distinctly tracked also varies among fuel cycle simulator tools. Some (e.g., COSI [15], DANESS [93], ORION [37], and VISION [15, 81, 101, 103]) are capable of tracking thousands or arbitrary numbers of isotopes. Others (e.g., NUWASTE [2]) track tens of isotopes, while still others neglect isotopic granularity (e.g., CAFCA [38]).

2.1.3 Accessibility

While these tools have contributed to analysis of fuel cycle effects on repository metrics, none address radionuclide contaminant transport in generic geologic media, and many (e.g., COSI [15], DANESS [93], ORION [37], NUWASTE [2], and VISION [15, 81, 101, 103]) are too restrictively distributed or licensed for broad use and development.

The current capabilities of these tools suggest that sensitivity of repository performance metrics to fuel cycle decisions can be calculated using a variety of methods that have yet to be explored. Based on the flexibility of discrete material tracking, the power of dynamic modeling, and the flexibility of open access the CYDER tool has emphasized those strategies. Also, recognizing the need for a tool that analyzes repository performance

for generic geologic settings, the CYDER tool employs both thermal and contaminant transport capabilities.

2.1.4 Repository Focused Fuel Cycle Analyses

While top level fuel cycle system analyses fail to incorporate repository models, some repository focused fuel cycle sensitivity analyses have been conducted using existing tools. Most domestic repository focused analyses have emphasized used fuel disposition and waste management in the Yucca Mountain Repository Site (YMR). These have been conducted by Ahn [5], Bauer [12], Li [62], Piet [77], Radel [82], Wigeland [97, 98], and others. With a focus on YMR capacity, repository performance metrics of interest for these analyses were heat, source term, and more global environmental impact metrics.

The Total System Model (TSM) code, developed at Office of Civilian Radioactive Waste Management (OCRWM) is a very detailed model of the Yucca Mountain disposal system. It includes transportation issues and detailed emplacement timing and strategy models, but considers only the fuel cycle associated with the current U.S. reactor fleet. Casks are modeled discretely and radionuclide and heat transport are modeled in great detail. This level of detail results in a dramatically extended run time making this model inappropriate for top level fuel cycle systems analysis. The TSM model can only be run by its development team and runs a typical simulation, processing 70,000 MTHM, in 12-15 hours [91].

The TSM framework is based on the commercial SimCAD platform. The simulation steps through time in 8 hour time steps during the waste cask transportation, processing and emplacement. This event based simulator is primarily focused on the operation stage of the Yucca Mountain repository, but is equipped with a thermal management model that informs waste package emplacement.

2.2 Disposal Environment Concepts

A suite of three geologic media and four disposal concepts of interest were chosen to capture those found in the following review of international and domestic efforts. CYDER has been developed to model granite, clay, and salt geologic environments with various layouts and an array of canonical engineered barrier component models.

Geologic disposal concepts that have been investigated internationally, with the exception of YMR, can be characterized as enclosed concepts in saturated, reducing environments. Saturated concepts are those located below the water table such that, in contrast to YMR, the porosity within the rock matrix as well as fractures and other open spaces is suffused with water. An enclosed concept is one that neither relies on ventilation shafts nor an extended open period after waste emplacement. In low permeability rock formations (clay/shale, granite, salt), an enclosed concept does not permit significant oxygen entry, typically resulting in chemically reducing environments.

Chemically reducing geologic environments are reducing insofar as they induce reduction of water flowing through them. That is, reduction and oxidation reactions in these environments proceed in a reducing direction. This attribute has the primary effect of slowing corrosion, dissolution, and alteration rates in materials that are subject to degradation. A reducing disposal environment also lowers solubility limits and increases sorption of many actinide species. The dominant dose contributors in reducing environments are therefore the soluble, long lived fission and activation products such as ^{129}I and ^{79}Se [61, 74].

Various engineered barrier system components have also been modeled as a part of this effort. Specifically, in order to cover the option space demonstrated by both domestic and international repository concepts, models were developed which can interchangeably represent concrete, salt, and bentonite buffer and backfill options as well as waste package

and waste form concepts which can be distinguished by their alteration, corrosion, and other degradation behaviors.

2.2.1 Clay Disposal Environments

Clays, including a range of claystones, shales, and argillites, have been investigated in Belgium, France, Japan, and Switzerland [61] as well as the US [24]. Due to low permeability and few fractures in clays, diffusion is the dominant transport mechanism. Additionally, clays tend to have high sorption capacity for cations, which reduces the mobility of contaminants present in clays as cations such as the lanthanides and americium [42]. A less attractive quality of clay is a low thermal limit around 100°C temperature limit to prevent alteration [40]. Some characteristics of clay disposal concepts are given in Table 2.1.

Clay Repository Features			
Hydrology	Geochemistry	Design Concepts	Thermal Behavior
Very low conductivity	Reducing	no/bentonite/concrete backfill	alteration limited
High porosity (up to 0.5)	Saline	~ 500 m deep	100° C limit
Low effective porosity	Saturated	closed horizontal or vertical emplacement	
Slow water velocity			
diffusion dominated			

Table 2.1: Clay geologic repository concepts demonstrate certain dominant physical phenomena.

2.2.1.1 Disposal System Components

The French ANDRA analysis modeled borosilicate glass as well as ceramic oxide waste forms within carbon steel waste packages in combination with a bentonite buffer material and a crushed clay or shale backfill [8]. The Belgian reference concept focused on a highly

plastic Boom Clay, which eventually completely seals around stainless steel, nickel, or titanium waste packages [75]. The Swiss concept modeled glass waste forms in stainless steel waste packages with a bentonite buffer and a bentonite and sand backfill [55]. Each of these concepts considered horizontal emplacement in multiple-package emplacement drifts.

2.2.1.2 Hydrology

In a clay disposal environment, exceptionally low interconnected porosity and very little fracturing result in a very low overall hydraulic conductivity and diffusion dominated water movement.

2.2.1.3 Geochemistry

This environment is very reducing in both the near and far field, its salinity increases with depth, and its pH is expected to be near neutral. However, for some concepts incorporating cementitious backfill materials for protection of steel, the pH can become significantly alkaline, resulting in expedited alteration of glass waste forms, bentonite buffers, and the clay matrix [8].

Radionuclides that are relatively highly mobile in a clay environment dominate potential long-term dose to the public from clay repository concepts. For most fuel cycles, these include ^{129}I , ^{79}Se , and ^{36}Cl [89].

2.2.1.4 Thermal Behavior

Heat limits in clay are based on the domain of known behavior in clay and the tendency for bentonite fill material to lose its isolating properties with high temperatures [8, 80]. The alteration of high smectite bentonite to non-expandable clays is a primary limitation

for heat tolerance in the clay concept. The isolation characteristics of bentonite buffer materials are reduced after this alteration. The time integral of this phenomenon determines total bentonite alteration. While short bursts of heat might be allowable, because the bentonite will not alter immediately, the kinetic alteration into smectite clays is hastened by temperatures above approximately 100°C [80]. Well understood behavior for argillite and bentonite buffer backfill is conservatively assumed by the ANDRA assessment to occur only under 90°C , which is effectively a limit at the waste package interface with the bentonite buffer material [8]. The National Cooperative for the Disposal of Radioactive Waste (NAGRA) Opalinus Clay assessment less conservatively uses a maximum heat limit in the bentonite buffer of 125°C [54].

The thermal conductivity of clay is also typically lower than $2\text{ W/m}\cdot\text{K}$. Accordingly, thermal loading constraints are more restrictive than in more conductive materials. In particular, Belgium (ref. [75]) used values between 1.25 and $1.7\text{ W/m}\cdot\text{K}$, France (ref. [8]) used values between 1.9 and $2.7\text{ W/m}\cdot\text{K}$, and Switzerland (ref. [55]) used $1.8\text{ W/m}\cdot\text{K}$.

2.2.2 Granite Disposal Environments

Granite disposal concepts have been considered in Finland, France, Japan, Sweden, China, Spain, the Czech Republic, South Korea, and Switzerland [9, 61] as well as the US [40].

Attributes of granite that make it an attractive candidate geologic medium for nuclear waste disposal include its very low porosity and permeability and high thermal conductivity. Fracturing in granite, however, has a negative effect on the isolation properties of the rock. Some characteristics of granite disposal concepts are given in Table 2.2.

Granite Repository Features

Hydrology	Geochemistry	Design Concepts	Thermal Behavior
Low porosity (~ 0.01) Fractures	Reducing in Near Field Slightly Oxidizing in Far Field	Single WP tunnels Carbon-Steel [9]or	Closed Bentonite Limit $100^{\circ}C$
Low permeability	Increasing saline with depth [61]	Copper overpack	
High Water Velocity in Fractures	Cement causes alkalinity [9] Saturated or Unsaturated	Bentonite buffer Crushed granite backfill [61] $\sim 500m$ deep	

Table 2.2: Granite repository concepts demonstrate certain dominant physical phenomena.

2.2.2.1 Disposal System Components

The Swedish KBS-3 concept includes ceramic oxide spent fuel waste forms within a steel shell and copper waste package buffered by bentonite clay and backfilled with clay and sand and emplaced vertically in horizontal drifts [1]. A similar Czech Republic repository concept consists of borosilicate glass waste forms within a stainless steel Universal Canister waste package, vertically emplaced in horizontal drifts and with a bentonite buffer and backfilled with a clay and sand mixture. The Spanish concept is almost identical to these, except emplacement is horizontal within the horizontal repository drifts [61].

2.2.2.2 Hydrology

In the granite disposal environment, a low porosity is combined with higher expected water velocity (relative to other repository concepts in this work) and significant fracturing. The overall granite hydraulic conductivity is still typically low [40, 86]. Within this environment, the water behavior in the far field must be modeled as both diffusive and advective.

2.2.2.3 Geochemistry

This environment is very reducing in the near field and slightly less so in the near surface far field due to far field fracturing in the granite near the surface. Most importantly, this results in higher actinide solubilities in that region. Salinity in the granite environment increases monotonically with depth. At a typical concept depth of 500m, the repository is therefore expected to be in a location of high salinity, an indicator of historically low fluid flow but resulting in increased corrosion rates and for some radionuclides, changed solubilities [9]. It is expected that the pH will be near neutral in this environment except with the introduction of concretes, due to which the pH becomes significantly alkaline, resulting in more rapid alteration of bentonite buffers.

The relatively fast advective pathways in fractures have the effect of increasing the importance of ^{234}U in the initial waste stream. While ^{234}U and its decay daughter ^{230}Th are not very mobile in a reducing environment, their subsequent decay daughter ^{226}Ra is highly mobile. ^{226}Ra is therefore a dominant dose contributor in granite [89], while in many other geologies, the 1601 year half life of ^{226}Ra is too short for a significant quantity to traverse the diffusive pathway.

2.2.2.4 Thermal Behavior

In the absence of a bentonite limitation (i.e., concepts with non-bentonite buffers), a thermal limit within the granite itself is greater than 200°C , limited by the increased risk of micro-cracking. Mechanical stresses and strains in the matrix due to heating at this level were analyzed by ANDRA and shown to have a negligible effect of flow behavior in granite. Similarly, thermo-hydraulic effects due to thermally induced fluid density changes are expected to be slight [9]. Similarly, for reasons of buffer isolation integrity, the Czech and Spanish granite disposal concepts both maintained a thermal limit at the waste package

interface with the buffer of $100^{\circ}C$. [61]

This relatively high resistance to heat induced mechanical failure is due to the high thermal conductivity of granite, which is typically found to be between 2.4 and 4 W/m·K. In particular Sweden (ref. [1]) used 3.4 - 4 W/m·K and 2.45 - 2.9 W/m·K, France (ref. [8]) used 2.4 - 3.8 W/m·K, and Finland (ref. [78]) used 2.3 - 3.2 W/m·K.

The effective thermal limit for granite disposal concepts, however, is usually related to the bentonite limit, which is similar to the bentonite limits of clay concepts discussed in Section 2.2.1.4.

2.2.3 Salt Disposal Environments

Salt disposal concepts have been investigated in Germany and demonstrated for non-heat-generating waste at the Waste Isolation Pilot Plant (WIPP) facility in the US. Salt demonstrates many attractive properties including ease of mining, creep behavior over time, which is expedited by heat, low permeability, and a high thermal conductivity, which affords a high temperature limit near $200^{\circ}C$ [40]. Some characteristics of salt disposal concepts are given in Table 2.3.

Salt Repository Features			
Hydrology	Geochemistry	Design Concepts	Thermal Behavior
Dry Waste Package	Reducing in Near Field	Alcove Emplacement	$180^{\circ}C$ limit [61]
Dry Backfill	Far Field Slightly Oxidizing	Crushed Salt Backfill	Heat induced creep sealing
Saturated Far Field Very low permeability Brine pockets in far field	Very saline brines	$\sim 500m$ deep Multiple Packages Breached only from intrusion	Closed limited data

Table 2.3: Salt geologic repository concept demonstrates certain dominant physical phenomena.

2.2.3.1 Disposal System Components

German and United States salt concepts include drifts or alcoves, respectively, in which waste packages are placed. The space is then backfilled with crushed salt [61]. The consolidation properties of the backfill and salt are of great isolation importance. The infinitesimally small hydraulic conductivity of consolidated rock salt has the effect of nullifying the possibility of any releases without a disruption scenario [20].

2.2.3.2 Hydrology

In a rock salt or salt dome disposal environment, a very low porosity combined with negligible water velocity and effectively no fracturing results in a salt hydraulic conductivity that is exceptionally low. Within this environment, extraordinarily slow diffusive speed out of the repository dominates the isolation behavior. Candidate salt formations are remarkably uniform and their accessible porosity is near negligible, so almost no water movement is expected to occur.

2.2.3.3 Geochemistry

This environment is very reducing in the near field and slightly less so in the far field [24]. Very high salinity expedites corrosive processes, but the engineered barrier system is of limited importance in this concept in which the diffusive geologic salt barrier dominates isolation integrity. It is expected that the pH will be near neutral in this environment [24, 61].

2.2.3.4 Thermal Behavior

Response of a salt repository to heat has a significant mechanical component. Bulk heating of a salt repository matrix causes coalescing of the salt surrounding the heat source. In

the case of a nuclear waste repository, this phenomenon increases isolation capability of the salt. A heat limit, then, is difficult to characterize, but evolution of the heat in a salt environment is of great importance to radionuclide transport modeling.

The German salt repository concept maintains a 180°C temperature limit. The technical basis for this limit has to do with the concern that at temperatures above 220°C differential densities in the salt formation may drive the movement of brine inclusions and potentially facilitating radionuclide transport [20, 59, 61].

Notably, the crushed salt backfill in most concepts has low conductivity, which increases the sensitivity of rock salt temperature on emplaced package temperature. However, as the crushed salt coalesces with heat over time, its thermal conductivity increases to approach that of intact salt. Further investigation toward a comprehensive model of the thermal behavior of dry salt has been recommended both domestically and internationally [23].

2.2.4 Deep Borehole Disposal Environments

Deep Borehole disposal system concepts are being evaluated in the UK, Sweden and the United States [24, 61]. Attributes of this concept that are favorable for waste isolation include the stability of the crystalline basement rock in which the borehole emplacement would occur and the elongated diffusion path length for release. The potential technical difficulty of well controlled emplacement at great depth is an unfavorable attribute, however [40]. Some characteristics of deep borehole disposal concepts are given in Table 2.4.

2.2.4.1 Disposal System Components

In deep borehole concepts, many types of waste form and waste package material are emplaced at great depths, typically between 2 and 5 km [24, 40] in a crystalline rock such as granite basement rock. In each borehole, hundreds of canisters are stacked vertically

Borehole Repository Features

Hydrology	Geochemistry	Design Concepts	Thermal Behavior
Crystalline rock Low porosity (~ 0.01)	Reducing at depth Less Reducing at surface	$\sim 5km$ deep disposal in lower 2km	cracking unimportant may affect flow
Limited fracturing at depth	limited solubility	1km bentonite seal	high conductivity
Rock Permeability ($\sim 10^{-19}$)	enhanced sorption	bentonite grout	high density
EBS Permeability ($\sim 10^{-16}$)	high salinity	bentonite plugs	
Very Limited Upward Flow	saturated	400 packages per borehole closed	

Table 2.4: Borehole geologic repository concept demonstrates certain dominant physical phenomena.

in the deepest section. In some concepts, dense bentonite plugs are stacked between the packages. Above the packages, swelling bentonite clay, asphalt and concrete provide a seal for the upper few kilometers [24].

2.2.4.2 Hydrology

In the deep borehole crystalline basement rock disposal environment, low porosity combined with only minor fracturing results in an overall hydraulic conductivity which is very low. Thermally driven, upward water velocity is the primary driver for solute movement along the 2-5 kilometer diffusive path to the surface where fresh water aquifers may exist [24]. Without the introduction of a fast pathway (e.g., an intersecting fracture or human intrusion) the length of the diffusive pathway has the effect of making the engineered barrier component choices irrelevant since no known engineered barrier choice can be expected to outlast the timescale of the diffusive pathway.

2.2.4.3 Geochemistry

This environment is very reducing in the near field and less in the very far field near the earth's surface. The very high expected salinity of this environment, due to its depth, indicates historically low flow. While this increases corrosion rates of engineered barriers, the isolation worth of this concept does not depend significantly on the engineered barrier components, relying instead on the diffusion path length.

2.2.4.4 Thermal Behavior

Since the crystalline basement rock in which deep borehole concepts are envisioned is typically granite, the thermal behavior of the deep borehole environment is identical to the granite case, except the bentonite buffer limitation is no longer applicable. Also, the 200°C limitation in order to avoid microfissures could be shown to be irrelevant in light of the great distance to the surface. That is, even if the damage zone in the vicinity of the emplaced waste packages is enlarged significantly by high heat load, the kilometers of diffusion length to the surface will still dominate the isolation behavior of the repository.

2.3 Analytical Models of Radionuclide Transport

Models of radionuclide contaminant transport address radionuclide transport through some or all of the release pathway made up of waste forms, waste packages, engineered barrier systems, and geologic media. A model of transport through the repository typically incorporates radionuclide release via waste form degradation, waste package failure, then advective and diffusive transport through the engineered barrier system and geologic medium. Some models also incorporate advective fast pathways introduced by tectonic events or human intrusions.

2.3.1 Waste Form Release Models

Radionuclide release, the mass transfer of a radionuclide from its waste form into surrounding water, from various possible waste form types will be dominated by an array of degradation, alteration, and dissolution phenomena. Some phenomena dominating the release from canonical waste forms such as Commercial Spent Nuclear Fuel (CSNF), DOE Spent Nuclear Fuel (DSNF), and borosilicate glasses are listed in Table 2.5.

Waste Form Types			
WF Type	SubTypes	Contents	Release Drivers
Once Through	CSNF Ceramic Oxide	Nominal Burnup UOx & MOX	redox reactions
	CSNF Ceramic Oxide	High Burnup	redox reactions, heat
	HTGR TRISO Graphite	High Burnup	graphite reactions
	DSNF Metal	High Burnup N Reactor Fuel	metal reactions, heat
Borosilicate Glass	DSNF Carbides	Fast Reactor Fuels	carbide reactions, heat
	DSNF Ceramic Oxides	Research Reactor Fuels	redox reactions, heat
Glass Ceramic	Current	MA's Cs/Sr	heat, glass alteration
	Future	Mo, no MA no Cs/Sr	glass alteration
Glass Ceramic	Glass Bonded Sodalite	Echem processed oxide fuels	ceramic, redox, glass reactions
Metal Alloy	From Echem	Cladding, noble metals	metal reactions, heat
	From Aqueous	transition metals	metal reactions, heat
Advance Ceramic		volatized iodine	ceramic reactions, redox
Salt	Cementitious Sodium	separated streams	alkaline reactions, dissolution

Table 2.5: An array of waste forms developed for nuclear wastes have a corresponding array of dominant release mechanisms [14].

2.3.1.1 Degradation Rates

An initial breach of the primary barrier, which exposes the waste form to water, typically triggers degradation of the waste form [17]. Degradation behaviors depend strongly water chemistry, but primarily on material properties of the waste form. In the absence of detailed knowledge about long term waste form material behavior, however, waste form degradation can be modeled as a purely rate based model,

$$\begin{aligned}
V_i(t) &= V_i(0) \left(1 - \int_0^t f(\dots) dt \right) \\
&= \text{intact waste form volume } [m^3]
\end{aligned}
\tag{2.1}$$

where

$$f(\dots) = \text{a known degradation rate function} \tag{2.2}$$

In the case of saturated repository concepts, degradation is often modeled to begin immediately at emplacement [41]. However, in models of unsaturated media [4, 5], the waste form may not come into contact with water immediately, and therefore degradation will not begin until the onset of water contact. Either environment can be represented by the general expression,

$$V_i(t) = V_i(0) \left(1 - \int_0^t f(\dots) H(t - t_{w_{pf}}) dt \right). \tag{2.3}$$

where

$t_{w_{pf}}$ = time of waste package failure

$H(t - t_{w_{pf}})$ = Heaviside step function

$$= \begin{cases} 0 & t < t_{w_{pf}} \\ 1 & t \geq t_{w_{pf}} \end{cases} \tag{2.4}$$

Importantly, the rate is often assumed to be slower in reducing environments than

oxidizing ones [89].

In either case, radionuclide release is often modeled as congruent with the degradation of the waste matrix. That is, release is modeled as unimpeded by sorption or solubility and becomes available according to the fractional degradation rate until the waste form is completely degraded [4, 5].

If congruent release neglects transport limiting factors such as solubility limitation, it is most appropriate when applied to highly soluble radionuclides. In [4, 5] the transport of highly soluble radionuclides (those with high solubility limits) are modeled as infinitely soluble in this way. In an oxidizing environment, radionuclides of this type include most of the fission products, but not the actinides.

2.3.1.2 Solubility Limitation

In order to account for solubility limitation, an upper limit of elemental dissolved concentration, the reduced mobility of radionuclides with lower solubilities can be modeled [41] as a reduction in the amount of solute available for transport. For radionuclides with low solubility, the mass fraction released from the waste matrix is constrained to less than the solubility limit such that

$$m_i(t) \leq V(t)C_{sol,i} \quad (2.5)$$

where

m_i = mass of isotope i in volume V [kg]

V = a distinct volume of fluid [m^3]

$C_{sol,i}$ = the maximum concentration of i [$kg \cdot m^{-3}$].

That is, the mass m_{1i} in kg of a radionuclide i dissolved into the waste package void volume V_1 in m^3 , at a time t , is limited by the solubility limit, the maximum concentration, C_{sol} in kg/m^3 at which that radionuclide is soluble [41].

In the Ahn models [4, 5], radionuclides with lower solubility limits are modeled with a solubility limited release model. Solubility values are assumed from TSPA for this model, and elements with a solubility of less than 5×10^{-2} mol/ m^3 are taken to be “low.” Elements in this “low” category include Zr, Nb, Sn and some toxic actinides such as Th and Ra for an oxidizing, unsaturated environment similar to YMR. It should be noted that in a reducing environment, the actinides are not as mobile, and the high and low solubility radionuclides will differ from this model. This model suggests that dissolution of radionuclides into the water is dominated by diffusion, which is largely dependent upon the concentration gradient between the waste matrix and the water.

2.3.1.3 Flow Assumptions

Water heavily affects the waste form degradation rate and is treated differently in various models. Some “flow through” models assume water moves through the waste packages at a constant volumetric rate. Ahn [5], for example models the water flow beginning at one waste package and travelling through the matrix and buffer space to the next waste package, contacting each waste package consecutively and then flowing on into the near

field. In this way, the water is increasingly contaminated as its path through the waste packages proceeds. Others adopt assumptions incorporating climate-based predictions of hydrologic activity [5].

2.3.2 Waste Package Failure Models

Waste package failure modes vary between models. Many analytic models of canister failure incorporate their own hydrologic approximations of canister degradation or make simpler assumptions of immediate waste canister failure in order to focus on degradation and radionuclide release.

Waste package failure depends on near field environmental factors such as decay heat and water chemistry. The radionuclide release rate from a waste package depends on the character of the waste form matrix and water flow as well as elemental solubility, sorption, and diffusion.

Waste package failure can, in general, be represented with an expression of the number of failed waste packages failing per unit time, n_F . This is a simple product between the initial number of waste packages, N , and the rate, f , of failure

$$n_F = N \cdot f(). \quad (2.6)$$

Some current common models addressed in this literature review appear in Table 2.3.2.

2.3.2.1 Physical Model

When enough data exists, the waste package failure rate f can be represented more realistically by fractional destruction according to experimentally observed corrosion and

Current Waste Package Failure Models

Model	WP Failure Mode	Waste Form	Details
TSPA	EBSFAIL		300,000 years
Ahn 2003	Instantaneous Failure	Borosilicate Glass	$t = 0$
Ahn 2007		CSNF UO_2 matrix Borosilicate Glass Naval UO_2 matrix	$T_f = 75,000$ years $T_f = 75,000$ years $T_f = 75,000$ years
Li	EBSFAIL		300,000 years
Hedin 2003	Instantaneous	Copper KBS-3 Concept	$t_{delay} = 300$ years

Table 2.6: The above represent some current methods by which waste package failure rates are modeled.

dissolution rate functions. However, this can be complicated to model even if the data exists. In particular, the corrosion rate will depend on the chosen material as well as hydrologic and thermal conditions. Specifically, corrosion rates for the same material are very different under dry oxidizing conditions and wet reducing conditions.

The rate f of package failure in this case will be a function of time t , temperature T , and other physical parameters.

$$f() = N \cdot f(t, T, \dots). \quad (2.7)$$

2.3.2.2 Degradation Rate Based

Rather than a discrete model, in which barriers fail completely at a collective rate, a fractional degradation rate per barrier can be used. For this type of model, the intact volume decreases at a fractional rate,

$$V_i(t) = V_i(0) \left(1 - \int_0^t f(\dots) dt \right) \quad (2.8)$$

which, for a constant rate, becomes

$$V_i(t) = V_i(0)(1 - t). \quad (2.9)$$

2.3.2.3 Probabilistic

When a probability distribution of waste package failure is available, perhaps from extrapolated empirical observations, the discrete waste packages can be modeled to fail according to that distribution. For example, if the expected lifetime of a waste package is some known t_F , a Gaussian distribution around t_F would provide a probability density function for waste package failures per time step, $f(t)$,

$$f() = f(t). \quad (2.10)$$

Expressed with a cumulative distribution function $F(t)$ rather than the probability distribution function, equation (2.7) becomes

$$\sum_{t=0}^{t=t} n_F(t) = N \cdot F(t). \quad (2.11)$$

A particularly appropriate probability distribution for use in the case of failed engineered barriers is the Weibull distribution, which has a flexible shape capable of modeling a range of failure rates and can provide reasonably accurate predictions of failure based on small empirical data sets [67]. The Weibull distribution is expressed as

$$f(t, \lambda, k) = \begin{cases} \frac{k}{\lambda} \left(\frac{t}{\lambda}\right)^{k-1} e^{-(t/\lambda)^k} & t \geq 0, \\ 0 & t < 0. \end{cases} \quad (2.12)$$

In this expression, k is a shape parameter and λ is a scale parameter. The time to failure, t , in the Weibull distribution gives a distribution for which the failure rate is proportional to a power of time [76]. Its complementary cumulative distribution function is

$$F(t, \lambda, k) = 1 - e^{-(t/\lambda)^k}. \quad (2.13)$$

For $k < 1$, the rate of failure will decrease over time, while for a value of $k > 1$, the rate increases over time, appropriate for the aging process of materials [76].

2.3.2.4 Instantaneous

The instantaneous case is a special case of the probabilistic situation. Specifically, the probability density function is clearly just the Dirac delta function, with n_F being the number of failed waste packages per unit time, N being the total number of waste packages, and t_F being the time to failure,

$$f() = \delta(t - t_F). \quad (2.14)$$

The Hedin model of waste package failure is effectively instantaneous, but limited by a release resistance coefficient [41]. The release is assumed to occur through a hole in the

waste canister that exists throughout the simulation, and the resistance coefficient limiting flow through the hole represents the magnitude of the canister flaw in combination with the buffer-geosphere interface [41]. A special case of this is instantaneous waste package failure, in which all waste packages simultaneously such that failure occurs either at the onset of the simulation or at some distinct time during the simulation.

2.3.3 Radionuclide Transport Through Secondary Engineered Barriers

When the waste package is breached and radionuclides are released from the waste form, radionuclides are transported through the secondary engineered barrier, which includes the buffer, backfill, and tunnel wall. After transport through the secondary EBS, radionuclides reach the geologic medium.

Diffusive and advective transport occur in the barrier matrix both before and after degradation. The same models of waste package failure (instantaneous, rate based, and probabilistic) can be applied to secondary engineered barriers (i.e., buffer materials). While concretes are expected to degrade over time, bentonite buffers are quite stable in a reducing environment and help to keep the environment reducing. Furthermore, if preserved by a low heat environment, plastically deforming bentonite clays tend to swell over time and exhibit increased isolating behavior.

Before degradation, transport is primarily diffusive. Thereafter, transport can become advective due to cracking. Radionuclide transport through the EBS and host rock is driven by diffusion as well as advection. Radionuclide transport is retarded by sorption, limited by solubility, and possibly enhanced by colloidal mobility [17].

2.3.4 Hydrologic Transport

Transport through the geosphere in clay, shale, granite, and salt can largely be characterized as solute transport in permeable porous media. While clay, shale and salt do not exhibit significant fracturing and can often be modeled as homogeneous, granite is characterized as a fractured permeable porous media. Solute transport in both fractured and homogeneous permeable porous media has both porous and fracture flow paths and involves advection, hydraulic dispersion, and diffusion phenomena.

Advection is transport driven by bulk water velocity, diffusion is the result of Brownian motion across concentration gradients, and hydraulic dispersion is transport resulting from heterogeneities in the water velocity field. Fundamentally, the effect of these flows on mass transport through a representative control volume is captured by the conceptual expression

$$\text{In} - \text{Out} = \text{Change in Storage} \quad (2.15)$$

Rearranging 2.15 and defining incoming and outflowing fluxes in a control volume, solute transport in a permeable medium of homogeneous porosity can be written (as in Schwartz and Zhang [86])

$$\theta \frac{\partial C}{\partial t} = -\nabla \cdot (F_c + F_{dc} + F_d) + m \quad (2.16)$$

where

$$\theta = \text{solute accessible porosity } [\%]$$

$$C = \text{concentration } [kg \cdot m^{-3}]$$

$$t = \text{time } [s]$$

$$\begin{aligned} F_c &= \text{advective flow } [kg \cdot m^{-2} \cdot s^{-1}] \\ &= \theta v C \end{aligned}$$

$$\begin{aligned} F_{dc} &= \text{dispersive flow } [kg \cdot m^{-2} \cdot s^{-1}] \\ &= \alpha \theta v \nabla C \end{aligned}$$

$$\begin{aligned} F_d &= \text{diffusive flow } [kg \cdot m^{-2} \cdot s^{-1}] \\ &= \theta D_e \nabla C \end{aligned}$$

$$m = \text{solute source } [kg \cdot m^{-3} \cdot s^{-1}].$$

In the expressions above,

$$v = \text{advective velocity } [m \cdot s^{-1}]$$

$$\alpha = \text{dispersivity } [m]$$

$$D_e = \text{effective diffusion coefficient } [m^2 \cdot s^{-1}]$$

and

$$\theta \cdot v = \text{Darcy flux } [m \cdot s^{-1}]. \tag{2.17}$$

The method by which the dominant solute transport regime (diffusive or advective) is determined for a particular porous medium is by use of the dimensionless Peclet number,

$$\begin{aligned}
Pe &= \frac{\theta v L}{\alpha \theta v + D_e}, \\
&= \frac{\text{advective rate}}{\text{diffusive rate}}
\end{aligned}
\tag{2.18}$$

where

$$L = \text{transport distance [m]}.$$

For a high Pe number, advection is the dominant transport regime, while diffusive or dispersive transport dominates for a low Pe number. If one of these terms can be neglected, the solution is simplified.

Otherwise, the analytical expression in equation (2.16) was the foundation of simplification by regression analyses for the radionuclide transport interface between components of the repository system model representing permeable porous media.

It is customary to define the combination of molecular diffusion and mechanical mixing as the dispersion tensor, D ,

$$D = \alpha v + D_e \tag{2.19}$$

such that the mass conservation equation becomes:

$$\nabla(\theta D \nabla C) - \nabla(\theta v) = \frac{\partial(\theta C)}{\partial t} \tag{2.20}$$

Sorption includes both absorption and adsorption. Absorption is the incorporation of a substance of one state into another of a different state. Adsorption is the interaction of a dissolved species with a surface that removes that species from the dissolving medium models. During sorption, contaminants are removed from the water and taken up by the walls of pores or fractures in the rock matrix. The process that is the reverse of sorption is desorption in which the contaminant is returned to the pore or fracture fluid from the matrix [3] . Reversible sorption is typically expressed in terms the mass of a radionuclide sorbed into the rock and the mass left in solution. Sorption is a sensitive function of the redox state of the environment. Adding sorption to equation (2.20), by accounting for a change in mass storage,

$$\nabla (\theta D \nabla C) - \nabla (\theta v) = \frac{\partial(\theta C)}{\partial t} + \frac{\partial(s \rho_b)}{\partial t} \quad (2.21)$$

where

s = solid concentration [kg/kg]

ρ_b = bulk (dry) density [kg/m^3].

If sorption is approximated as a linear equilibrium, reversible reaction,

$$s = K_d C \quad (2.22)$$

where

$$K_d = \text{the distribution coefficient } [m^3/kh],$$

then equation (2.21) can be rewritten in terms of the so-called retardation factor,

$$\nabla (\theta D \nabla C) - \nabla (\theta v) = R_f \frac{\partial \theta C}{\partial t} \quad (2.23)$$

where

$$\begin{aligned} R_f &= \text{retardation factor} \\ &= 1 + \frac{\rho_b K_d}{\theta}. \end{aligned} \quad (2.24)$$

Finally, a phenomenon called colloidal mobility can enhance radionuclide transport in some geologic media. Mineral colloids, which are suspended molecular solids within a liquid emulsion, are expected in the solution saturating the geologic environment. Colloids present in the near field dissolving solution have an effect on the mobility of radionuclides. Studies addressing the subtle differences between resultant behavior of various isotopes indicate that colloidal mobility can be modeled as a correction factor to the sorption coefficient [17].

For uniform flow, the dispersion tensor, D , becomes

$$\begin{aligned}
D_x &= D_L \\
&= \alpha_L v_x + \tau D_e
\end{aligned} \tag{2.25}$$

$$\begin{aligned}
D_y &= D_{TH} \\
&= \alpha_H v_x + \tau D_e
\end{aligned} \tag{2.26}$$

$$\begin{aligned}
D_z &= D_V \\
&= \alpha_V v_x + \tau D_e
\end{aligned} \tag{2.27}$$

where

D_e = effective diffusion coefficient [m^2/s]

α_L = longitudinal dispersivity [m]

α_H = horizontal dispersivity [m]

α_V = vertical dispersivity [m]

and

$$\tau = \text{tortuosity.} \tag{2.28}$$

For unidirectional flow, the unidirectional dispersion tensor gives

$$D_x \frac{\partial^2 C}{\partial x^2} + D_y \frac{\partial^2 C}{\partial y^2} + D_z \frac{\partial^2 C}{\partial z^2} + v_x \frac{\partial C}{\partial x} = R_f \frac{\partial(\theta C)}{\partial t}. \tag{2.29}$$

In the case of no flow, equation (4.2) simplifies to the diffusion equation,

$$D_x \frac{\partial^2 C}{\partial x^2} + D_y \frac{\partial^2 C}{\partial y^2} + D_z \frac{\partial^2 C}{\partial z^2} = R_f \frac{\partial(\theta C)}{\partial t}. \quad (2.30)$$

Solutions to these equations can be categorized by their boundary conditions. The first, or Dirichlet type boundary conditions define a specified species concentration on some section of the boundary of the representative volume,

$$C(\vec{r}, t) = C_0(\vec{r}, t) \text{ for } \vec{r} \in \Gamma. \quad (2.31)$$

The second type or Neumann type boundary conditions describe a full set of diffusive fluxes at the boundary of the domain

$$D \frac{\partial C(\vec{r}, t)}{\partial r} = \theta \vec{J} \text{ for } \vec{r} \in \Gamma. \quad (2.32)$$

where

\vec{r} = position vector

Γ = domain boundary

\vec{J} = solute mass flux [$kg/m^2 \cdot s$].

The third, Cauchy, type defines a linear combination of the concentration gradient and a concentration at that boundary,

$$-D \frac{\partial C(\vec{r}, t)}{\partial r} \Big|_{r \in \Gamma} + v_z C_j \Big|_{r \in \Gamma} = \text{a known value [kg/m}^2\text{s]} \quad (2.33)$$

2.4 Analytical Models of Heat Transport

A repository performance simulator appropriate for dynamic systems analysis must arrive at an appropriate notion of heat-based waste loading and repository capacity. This requires a model which addresses heat transport through the repository as a function of spatial repository layout, waste stream decay heat, and heat transfer properties of the engineered barrier system and host rock. This model must sufficiently solve for peak temperatures at locations where thermal constraints are considered, which are in most cases at the waste package interface with the buffer material and the buffer material interface with the host rock. These heat limits were discussed in Section 2.2.1.4.

Heat transfer in these concepts will be dominated by conductive heat transfer. In a saturated closed system, very few air gaps will exist such that heat transfer by radiation is likely to be negligible. Similarly, since water velocities are comparatively low, heat transfer by mass transfer or by convection will be small relative to conduction.

A discussion of conductive heat transport follows.

2.4.1 Conduction

Conductive heat transfer occurs as a result of a temperature gradient. Heat flows diffusively from the hotter material to the cooler material over time and steadily approaches thermal equilibrium. The general form of the conduction equation can be expressed

$$\nabla^2 T + \frac{q'''}{k} = \frac{1}{\alpha} \frac{\partial T}{\partial t}, \quad (2.34)$$

which with no heat source becomes the transient Fourier equation,

$$\nabla^2 T = \frac{1}{\alpha_{th}} \frac{\partial T}{\partial t}, \quad (2.35)$$

or which becomes the Laplace equation in steady state,

$$\nabla^2 T = 0. \quad (2.36)$$

At steady state, the conduction equation becomes the Poisson equation,

$$\nabla^2 T + \frac{q'''}{k} = 0. \quad (2.37)$$

An areal heat flux, $q''[W/m^2]$ can be derived from an integration of Poisson's equation (2.37) and expressed in terms of the thermal conductivity of the material, $k[W \cdot m^{-1} \cdot K^{-1}]$, and the temperature gradient $\nabla T[K/m]$ by the expression

$$q'' = -k\nabla T. \quad (2.38)$$

For the one dimensional case, equation 2.38 can be approximated using a finite difference method. For a body at x_1 with temperature T_1 and a body with temperature T_2 at position x_2 ,

$$q_x'' = -k_x \frac{dT}{dx} \quad (2.39)$$

$$= -k_x \frac{(T_1 - T_2)}{x_1 - x_2}. \quad (2.40)$$

2.4.2 Lumped Parameter Model

The lumped heat capacitance model reduces a thermal system into discrete lumps for an approximate solution of transient heat transfer. Such an approximation is appropriate when it can be assumed that the temperature gradient within each lump is approximately uniform. The appropriateness of this approximation can be quantitatively expressed by comparison of the Biot number,

$$Bi = \frac{hL}{k}. \quad (2.41)$$

The Biot number indicates the relative speeds with which heat conducts within an object and across the boundary of that object. If the Biot number is low (< 0.1), and therefore conduction is faster within the object than at the boundary, the assumption of a uniform internal temperature is appropriate and the lumped parameter model may be expected to give a result within 5% error [51]. This assists in choosing the size of distinct lumps within a conceptual model.

The lumped capacitance model can address multiple media and multiple heat transfer modes. The rate of heat transfer \dot{q} [$Wm^{-2}K^{-1}s^{-1}$] through a circuit is simply given as the quotient of the temperature difference and the sum of thermal resistances, R_i [$W \cdot K^{-1}$], of the multiple lumps

$$\dot{q} = \frac{\Delta T}{\sum_{i=0}^N R_i}. \quad (2.42)$$

By representing the various modes of heat transport (i.e. conduction, convection, radiation, and mass transfer) with various expressions for resistance, the lumped capacitance model provides a solution to the transient problem described by the energy balance,

$$\begin{aligned} (\text{Energy added to body } j \text{ in } dt) &= (\text{Heat out of adjacent bodies into body } j) \\ c_j \rho_j V_j dT_j(t) &= \sum_{i=0}^{i=N} [q_{i,j}] dt, \end{aligned} \quad (2.43)$$

where $c_j \rho_j V_j$ is the total lumped thermal capacitance of the body.

For example, in the case of a simple convective circuit between two bodies, i and j , the resistance of j can be described as

$$R_{conv} = 1/hA \quad (2.44)$$

such that

$$c_j \rho_j V_j dT_j(t) = \sum_{i=0}^{i=N} [hA_j (T_i - T_j(t))] dt. \quad (2.45)$$

$$(2.46)$$

A time constant appears under integration that describes the speed with which the body j changes temperature with respect to the maximum temperature change,

$$\int_{T_j=T_0}^{T_j(t)} \frac{dT_j(t)}{T_i - T_j} = \frac{hA_j}{c_j\rho_jV_j} \int_0^t dt \quad (2.47)$$

$$-\ln \frac{T_i - T_j(t)}{T_i - T_0} = \frac{hA_j}{c_j\rho_jV_j} t \quad (2.48)$$

$$\frac{T_i - T_j(t)}{T_i - T_0} = e^{-(hA_j/c_j\rho_jV_j)t} \quad (2.49)$$

such that

$$\frac{T_j(t) - T_i}{T_i - T_0} = 1 - e^{-t/\tau} \quad (2.50)$$

where

$$\tau = (c_j\rho_jV_j/hA_j). \quad (2.51)$$

The time constant, τ is the time it takes for the body to change $(1 - (1/e))\% \Delta T$ and is equal to the product of the thermal capacitance and thermal resistance between the body and its surroundings, CR , analogous to an electrical circuit [31].

This is the case for all resistances, R_i representing modes of heat transfer. Thus, one can say, in general

$$\tau_j = c_j\rho_jV_jR_j. \quad (2.52)$$

2.4.3 Specific Temperature Integral

Linear mass loading (*tonnes/m*), linear thermal loading (W/m) and areal power density (W/m^2) are common metrics for describing the loading of the repository. While these metrics are informative for mass capacity and power capacity respectively, they fail to reflect differences in thermal behavior due to varying SNF compositions. A closer look at the isotopics of the situation has proven much more applicable to thermal performance studies of the repository, and the preferred method in the current literature relies on specific temperature integrals.

Specific temperature integrals model the thermal source as linear along the emplacement paths, similar to the line loading and areal power density metrics. However, a temperature integral takes account of heat transfer behavior in the rock, includes the effects of myriad SNF compositions, and gives the thermal integration over time for any specific location within the rock. Man-Sung Yim calls this the Specific Temperature Increase method [64] though other researchers have other names for this method. Tracy Radel calls her temperature metric at a point in the rock the Specific Temperature Change [81].

In a repository with linear drifts, the heat flux from the drifts can be expressed as the superposition of the linear heat flux contributions of all the radionuclides in the waste. The temperature change, more importantly can be expressed as a superposition of the temperature change contributions due to each radionuclide. Each radionuclide contributes in proportion to its decay heat generation and its weight fraction of the SNF. With information about isotopic composition of the SNF, the Specific Temperature Increase can determine the maximum thermal capacity of the repository in terms of tonnes/m. The length based accounting in $\frac{t}{m}$ is converted to $\frac{t}{Repository}$ by multiplication with the total emplacement tunnel length of the repository.

2.5 Computational Models of Radionuclide

Transport

Computational models of radionuclide transport seek to quantify the spatial and temporal movement of radionuclides within a repository. Many such models are detailed with respect to their fine spatial and temporal resolution or with respect to the incorporation and coupling of numerous physical phenomena. Current computational models addressing various geologic media and emplacement geometries will be reviewed here that utilize finite difference and finite element methods in many dimensions, sophisticated numerical solvers, and other high fidelity approaches.

A number of efforts to model radionuclide transport through geologic repository concepts have been made internationally and domestically. These efforts, the geologic media they address, and some features of their methods will be discussed here and appear in Table 2.7.

2.5.1 European RED-IMPACT

The RED-IMPACT assessment compared results from European fuel cycle codes for various specific waste packages, forms, radioactive and radiotoxic inventories, reprocessing discharges, waste package thermal power, corrosion of matrices, transport mechanisms, and resulting doses. Granite, clay and salt were analyzed by various countries. The studied concepts are listed in table 2.8.

2.5.2 UFD Generic Disposal System Models

The UFD campaign has produced a suite of tools for analysis of various geologic disposal environments. Teams from Argonne National Laboratory, Lawrence Berkeley National

Radionuclide Transport Models for Various Geologic Media

Source (Who)	Nation (Where)	Medium (What)	Methodology (How)
Enresa [61]	Spain	Granite	GoldSim Proprietary Framework ^{129}I primary contributor
SCK-CEN [61]	Belgium	Clay	Features, events, processes ^{129}I primary contributor
GRS [61]	Germany	Salt	Systematic Performance Assessment ^{135}Cs , ^{129}I , ^{226}Ra , ^{229}Th
NCSU(Nicholson) [63]	USA	Yucca Tuff	TSPA codes EBSREL and EBS-FAIL
NAGRA [54, 55]	Switzerland	Opalinus Clay	TAME code
ANDRA [8]	France	Argillite	Very detailed CEA code Mostly homogeneous medium ^{129}I primary contributor
ANDRA [9]	France	Granite	Very detailed CEA code Involves fractured medium ^{129}I primary contributor
SKB [1]	Sweden	Forsmark Laxemar	HYDRASTAR solute transport FracMan for fractures

Table 2.7: Computational methods by which to evaluate source term dependence of waste package failure, transport through the EBS and hydrogeologic transport. The latter two parts vary significantly among host formations.

International Repository Concepts

Medium	Nation	Waste Stream	Metric	Institution
Granite	Spain	HLW	Heat Load	Enresa
Granite	Czech Rep.	HLW	Heat Load	NRI
Clay	Belgium	HLW	Heat Load	SCK-CEN
Salt	Germany	HLW	Heat Load	GRS
Granite	Spain	HLW	Dose	Enresa
Clay	Belgium	HLW	Dose	SCK-CEN
Clay	France	HLW	Dose	CEA
Salt	Germany	HLW	Dose	GRS
Granite	Czech Rep.	ILW	LT Dose	NRI
Granite	Spain	ILW	LT Dose	Enresa
Clay	Belgium	ILW	LT Dose	SCK-CEN
Granite	Spain	HLW/ILW/Iodine	LT Dose	Enresa
Clay	Belgium	HLW/ILW/Iodine	LT Dose	SCK-CEN

Table 2.8: International repository concepts evaluated in the RED Impact Assessment.[61]

Laboratory, Los Alamos National Laboratory, and Sandia National Laboratory have developed models of generic clay, granite, and salt disposal environments respectively.

Sandia is simultaneously constructing a deep borehole disposal system model in crystalline rock. Each generic disposal system model performs detailed calculations of radionuclide transport within its respective geologic medium [24].

The radionuclide transport calculations for the geologically distinct models are performed within the GoldSim simulation platform. GoldSim is a commercial simulation environment [33, 34]. Probabilistic elements of the GoldSim modeling framework enable the models to incorporate Features, Events, and Processes (FEPs) expected to take place probabilistically during the evolution of the repository [24].

Cells within GoldSim represent components of the waste disposal system and are linked by diffusive, advective, precipitated, direct, or otherwise filtered mass transfer links and pipes.

2.5.2.1 Clay/Shale GDSM

The Clay GDSM is being pursued by the team at Argonne National Laboratory (ANL) and was the primary model with which this work conducted parametric regression analyses.

The Clay GDSM models a single waste form, waste package, EBS, Excavation Disturbed Zone (EDZ), and far field zone. This waste unit cell is modeled with boundary conditions such that it may be repeated throughout the extent of a repository configuration.

The waste form and engineered barrier system are modeled as well-mixed volumes and radial transport away from the cylindrical base case unit cell is modeled as one dimensional.

Two radionuclide release pathways are considered. One is the nominal, undisturbed case, while the other is a fast pathway simulating a disturbed case [24].

2.5.2.2 Granite GDSM

Los Alamos National Laboratory (LANL) has created a model of the granite repository concept in a saturated, reducing environment. Waste form degradation is modeled as a constant, fractional rate to represent dissolution for both canonical borosilicate glass and commercial used fuel waste forms. Though waste package failure is assumed to be instantaneous, waste package release into the near field is solubility limited as is the near field to far field interface. Transport through the buffer is modeled as entirely diffusive coupled with sorption. Advection is neglected. The far field was represented using a model that includes advection, diffusion and sorption. Specifically, the Finite Element Heat and Mass Transfer (FEHM) code was coupled into GoldSim to represent the far field.

2.5.2.3 Salt GDSM

The salt repository concept has an alcove gallery geometry and is located in a bedded salt formation. The formation is located in a reducing, saturated environment. Once waste packages are horizontally placed in a corner of the alcove, the space is backfilled with crushed salt.

Decay heat induced salt consolidation and brine flow are primary focuses of this analysis and inform radionuclide transport calculations. A constant, temperature independent annual degradation rate model is used to represent waste form dissolution for both canonical borosilicate glass and commercial used fuel waste forms.

Waste package failure is conservatively assumed to be instantaneous, and all near field components are modeled as a single mixed cell, the water volume of which is determined by the bulk volumes and degraded porosities of contained materials (e.g. crushed salt). A block of rock below the salt provides the pathway interface to an aquifer below. Radionuclide transport into that interface is modeled as diffusive, advective, and solubility limited.

The far field is modeled using an equilibrium sorption model in addition to solubility limited diffusion and advection. In such an equilibrium sorption model, the sorption to precipitation balance is assumed to be at a reaction equilibrium. In this way, the partitioning coefficient K_d is used to quantify the ratio between dissolved and undissolved reactant. Radionuclide transport in the far field takes place for 5km, and ends in a biosphere model.

Two radionuclide release pathways are considered. One is the nominal, undisturbed case, which the other is a fast pathway simulating a disturbed case [24].

2.5.2.4 Deep Borehole GDSM

The deep borehole model concept consists of some 400 waste canisters in a 5km deep hole within a low permeability, high salinity region characteristic of crystalline rock formations at depth. The lower 2km of the hole are filled by waste packages as well as spacing and sealing plugs. A 1km sealing zone extends above the waste disposal region.

As with the salt model, a constant, temperature independent annual degradation rate model is used to represent waste form dissolution for both canonical borosilicate glass and commercial used fuel waste forms. Waste package failure is conservatively assumed to be instantaneous.

Flow in the vicinity of the borehole was modeled using tabulated groundwater flow velocities obtained from simulations run using the FEHM code meshed in three full dimensions with the CUBIT Geometry and Mesh Generation Toolkit (CUBIT) meshing tool [24].

2.5.3 Li Model [63]

In a case study evaluating transmutation effects on repository benefit, Jun Li approximated Yucca Mountain Repository performance for three fuel cycles. As a function of time, water enters the Engineered Barrier System and corrodes the waste packages. These fail and from the failed waste packages radionuclides are released according to advective transfer. Further transport through the near and far field rock medium is modeled in two modes, one representing the unsaturated zone, and one representing the saturated zone.

Waste package failure and radionuclide release are modeled with two Total System Performance Assessment for the Yucca Mountain License Application (TSPA) code modules called EBSFAIL and EBSREL. The waste package failure rate is determined from EBSFAIL, which incorporates waste form chemistry, humidity, oxidation, etc and upon contact from water begins the degradation process. The results of EBSFAIL become the input to EBSREL, which models corresponding radionuclide release from those failed waste packages. Mass balance governing the radionuclide release rate in this model allows advective transfer to dominate and takes the form:

$$\dot{m}_i = w_{li}(t) - w_{ci}t - m_i\lambda_i + m_{i-1}\lambda_{i-1}.$$

In this expression, $w_{li}(t)$ is the rate [mol/yr] of isotope i leached into the water. It is a function of water flow rate, chemistry, and isotope solubility. m_i describes the mass of isotope i , and λ_i [s^{-1}] describes its decay constant. Finally, $w_{ci}(t)$ describes the advective transfer rate [mol/yr] of the isotope i . This model defines w_{ci} as:

$$w_{ci}(t) = C_i(t)q_{out}(t). \quad (2.53)$$

where q_{out} is the volumetric flow rate of the water [m^3/yr], and C_i is the concentration

on isotope i in the waste package volume m_i/V_{wp} in $[mol/m^3]$. These assumptions fail to take into account any differences in the varying solubilities of the isotopes, but are quite sensitive to the concentration of an isotope i in the waste package volume.

2.5.4 ANDRA Dossier 2005

The ANDRA Dossier 2005 studies, developed for the French radioactive waste disposal program, provided detailed radionuclide transport calculations for both argillite, a clay-rich rock, and granite formations.

In particular, in the ANDRA clay model, complicated saturation and resaturation phenomena are neglected and it is assumed that the initial repository condition is fully resaturated. Additionally, it conservatively assumes that the excavation disturbed zone does not heal. Rather, it is modeled in its damaged state immediately after excavation and forever thereafter.

This model only tracks 15 radionuclides of importance. These are chosen to be those with half lives over 1000 years and most toxicity or mobility [8]. The behavior of radionuclides in glass vitrification forms are categorized into mobile, intermediate, and well retained elements.

Some specific codes and the method with which they were used in the ANDRA clay assessment are listed in Table 2.9.

Waste form dissolution and package release was assumed to be immediate for some waste forms and corrosion rate based for those where appropriate data were available. Vitrified waste package releases were either modeled with a simple model or a two phase model. In the first phase dissolution is treated by a rate model until silica saturation in the surrounding environment. In the second phase, dissolution kinetics decreases to a residual rate.

Detailed Nuclide Transport Models Used in the ANDRA analysis.

Models	Codes
Groundwater flow and particle tracking in continuous porous media	Connectflow (3D finite element) Geoan (3D finite differences). Porflow (3D finite differences).
Groundwater flow and particle tracking in discrete fracture networks.	Connectflow (3D finite elements). FracMan (discrete fracture networks) and MAFIC (3D finite elements).
Transport in continuous porous media.	PROPER (finite differences), Goldsim (control volumes), and Porflow (control volumes?).
Transport in discrete fracture networks.	PROPER (1D stream tube concept). PathPipe (networks of tubes) and Goldsim (networks of 1D pipes).

Table 2.9: Similar to the Total System Performance Assessment, ANDRA’s analyses are a coupled mass of many codes. Table reproduced from Argile Dossier 2005 [8]

Transport through the backfill is modeled as diffusive, with high permeability after degradation. The excavation disturbed zone has both a fracture zone and a microfissure zone. In the host formation, movement is dominated by diffusion, and advection is modeled, but is negligible.

2.6 Detailed Computational Models of Heat Transport

Detailed heat transport models seek to quantify the heat evolution within a repository environment due to heat generating waste forms. Such models are detailed with respect to their spatial and temporal resolution or with respect to the incorporation and coupling of numerous physical phenomena. Such codes typically utilize finite difference or finite element methods in many dimensions or sophisticated numerical solvers, respectively.

S]

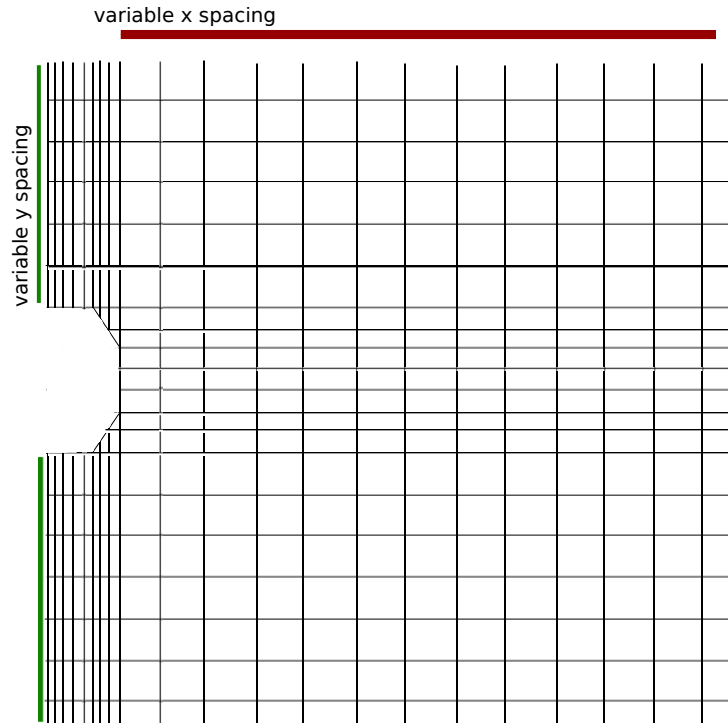


Figure 2.1: The geometry of the SINDA\G thermal model can be adjusted in two dimensions, altering the tunnel spacing and the vertical distance from the aquifer.

2.6.1 ANL SINDA\G Model

This model, created at ANL uses the Systems Improved Numerical Differencing Analyzer \ Gaski (SINDA\G) lumped capacitance solver [32]. This model was originally created to evaluate the effects of advanced separations efficiencies on the thermal performance of the YMR. It is geometrically adjustable in two dimensions, as is demonstrated in Figure 2.1. The tunnel size is a fixed parameter in the model, but the optimal drift spacing for a particular waste stream and package loading is solved for with an optimization loop within this model.

The SINDA\G lumped capacitance solver solves a thermal circuit, for which connecting

nodes may be of four types corresponding to the four modes of heat transfer. Nodes, treated as resistors, are connected by conduction, convection, radiation, and mass flow heat transfer links. As discussed in Section 2.4.2, these are represented by

$$R_{cond} = \frac{L}{K_{th}A} \quad (2.54)$$

$$R_{conv} = \frac{1}{hA} \quad (2.55)$$

$$R_{mf} = \frac{1}{\dot{m}c_p} \quad (2.56)$$

$$R_{rad} = \frac{1}{\sigma F_{ij}A [T_i + T_A + T_j + T_A] [(T_i + T_A)^2 + (T_j + T_A)^2]} \quad (2.57)$$

where

$$K_{th} = \text{thermal conductivity}[W \cdot m^{-1} \cdot K^{-1}]$$

$$A = \text{area}[m^2]$$

$$c_p = \text{specific heat capacity}[J \cdot K^{-1}]$$

$$h = \text{heat transfer coefficient}[W \cdot m^{-1} \cdot K^{-1}]$$

$$\dot{m} = \text{mass transfer rate}[kg \cdot s^{-1}]$$

$$T_i = \text{lump temperature}[^{\circ}C]$$

$$T_A = \text{absolute temperature}[^{\circ}C]$$

$$F_{ij} = \text{radiation interchange factor}[-].$$

With these representations of thermal resistance, a lumped parameter model required an analysis that determines the appropriate length scale for the lumped parameter approximation.

Given one or more heat constraints, the ANL model optimizes spatial waste loading in order to meet those constraints with maximal waste loading. For example, given a thermal limit at the edge of the waste package, the model utilizes the SINDA\G solver to determine the two dimensional heat evolution of the repository as a result of a given waste package composition for various drift spacings and arrives at an ideal drift spacing by iteration.

2.6.2 LLNL MathCAD Model

A semi-analytic model, created at Lawrence Livermore National Laboratory (LLNL) for the UFD campaign seeks to inform heat limited waste capacity calculations for a range of potential host media and for many waste package loading densities, and for many fuel cycle options [35, 36, 40]. It employs an analytic model from Carslaw and Jaeger [21] and is implemented in MathCAD [79]. The integral solver in the MathCAD toolset is the primary calculation engine for the semi-analytic MathCAD thermal model, which relies on superposition of integral solutions.

The model consists of two conceptual regions, an external region representing the host rock and an internal region representing the waste form, package, and EBS within the excavated disposal tunnel radius. The first region is taken to be a transient calculation unit. Since the thermal mass of the EBS is small in comparison to the thermal mass of the host rock, the internal region is treated as quasi-steady state. The transient state of the temperature at the calculation radius is found with a convolution of the transient external solution with the steady state internal solution. The process is then iterated with a one year resolution in order to arrive at a temperature evolution over the lifetime of the repository.

Figure 2.2 shows the geometric layout of the semi-analytic LLNL model in which the

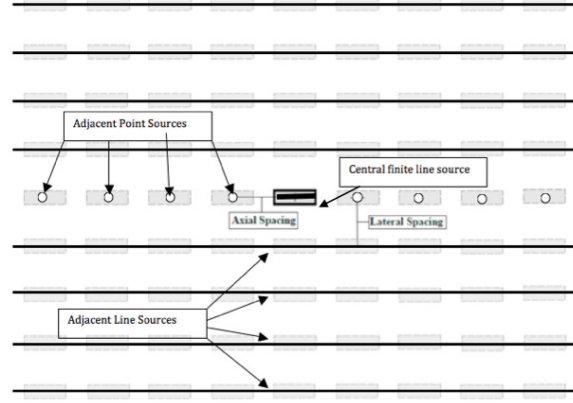


Figure 2.2: The central package is represented by a finite line source, adjacent packages in the central drift are represented as points, and adjacent disposal tunnels are represented as infinite lines. [36].

central package is represented by the finite line solution

$$T_{line}(t, x, y, z) = \frac{1}{8\pi K_{th}} \int_0^t \frac{q_L(t')}{t-t'} e^{\frac{-(x^2+z^2)}{4\alpha_{th}(t-t')}} \cdot \left[\operatorname{erf} \left[\frac{1}{2} \frac{\left(y + \frac{L}{2}\right)}{\sqrt{\alpha_{th}(t-t')}} \right] - \operatorname{erf} \left[\frac{1}{2} \frac{\left(y - \frac{L}{2}\right)}{\sqrt{\alpha_{th}(t-t')}} \right] \right] dt', \quad (2.58)$$

adjacent packages within the central tunnel are represented by the point source solution

$$T_{point}(t, r) = \frac{1}{8K_{th}\sqrt{\alpha_{th}\pi^{\frac{3}{2}}}} \int_0^{-t} \frac{q(t')}{(t-t')^{\frac{3}{2}}} e^{\frac{-r^2}{4\alpha_{th}(t-t')}} dt', \quad (2.59)$$

and adjacent disposal tunnels are represented by infinite line source solutions

$$T_{\infty line}(t, x, z) = \frac{1}{4\pi K_{th}} \int_0^t \frac{q_L(t')}{t-t'} e^{\frac{-(x^2+z^2)}{4\alpha_{th}(t-t')}} dt' \quad (2.60)$$

in infinite homogeneous media, where

$$\alpha_{th} = \text{thermal diffusivity } [m^2 \cdot s^{-1}]$$

$$q(t) = \text{point heat source}[W]$$

and

$$q_L(t) = \text{linear heat source}[W \cdot m^{-1}]$$

Superimposed point and line source solutions flexibly accommodate various repository layouts.

2.6.3 Yucca Mountain Layout Analyses

The repository layout has a significant influence on its heat transfer properties. Waste package spacing in drifts, boreholes, or alcoves, tunnel spacing, and multiple gallery level designs all define available heat loading. For example, in the YMR, a variety of parameters have been shown to affect the potential repository waste loading density.

The YMR statutory limit of once-through, thermal PWR waste was 70,000 Metric Tons of Heavy Metal (MTHM) of waste. That is to say, the statutory line load limit is approximately 1.04 tonnes/m for 67km of planned emplacement tunnels (with 81 meters between drifts). The Office of Civilian Radioactive Waste Management Science and Engineering Report gives this basic “statutory limit”, but suggests an inherent design flexibility that could allow for expansion. Multiple efforts have adjusted various repository layout parameters in order to develop expanded capacity models of the YMR. Some of

these efforts are detailed in Table 2.10.

Yucca Mountain Footprint Expansion Calculations

Author	Max. Capacity <i>tonnes</i>	Footprint <i>km²</i>	Details
OCRWM	70,000 97,000 119,000	4.65 6 7	“statutory case” “full inventory case” “additional case”
Yim, M.S.	75,187 76,493 95,970 82,110	4.6 4.6 4.6 4.6	SRTA code STI method 63m drift spacing 75 yrs. cooling
Nicholson, M.	103,600	4.6	drift spacing
EPRI	63,000 126,000 189,000 189,000 252,000 378,000 567,000	6.5 13 6.5 6.5 6.5 13 13	Base Case CSNF expanded footprint multi-level design grouped drifts hybrid hybrid hybrid

Table 2.10: Various analyses based on heat load limited repository designs have resulted in footprint expansion calculations of the YMR.

This inherent flexibility can come from an increase in the areal extent of the repository footprint, the density of drifts, or vertical expansion. The “full inventory” Yucca Mountain design alternative gives a maximum repository capacity of 97,000 tonnes. In addition, the current design for the repository has flexibility for “additional repository capacity” which would give a 119,000 tonne capacity at 1.04 tonnes/m. [26]

In addition to variable drift spacing, other modifications to repository layout have had promising results in terms of heat-limited repository capacity. The Electric Power Research Institute (EPRI) in their Room at the Mountain study found that with redesign of the repository an increased capacity of at least 400% (295 kilotonnes once-through SNF) and up to 900% (663 kilotonnes) could be expected to be achieved. Proposed design changes

include decreased spacing between drifts, a larger areal footprint, vertical expansion into second and third levels of repository space, and hybrid solutions involving combinations of these ideas. In particular, EPRI suggests either an expansion of the footprint with redesign of the current line load design plan or a multi-level plan that repeats the footprint and line load design of the current plan [57].

Layout options such as age based fuel mixing also allows for decreases in drift spacing. In aged based fuel mixing, aged (long cool time) SNF is loaded in a mixture with young SNF. This age based fuel mixing has been shown to achieve a 48% increase in the repository capacity as constrained by heat load [68]. This factor uses a fiducial default footprint of 4.6km^2 used in the NRC TSPA. The reported 48% increase in capacity results in total repository capacity of 103,600 tonnes [99].

2.6.4 Other Numerical Methods

Codes used by repository modeling efforts investigated in this review include finite difference codes, finite element codes, and specific temperature integrals. Some efforts and their methods are listed in Table 2.11.

Models of Heat Load for Various Geologic Media

Source (Who)	Nation (Where)	Medium (What)	Methodology (How)
Enresa [61]	Spain	Granite	CODE_BRIGHT 3D Finite Element
NRI [61]	Czech Rep.	Granite	Specific Temperature Integral
ANDRA [9]	France	Granite	3D Finite Element CGM code
SKB [1]	Sweden	metagranite	1D-3D Site Descriptive Models
SCK·CEN [61]	Belgium	Clay	Specific Temperature Integral
ANDRA [8]	France	Argillite	3D Finite Element CGM code
NAGRA [54, 55]	Switzerland	Opalinus Clay	3D Finite Element CGM code
GRS [61]	Germany	Salt	HEATING (3D finite difference)
NCSU(Li) [62]	USA	Yucca Tuff	Specific Temperature Integral
NCSU(Nicholson) [68]	USA	Yucca Tuff	COSMOL 3D Finite Element
Radel & Wilson [81]	USA	Yucca Tuff	Specific Temperature Change

Table 2.11: Methods by which to calculate heat load are independent of geologic medium. Maximum heat load constraints, however, vary among host formations.

3 MODELING PARADIGM

The modeling paradigms of the CYCLUS simulation platform and the CYDER disposal system simulator are described here. The modular design of both tools, the interface between them, and the interfaces defining components of the CYDER disposal system model are discussed.

3.1 Cyclus Simulator Paradigm

The CYDER disposal system simulator is designed to operate within the CYCLUS fuel cycle simulation framework [102] from the University of Wisconsin (UW) Madison. Modular features within the CYCLUS software architecture provide a great deal of flexibility, both in terms of modifying the underlying modeling algorithms and exchanging components of a fuel cycle system.

The CYCLUS fuel cycle simulator is the result of lessons learned from experience with previous nuclear fuel cycle simulation platforms. The modeling paradigm follows the transaction of discrete quanta of material among discrete facilities, arranged in a geographic and institutional framework, and trading in flexible markets. Key concepts in the design of CYCLUS include open access to the simulation engine, modularity with regard to functionality, and relevance to both scientific and policy analyses. The combination of modular encapsulation within the software architecture and dynamic module loading allows for robust but flexible reconfiguration of the basic building blocks of a simulation without alteration of the simulation framework.

The modeling paradigm adopted by CYCLUS includes a number of fundamental concepts that comprise the foundation on which other, more flexible, design choices have been made.

3.1.1 Dynamic Module Loading

The ability to dynamically load independently constructed modules is a key feature of the CYCLUS simulator. Dynamically-loadable modules are the primary mechanism for extending CYCLUS' capability. The primary benefit of this approach is encapsulation: the core of the code is completely independent of the individual models. Thus, any customization or extension is implemented only in the loadable module. A secondary benefit is the ability for contributors to choose different distribution and licensing strategies for their contributions. By allowing models to have varied availability, the security concerns of developers can be assuaged (See Figure 3.1).

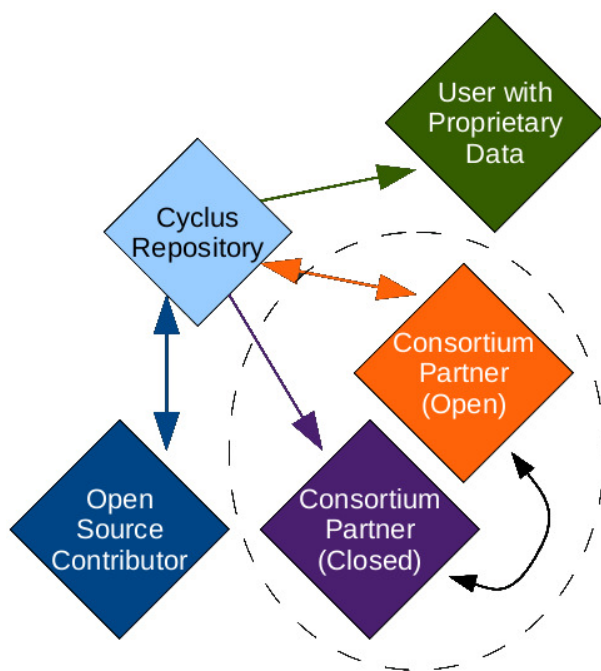


Figure 3.1: The CYCLUS code repository allows for varied accessibility [102].

This strategy also allows individual developers to explore different levels of complexity within their modules, including wrapping other simulation tools as loadable modules within the CYCLUS framework. This last benefit of dynamically-loadable modules addresses

another goal of CYCLUS: ubiquity amongst its potential user base. By engineering CYCLUS to easily handle varying levels of complexity, a single simulation engine can be used by both users interested in big-picture policy questions as well as users focused on more detailed, technical analyses.

3.1.1.1 Encapsulation

CYCLUS implements an encapsulated structure that takes advantage of object-oriented software design techniques in order to create an extensible and modular user and developer interface. A primary workhorse for this implementation is the notion of dynamic module loading in combination with well defined module interfaces within a region, institution, and facility hierarchy. In this paradigm, the shared interface of polymorphic objects is abstracted from the logic of their instantiation by the model definition they inherit.

In this way, CYCLUS allows a level of abstraction to exist between the simulation and model instantiation as well as between model instantiation and behavior. An interface defines the set of shared functions of a set of subclasses in an abstract superclass. In CYCLUS, the main superclasses are Regions, Institutions, and Facilities while their subclasses are the concrete available model types (e.g. a `RecipeReactorFacility`). See Figure 3.2 for a schematic.

The interface for `FacilityModel` objects is the set of virtual functions declared in the `FacilityModel` class and implemented in the concrete facility models that inherit from it. Through such an interface, the members of a subclass can be treated as interchangeable (polymorphic) instantiations of their shared superclass.

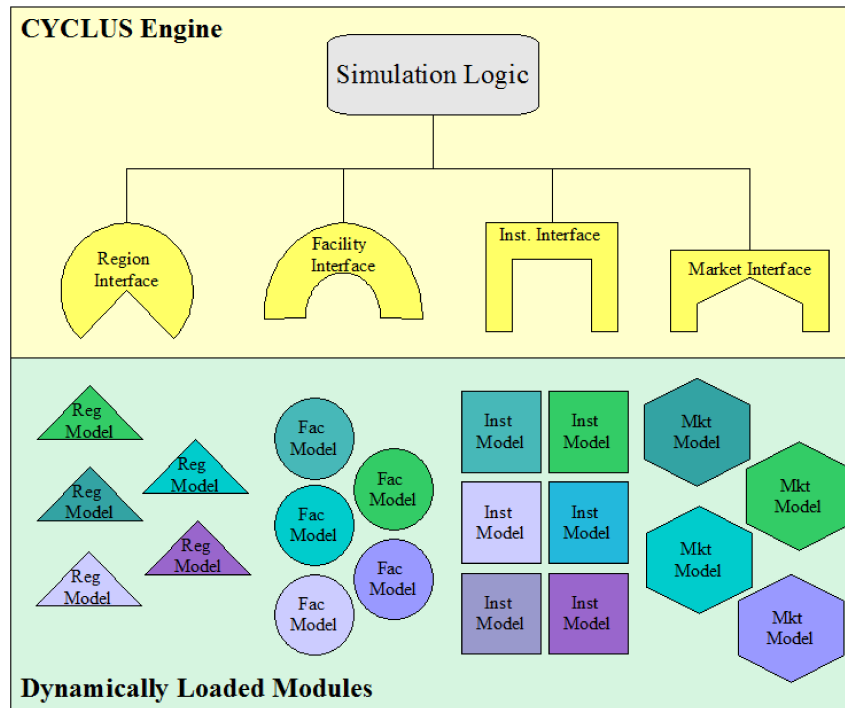


Figure 3.2: Modules are defined solely by their interfaces in a modular paradigm and can be arbitrarily interchanged with modules possessing equivalent interfaces.

3.1.1.2 Modularity and Extensibility

Modular software must have the traits of encapsulation and abstraction appropriate for a user or developer to flexibly make alterations to the simulation performance with minimal modification to the code. For extensibility, software should also be both robustly suited to the addition of classes and subclasses as well as suited to communication with other codes. In CYCLUS, addition of new models by dynamic loading is possible without any alteration of the software core. The modular design of CYCLUS stresses avoidance of rigidity, in which changes to the code are potentially difficult, and fragility, in which changes to the code are potentially damaging.

3.1.2 Market-based Material Transactions

The foundation of a simulation is a commodity market that collects offers and requests and matches them according to some algorithm. The user is able to select which type of algorithm is used for each market by selecting a `MarketModel` and configuring it with a particular set of parameters defined by that `MarketModel`. Changing the parameters of a market changes its performance and selecting a different `MarketModel` completely changes its behavior.

The transaction of nuclear materials takes place in markets that act as brokers matching a set of requests for material with a set of offers for that material. A variety of market models are available to perform this brokerage role. It is important to note that each market is defined for a single commodity and acts independently of other markets. Once the requests and offers have been matched by each market in a simulation, the facilities exchange material objects.

Facilities are deployed to issue offers and requests in these markets. Like markets, the user may select which type of algorithm is used for each facility by selecting a `FacilityModel` and configuring it with a particular set of parameters defined by that `FacilityModel`. Changing the parameters of a facility changes its performance and selecting a different `FacilityModel` completely changes its behavior. Multiple independent instances of each facility configuration can be deployed to represent individual facilities.

3.1.3 Discrete Materials and Facilities

The CYDER disposal system simulator that is the subject of this work is a facility model within the CYCLUS simulation paradigm. The CYCLUS modeling infrastructure is designed to be “agent based” such that every facility in a global nuclear fuel cycle is treated and acts individually. Each facility has two fundamental tasks: the transaction of goods or products

with other facilities and the transformation of those goods or products from an input form to an output form. For example, a reactor will receive fresh fuel assemblies from a fuel fabrication facility, transform them to used fuel assemblies using some approximation of the reactor physics, and supply those used fuel assemblies to a storage facility. In this manner, facilities can be thought of as black boxes in the simulation which request and produce resources as in Figure 3.3.

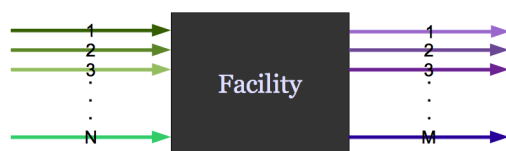


Figure 3.3: *CYCLUS* FacilityModels make offers ($1 \dots M$) and requests ($1 \dots N$).

A facility configuration is created by selecting a FacilityModel and supplying input parameters to define its performance. The same FacilityModel may be used for multiple facility configurations in the same simulation, each with parameter values appropriate for that facility configuration. Each FacilityModel independently enumerates the set of parameters that govern its performance.

Material movement is the primary unit of information in *CYCLUS*. Discrete materials passed, traded, and modified between and within facilities in the simulation are recorded at every time step. This material history is stored in the output dataset of *CYCLUS*. In addition to holding the map of isotopes and their masses, a material object holds a comprehensive history of its own path as it moves through models within the simulation.

3.1.4 Implications for Cyder

The above sections outline the CYCLUS fuel cycle simulation platform currently under development at UW in which the CYDER repository model at hand is implemented. Implemented as a facility within this framework, the CYDER interface conforms to the FacilityModel interface defined within the CYCLUS paradigm. CYDER is distinguished from other FacilityModels used in CYCLUS when it overrides and supplements these behaviors and data with its own functionality and the functionality of its subcomponents.

The CYDER repository is a subclass of the FacilityModel class. That is, the repository inherits data, parameters and behaviors from the CYCLUS simulation FacilityModel class. Though some FacilityModels make both requests and offers to the system, the CYDER model is a type of sink node, making only requests as in Figure 3.4.

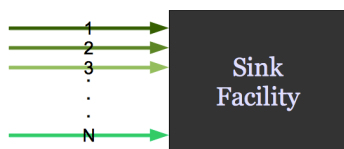


Figure 3.4: CYDER is a type of CYCLUS FacilityModel that makes only requests ($1 \cdots N$).

That interface requires that a capacity be defined by the repository at every CYCLUS time step so that the repository may make appropriate requests of disposable material.

The implementation of CYDER within CYCLUS also enables the capability for dynamic module loading possible within the CYCLUS paradigm allows the disposal system subcomponents to be interchangeably loaded at runtime, enabling comparison of various repository subcomponents, physical models of varying levels of detail.

3.2 Cyder Repository Modeling Paradigm

The CYDER disposal system simulator architecture is intended to modularly permit exchange of disposal system Component models (e.g., detailed nuclide transport model vs. less detailed) and data (e.g., exchange clay for granite geologic data) and accept arbitrary waste stream isotopic compositions. Finally, in order to participate in the simulation as a facility model, CYDER must make requests for spent material up to its capacity. Determination of the repository capacity for various types of spent fuel commodities comprises the interfacing functionality of the repository model.

3.2.1 Waste Stream Acceptance

The disposal system simulator must accept arbitrary spent fuel and high level waste streams. A waste stream is a material data object resulting from the CYCLUS simulated fuel cycle. As radionuclides are gained, lost, and transmuted within the spent fuel object, a history of its isotopic composition is recorded. It arrives at the repository and is emplaced if it obeys all repository capacity limits.

Since disposable material in most simulations of interest will be of variable composition and therefore heterogeneous in heat production capability, the disposal system simulator must be able to repeatedly recalculate its own capacity as new materials are offered. For waste streams that vary from each other in composition, the thermal capacity of the repository to receive that waste stream must therefore be recalculated. That capacity calculation will be discussed in Section 4.2.

3.2.2 Waste Stream Conditioning

Waste conditioning is the process of packing a waste stream into an appropriate waste form. As CYCLUS lacks a conditioning facility, the CYDER repository fulfills this need as a part of the repository behavior. As a waste stream is accepted into the repository, it is associated with a waste form according to its commodity name. This pairing is input by the user during simulation setup when a number of waste form Component configurations are specified and associated with allowed waste stream commodities. It is according to these pairings that CYDER loads discrete waste forms with discrete waste stream contaminant vectors as depicted in Figure 3.5.

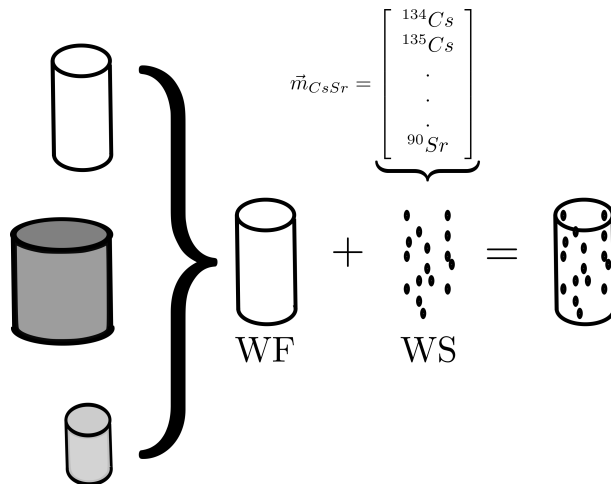


Figure 3.5: Waste streams are accepted and conditioned into the appropriate waste form, selected from an array according to user-specified pairings between commodities and waste forms.

3.2.3 Waste Form Packaging

Waste packaging is the process of placing one or many waste forms into a containment package. Once the waste stream has been conditioned into a waste form, that waste form

Component is loaded into a waste package Component, also according to allowed pairs dictated by the user, as depicted in Figure 3.6.

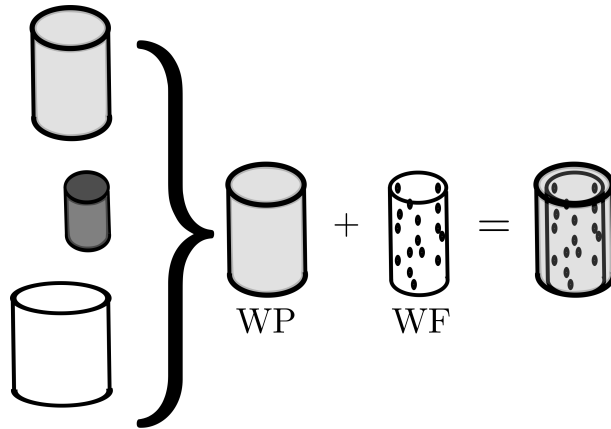


Figure 3.6: Waste forms are loaded into the appropriate waste package, selected from an array of choices according to user-specified pairings between forms and packages.

3.2.4 Package Emplacement

Finally, the waste package is emplaced in a buffer component, which contains many other waste packages, spaced evenly along an axis in the x-dimension within the larger repository grid. The location of each waste package within the repository grid is defined by the user input and depends on repository depth, Δz , waste package spacing, Δx , and tunnel spacing, Δy as in Figure 3.7.

3.2.5 Nested Components

The fundamental unit of information in the disposal system simulator is radionuclide contaminant presence at each stage of containment. The disposal system simulator, in this way, is fundamentally a tool to determine thermal and contaminant transport evolution as a result of an arbitrary waste stream. The disposal system simulator in this work conducts

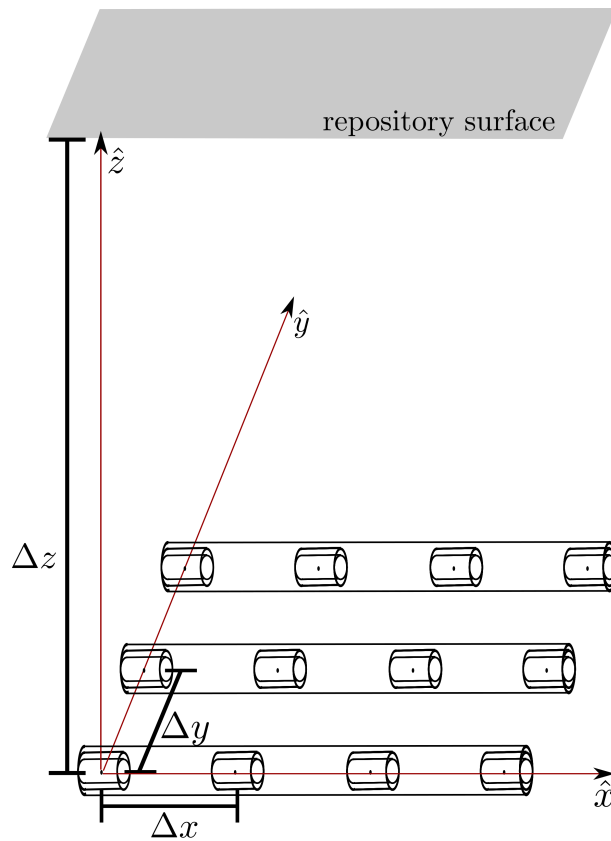


Figure 3.7: The CYDER repository emplacement geometry allows generic representation of all semi-regular two dimensional gridded layouts.

this calculation by treating each containment Component as a nested volume in a release chain.

Each Component is defined by a number of distinct object classes. Most importantly, those include a Geometry, some MaterialData, a ThermalModel, and a NuclideModel. It is also defined by the Parent Component which contains it and the Daughter Components which it contains. An emplaced waste package Component, for example, possesses a pointer to the buffer that surrounds it, its Parent Component. It also possesses a list of pointers to the waste form or waste forms within it, its Daughter Components.

3.2.5.1 Component Geometry

Each Component of the repository system (i.e. waste form, waste package, buffer, and geologic medium) is modeled as a discrete control volume. Each control volume performs its own mass balance at each time step and assesses its own internal heat transfer and degradation phenomena utilizing interface information provided by adjacent nested Components. The spatial extent of the control volume is defined by the Component Geometry, a class which keeps track of the inner and outer radii, length, and centroid coordinates of the (assumed cylindrical) volume.

3.2.5.2 Component Material Data

Each Component of the repository system possesses a notion of the material that it is made of. Supporting thermal and hydrologic data for canonical engineered barrier and geologic media is provided with the code in the `mat_data.sqlite` SQLite database.

Each table in the database holds data related to one of a canonical set of engineered barrier and geologic medium materials (e.g. clay, glass, etc.). The columns of that table hold data required to support all CYDER models. Thermal diffusivity and thermal conductivity comprise the thermal data in the table for each material. The hydrologic and chemical data in the database are included in one table for each material. Each table contains relative diffusivity coefficients, solubility limits, and sorption parameters for each element.

3.2.5.3 Component ThermalModel

Each Component possesses a thermal transport model that determines the temperature inside the Component over time. The thermal modeling options are discussed further in Section 4.2.

3.2.5.4 Component NuclideModel

Each Component possesses a radionuclide contaminant transport model that determines the contaminant transport inside the Component over time. The choices available for this NuclideModel are discussed further in Section 4.1.

3.2.6 Output Tables

CYDER output tables utilize the CYCLUS Table class and rely on the CYCLUS simulation logic to record table entries in the `cyclus.sqlite` output database. The current CYDER output database includes a number of tables. First, a repository parameters table, **cyder_params**, keeps data from the user input that parameterized the generic repository for reproducibility. Similarly, a Component parameters table, **cyder_components**, keeps data that parameterized each component, both from the user input and from the CYDER procedures that position and arrange these components. An example is shown in Figure 3.8. Finally, a contaminants table, **cyder_contaminants**, keeps track of the isotopic composition of the contaminants in each component as they move radially outward and a thermal table **cyder_thermal**. An example of the contaminants table is shown in Figure 3.9.

compID	parentID	compType	name	material_data	nuclidemodel	thermalmodel	innerradius	outerradius	x	y	z	
1	4	0	2	FF	clay	DEGRATE_NUCLIDE	STUB_THERMAL	3	100	0	0	0
2	5	0	0	BUFFER	clay	DEGRATE_NUCLIDE	STUB_THERMAL	2	3	50	0	100
3	6	0	4	WF	clay	DEGRATE_NUCLIDE	STUB_THERMAL	0	1	50	50	100
4	7	0	5	WP	clay	DEGRATE_NUCLIDE	STUB_THERMAL	1	2	50	50	100
5	8	0	4	WF	clay	DEGRATE_NUCLIDE	STUB_THERMAL	0	1	50	150	100
6	9	0	5	WP	clay	DEGRATE_NUCLIDE	STUB_THERMAL	1	2	50	150	100
7	10	0	4	WF	clay	DEGRATE_NUCLIDE	STUB_THERMAL	0	1	50	250	100
8	11	0	5	WP	clay	DEGRATE_NUCLIDE	STUB_THERMAL	1	2	50	250	100
9	12	0	4	WF	clay	DEGRATE_NUCLIDE	STUB_THERMAL	0	1	50	350	100
10	13	0	5	WP	clay	DEGRATE_NUCLIDE	STUB_THERMAL	1	2	50	350	100
11	14	0	4	WF	clay	DEGRATE_NUCLIDE	STUB_THERMAL	0	1	50	450	100
12	15	0	5	WP	clay	DEGRATE_NUCLIDE	STUB_THERMAL	1	2	50	450	100

Figure 3.8: An example of the CYDER component parameters table recorded for provenance in the cyclus.sqlite database.

CompID	Time	IsolD	MassKG	AvailConc
1	6	0	0.115044	0
2	6	0	0.0442478	0
3	6	0	0.840708	0
4	7	0	0	0
5	5	0	0	0
6	4	0	0	0
7	6	1	0.115044	0
8	6	1	0.0442478	0
9	6	1	0.840708	0
10	8	1	0.115044	0
11	8	1	0.0442478	0
12	8	1	0.840708	0
13	7	1	0	0

Figure 3.9: An example of the CYDER contaminants table in the cyclus.sqlite database.

4 METHODOLOGY

Each engineered barrier component within the CYDER disposal system simulator relies on a mass balance model, a mass transfer model, and a thermal model selected from those four presented in this chapter.

Mass balance calculations range from simplistic rate based models to more detailed solutions capturing the physics of advection, dispersion, sorption, and solubility. Mass transfer modes also range in complexity, including a fictionally simplistic forced transfer mode as well as modes capturing advection dominated, diffusion dominated, and coupled flow, respectively. In order to be interchangeable within the simulation, the radionuclide mass balance models have boundary interfaces designed to support the array of available mass transfer modes.

Thermal calculations are undertaken using a Specific Temperature Change (STC) model based on a thermal response database populated sufficiently to support thermal transport in clay, granite, and salt. This database captures the effect of thermal diffusivity, thermal conductivity, and varying waste isotopics.

4.1 Radionuclide Mass Transport In Cyder

The principal result of radionuclide contaminant transfer in CYDER is an assessment of radionuclide contaminants that reach the far field. This calculation is a key piece of information for repository performance assesment metrics regarding containment.

The CYDER model addresses this performance assesment by modeling the various engineered and natural containment barriers as finite control volumes connected by mass transfer interfaces. These approximations of mass transfer are based on parameters derived from the inventory and distribution of mass within adjacent control volumes. Meanwhile,

mass inventory is a simple sum of in and out flows, and mass distribution within the control volume is determined by the dominant physics of the mass balance model selected for that volume.

4.1.1 Time Stepping Algorithm

In CYDER, radionuclide contaminant flow is assumed to travel outward from the central Component (and up, in the \hat{k} direction). In order to conduct a mass balance in each Component at each time step, the mass flow and mass balance calculations proceed from the innermost Component to the outermost Component. As mass flows from inner components to outer components, the mass balances in both components are updated. Thus, nuclide release information is passed radially outward from the waste stream sequentially through each containment layer to the geosphere. This implicit time stepping method arrives at the updated state of each Component, radially outward, as a function of both the past state and the current state of the system.

At each component interface where mass transfer occurs and within each component where mass balances take place, the flow model is solved with the most up to date information available. To illustrate the algorithm by which mass flow calculations are conducted through the system of components at each time step, we will walk through the phases of a single time step for a simple pair of components. The source, i , is the inner and the sink, j , is the outer component.

4.1.1.1 Phase 1: Initial Conditions

The initial conditions in both the source and the sink at the beginning of a time step are equal to the final updated state of the previous time step. If this is the first time step, the global initial state of the repository system is used.

4.1.1.2 Phase 2: Interior Mass Balance

The mass distribution and concentration profile in the interior source volume i is solved based on the initial condition, any influxes, and the physics of its mass balance model. This calculation results in a contaminant mass distribution and concentration profile within the volume i at time t_n . For each of the models, the calculation behind this mass distribution and concentration profile is discussed in Section 4.1.3.

This mass distribution and concentration profile fully inform the conditions on the boundary at r_i and this information is made available to the external component, j .

4.1.1.3 Phase 3: Mass Transfer Calculation

The mass transfer from the source volume i to the sink volume j is calculated next, based on the up to date conditions at $0 \leq r \leq r_i$ determined in Phase 2 and the initial conditions in volume j where $r_i \leq r \leq r_j$. The mass transfer is calculated according to the mass transfer mode preference of the mass balance model of volume j .

The Degradation Rate and Mixed Cell models can be parameterized to utilize an explicit mass transfer mode that captures either advection, dispersion, or coupled flow. The Lumped Parameter and One Dimensional PPM models, on the other hand, use an implicit method by which the incoming mass flux is determined based on the expected concentration profile resulting from the internal Dirichlet boundary condition at r_i .

4.1.1.4 Phase 4: Exterior Mass Balance

When a mass flux $m_{ij}(t_n)$ is determined between volumes i and j , the mass is added to the exterior sink volume j . Accordingly, necessary updates are made to the mass balance and concentration profile. For each of the models, the calculation behind this mass distribution and concentration profile is discussed in Section 4.1.3.

4.1.1.5 Phase 5: Interior Mass Balance Update

When a mass flux $m_{ij}(t_n)$ is determined between volumes i and j , the mass is simultaneously added to the exterior sink volume j (as in phase 4) and extracted from the interior source volume i . When the material is extracted from the interior source volume, the contained mass distribution and concentration profile are updated to reflect this change,

$$m_i^*(t_n) = m_i(t_n) - m_{ij}(t_n). \quad (4.1)$$

4.1.2 Mass Transfer Modes

The mass transfer interfaces between the mass balance models are essential to the understanding of the CYDER paradigm. Depending on the mass balance model selected in the external of two components, mass transfer into that component is either explicit or implicit.

In the explicit mode, the mass transfer is chosen by the user among advective, dispersive, coupled or fixed flux and is calculated based on the conditions at the transfer boundary. The inventory in the components is then updated based on this transfer rate. While all components enable this on their outer boundary, only the mass balance models that are 0-dimensional in space (the Degradation Rate model and the Mixed Cell model) require explicit transfer on their inner boundary.

In the implicit mode, the mass balance model of the external component determines the inventory based on boundary conditions provided by the internal component. The appropriate mass is then transferred to accomplish the change in inventory.

In groundwater transport, contaminants are transported by dispersion and advection. It is customary to define the combination of molecular diffusion and mechanical mixing

as the dispersion tensor, D , such that, for a conservative solute (infinitely soluble and non-sorbing), the mass conservation equation becomes [86, 95, 96]:

$$J = J_{dis} + J_{adv}$$

where

$$\begin{aligned} J_{dis} &= \text{Total Dispersive Mass Flux [kg/m}^2\text{/s]} \\ &= -\theta(D_{mdis} + \tau D_m)\nabla C \\ &= -\theta D \nabla C \end{aligned}$$

$$\begin{aligned} J_{adv} &= \text{Advective Mass Flux [kg/m}^2\text{/s]} \\ &= \theta v C \end{aligned}$$

$$\tau = \text{Tortuosity [-]}$$

$$\theta = \text{Porosity [-]}$$

$$D_m = \text{Molecular diffusion coefficient [m}^2\text{/s]}$$

$$D_{mdis} = \text{Coefficient of mechanical dispersivity [m}^2\text{/s]}$$

$$D = \text{Effective Dispersion Coefficient [m}^2\text{/s]}$$

$$C = \text{Concentration [kg/m}^3\text{]}$$

$$v = \text{Fluid Velocity in the medium [m/s].}$$

For uniform flow in \hat{k} ,

$$J = \left(-\theta D_{xx} \frac{\partial C}{\partial x} \right) \hat{i} + \left(-\theta D_{yy} \frac{\partial C}{\partial y} \right) \hat{j} + \left(-\theta D_{zz} \frac{\partial C}{\partial z} + \theta v_z C \right) \hat{k}. \quad (4.2)$$

Solutions to this equation can be categorized by their boundary conditions. Those boundary conditions serve as the interfaces between components in the CYDER library of nuclide transport models by way of advective, dispersive, coupled, and fixed fluxes. This is supported by implementation in which vertical advective velocity is uniform throughout the system and in which parameters such as the dispersion coefficient are known for each component.

4.1.2.1 Explicit Advection Dominated Mass Transfer

The first, specified-concentration or Dirichlet type boundary conditions define a specified species concentration on some section of the boundary of the representative volume,

$$C(\vec{r}, t) \Big|_{\vec{r} \in \Gamma} = C_0(t) \quad (4.3)$$

where

\vec{r} = position vector

Γ = domain boundary .

The right hand side of the Dirichlet boundary condition can be provided by any mass balance model, j , at its external boundary, r_j , based on the concentration profile it calculates (see Section 4.1.3),

$$\begin{aligned}
C(z, t_n)|_{z=r_j} &= \text{fixed concentration in } j \text{ at } r_j \text{ and } t_n [kg/m^3]. \\
&= \begin{cases} \frac{m_d(t_n)}{V_d(t_n)}, & \text{Degradation Rate} \\ \frac{m_{df}(t_n)}{V_{df}(t_n)}, & \text{Mixed Cell} \\ C_{out}(t_n), & \text{Lumped Parameter} \\ C(r_j, t_n), & \text{One Dimensional PPM.} \end{cases} \quad (4.4)
\end{aligned}$$

In the Degradation Rate and Mixed Cell models, the Dirichlet boundary condition can be chosen to enforce an advective flux on the inner boundary. This choice is appropriate when the user expects a primarily advective interface between two components. The advective flux across the boundary between two components j and k ,

$$\begin{aligned}
J_{adv}(t_n) &= \text{potential advective flux at } t_n [kg/m^2/s] \\
&= \theta v C(z, t_n) \quad (4.5)
\end{aligned}$$

relies on the fixed concentration Dirichlet boundary condition at the interface, provided by the internal component.

The resulting mass transfer into the Degradation Rate or Mixed Cell model is, therefore,

$$m_{jk}(t_n) = A \Delta t \theta_k v C(z, t_n)|_{z=r_j} \quad (4.6)$$

where

$A =$ surface area normal to the flow direction [m^2]

$\Delta t =$ length of the time step [s].

4.1.2.2 Explicit Dispersion Dominated Mass Transfer

The second type, specified dispersive flux, or Neumann type boundary conditions describe a full set of concentration gradients at the boundary of the domain,

$$\left. \frac{\partial C(\vec{r}, t)}{\partial r} \right|_{\vec{r} \in \Gamma} = f(t) \quad (4.7)$$

$f(t) =$ known function .

The Neumann boundary condition can be provided at the external boundary of any mass balance model,

$$\left. \frac{\partial C}{\partial z} \right|_{z=r_j} = \text{fixed concentration gradient in } j \text{ at } r_j \text{ and } t_n [kg/m^3/s].$$

For mass balance models that are 0-dimensional in space (i.e. the Degradation Rate model and the Mixed Cell model), which lack spatial variation in the concentration profile, the differential must be approximated. Taking the center-to-center difference between adjacent components is one convenient way to make this approximation, and is the method implemented in CYDER, such that

$$\left. \frac{\partial C(z, t_n)}{\partial z} \right|_{z=r_j} = \frac{C_k(r_{k-1/2}, t_{n-1}) - C_j(r_{j-1/2}, t_n)}{r_{k-1/2} - r_{j-1/2}} \quad (4.8)$$

where

$$r_{j-1/2} = r_j - \frac{r_j - r_i}{2}$$

$$r_{k-1/2} = r_k - \frac{r_k - r_j}{2}.$$

However, for mass balance models that are 1-dimensional in space (i.e. the Lumped Parameter model and the One Dimensional PPM model), the derivative is taken based on the concentration profile in the internal component as it approaches the boundary. In component j , if it is a lumped parameter model, the profile is assumed to be a linear relationship between C_{in} and C_{out} , the gradient is

$$\left. \frac{\partial C(z, t_n)}{\partial z} \right|_{r_i \leq z \leq j} = \frac{C_{out} - C_{in}}{r_j - r_i}. \quad (4.9)$$

For the one dimensional permeable porous medium model, the analytical derivative of equation (4.54) is evaluated at r_j .

For mass transfer into the Degradation Rate and Mixed Cell models, the Neumann boundary condition can be chosen to enforce a dispersive flux on the inner boundary. This choice is appropriate when the user expects a primarily dispersive flow across the boundary. The dispersive flux in one dimension,

$$J_{dis} = \text{Total Dispersive Mass Flux [kg/m}^2\text{/s]}$$

$$= -\theta D \frac{\partial C}{\partial z}$$

relies on the fixed gradient Neumann boundary condition at the interface. The resulting mass transfer into the Degradation Rate or Mixed Cell model is, therefore,

$$m_{jk}(t_n) = -A\Delta t\theta_k D \frac{\partial C(z, t_n)}{\partial z} \Big|_{z=r_j}. \quad (4.10)$$

4.1.2.3 Explicit Coupled Advective Dispersive Mass Transfer

The third Cauchy type mixed boundary condition defines a solute flux along a boundary. The fixed concentration flux Cauchy boundary condition can be provided at the external boundary of any mass balance model. For a vertically oriented system with advective velocity in the \hat{k} direction,

$$-D \frac{\partial C(z, t)}{\partial z} \Big|_{z \in \Gamma} + v_z C(z, t) = v_z C(t) \quad (4.11)$$

where

$$C(t) = \text{a known concentration function [kg/m}^3\text{]}.$$

In the Degradation Rate and Mixed Cell models, the Cauchy boundary condition can be selected to enforce coupled advective and dispersive flow,

$$\begin{aligned} J_{coupled} &= J_{adv} + J_{dis} \\ &= \theta v C(z, t_n) - \theta D \frac{\partial C}{\partial z}. \end{aligned} \quad (4.12)$$

The resulting mass transfer into the Degradation Rate or Mixed Cell model is then,

$$m_{jk}(t_n) = A\Delta t \left(\theta_k v C(z, t_n)|_{z=r_j} - \theta_k D \frac{\partial C(z, t_n)}{\partial z} |_{z=r_j} \right). \quad (4.13)$$

4.1.2.4 Explicit Maximum Flow Mass Transfer

For debugging and testing purposes, the maximum flow mode transports all available material in a component into the component external to it.

The total available mass for each mass balance model can be expressed,

$$m_{jk}(t_n) = \begin{cases} m_{j,d}(t_n), & \text{Degradation Rate} \\ m_{j,df}(t_n), & \text{Mixed Cell} \\ \int C(z, t_n) dV_j, & \text{Lumped Parameter} \\ \int C(z, t_n) dV_j, & \text{One Dimensional PPM.} \end{cases} \quad (4.14)$$

The integrals for the Lumped Parameter model and the One Dimensional PPM model are calculated numerically.

4.1.2.5 Implicit Mass Transfer

On its inner boundary, the Lumped Parameter model uses the fixed concentration Dirichlet boundary condition directly in its solution such that,

$$C_{k,in}(t_n) = C(z, t_n)|_{z=r_j}. \quad (4.15)$$

The resulting mass transfer into the external component k containing the Lumped Parameter model is calculated by taking the integral of that concentration profile over the

volume,

$$m_{jk}(t_n) = \int C(z, t_n) dV_k - \int C(z, t_{n-1}) dV_k. \quad (4.16)$$

In the similar case of the One Dimensional Permeable Porous Medium Model, the Dirichlet boundary condition at the boundary is also used directly in the solution as C_0 such that,

$$C_{k,0}(t_n) = C(z, t_n)|_{z=r_j}. \quad (4.17)$$

The mass transfer on the inner boundary is again calculated by taking an integral of that profile over the volume,

$$m_{jk}(t_n) = \int C(z, t_n) dV_k - \int C(z, t_{n-1}) dV_k. \quad (4.18)$$

4.1.3 Mass Balance Models

The mass balance models selected to represent the physics of mass distribution within each component are selected from among four options. The Degradation Rate model and Mixed Cell model are control volumes that distribute contaminants between a liquid and a solid phase. These models calculate a homogenous concentration profile throughout the volume and are therefore zero-dimensional in space. The Lumped Parameter model and the

One Dimensional Permeable Porous Medium model, however, calculate one dimensional concentration profiles to arrive at a mass distribution throughout the volume.

These models are differentiated from one another by the physics that they capture as well as the detail and accuracy with which they capture it. Depending on the component being modeled, the user's available data, need for accuracy, and need for speed, some mass balance models will be more appropriate than others.

4.1.3.1 Degradation Rate Radionuclide Mass Balance Model

Many barrier materials in a repository environment degrade over time. The Degradation Rate mass balance model is the simplest implemented model and is most appropriate for rate based modeling of a degrading barrier volume. The Degradation Rate mass balance model does not attempt to model the physical mechanisms responsible for this degradation. Rather, it generically captures this behavior as a simple fractional degradation rate. The fundamental concept is depicted in Figure 4.1.

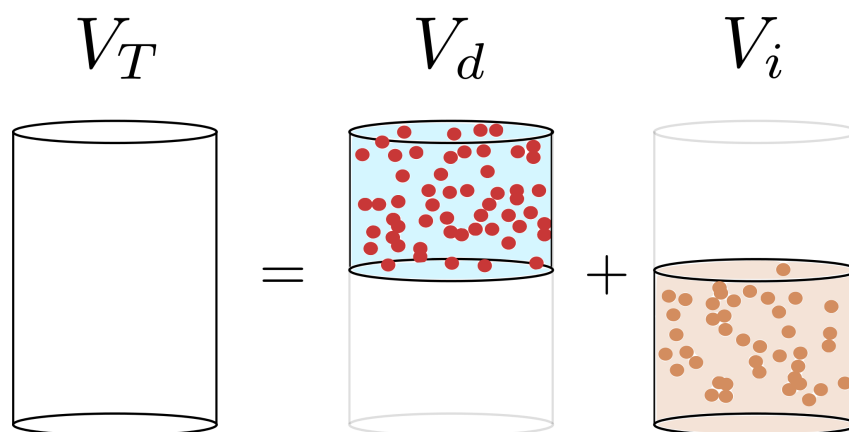


Figure 4.1: The control volume contains an intact volume V_i and a degraded volume, V_d . Contaminants in V_d are available for transport, while contaminants in V_i are contained.

For a situation as in CYDER and CYCLUS, with discrete time steps, the time steps are

assumed to be small enough to assume a constant rate of degradation over the course of the time step. The degraded volume, then, is a simple fraction, d , of the total volume, V_T , such that

$$V_T = V_i + V_d \quad (4.19)$$

where

$$V_d(t) = d(t)V_T$$

$$V_i(t) = (1 - d(t))V_T$$

$$V_T = \text{total volume } [m^3]$$

$$V_i(t) = \text{intact volume at time } t [m^3]$$

$$V_d(t) = \text{degraded volume at time } t [m^3]$$

and

$$\begin{aligned} d(t) &= \text{the fraction that has been degraded by time } t [-] \\ &= \sum_{n=0}^N f_n \Delta t \end{aligned}$$

where

$$f_n = \text{the constant rate over a time step } [1/s]$$

$$\Delta t = \text{the length of a time step } [s].$$

In this model, all contaminants in the degraded fraction of the control volume are available to adjacent components such that,

$$m_{jk}(t_n) = m_{j,d}(t_n) \quad (4.20)$$

where

$$\begin{aligned} m_{j,d} &= \text{mass in degraded volume of cell } j \text{ [kg]} \\ t_n &= \text{time [s]}. \end{aligned}$$

The total contaminants $m_{j,d}(t_n)$, available in the degraded volume at time t_n are calculated based on mass flux from the inner boundary, the updated mass in the degraded volume at the previous time step, and the mass released by degradation during the current time step. Specifically,

$$m_{k,d}(t_n) = m_{jk}(t_n) + m_{k,d}^*(t_{n-1}) + m_{k,i}^*(t_{n-1})f_n\Delta t \quad (4.21)$$

where

$m_{jk}(t_n)$ = incoming mass from the inner boundary [kg]

$m_{k,d}^*(t_{n-1})$ = mass in the degraded volume of k at the end of t_{n-1} [kg]

$m_{k,i}^*(t_{n-1})$ = mass in the intact volume of k at the end of t_{n-1} [kg]

f_n = degradation rate during the time step t_n [kg]

$\Delta t = t_n - t_{n-1}$ [s].

The concentration calculation results from the mass balance calculation in (4.21) to support parent components that utilize the Dirichlet boundary condition. For the degradation rate model, which incorporates no diffusion or advection, the concentration, C_j at r_j , the boundary between cells j and k , is the average concentration in degraded volume,

$$\begin{aligned} C_d &= \frac{m_d(t_n)}{V_d(t_n)} \\ &= \frac{\text{solute mass in degraded fluid in cell j}}{\text{degraded fluid volume in cell j}}. \end{aligned} \tag{4.22}$$

4.1.3.2 Mixed Cell Radionuclide Mass Balance Model

Slightly more complex, the Mixed Cell model incorporates the influence of porosity, elemental solubility limits, and sorption in addition to the degradation behavior of the Degradation Rate model. A graphical representation of the discrete sub-volumes in the mixed cell model is given in Figure 4.2.

After some time degrading, the total volume in the degraded region can be expressed as in equation (4.19). Additionally, the intact and degraded volumes can also be described

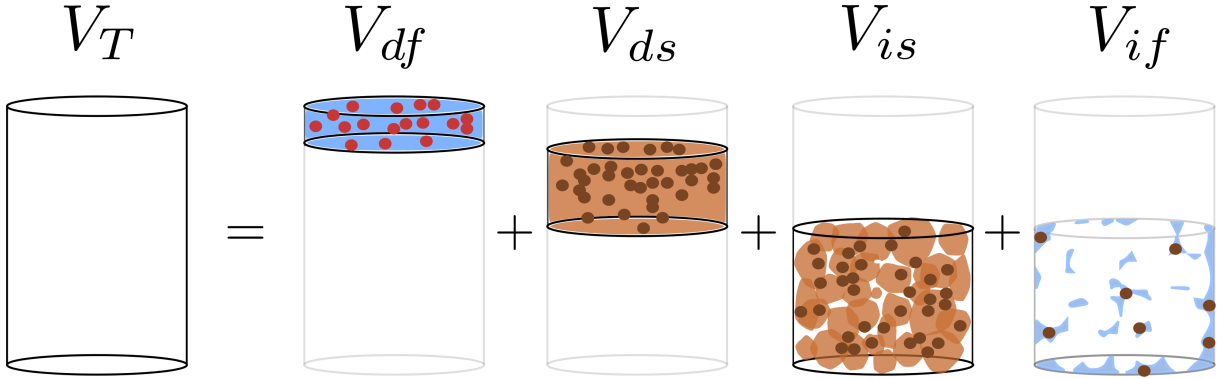


Figure 4.2: The degraded volume is modeled as a degraded solid volume, V_{ds} , and a degraded fluid volume, V_{df} . The intact volume is modeled as an intact solid volume, V_{is} , and an intact fluid volume V_{if} . Only contaminants in V_{df} are available for transport.

in terms of their constituent solid matrix and pore fluid volumes,

$$\begin{aligned}
 V_d(t_n) &= \text{degraded volume at time } t_n [m^3] \\
 &= V_{df}(t_n) + V_{ds}(t_n)
 \end{aligned} \tag{4.23}$$

where

$$\begin{aligned}
 V_{df}(t_n) &= \text{degraded fluid volume at time } t_n [m^3] \\
 &= \theta V_d(t_n)
 \end{aligned} \tag{4.24}$$

$$= \theta d(t_n) V_T \tag{4.25}$$

$$\begin{aligned}
V_{ds}(t_n) &= \text{degraded solid volume at time } t_n [m^3] \\
&= (1 - \theta)V_d(t_n)
\end{aligned} \tag{4.26}$$

$$= (1 - \theta)d(t_n)V_T \tag{4.27}$$

$$\begin{aligned}
V_i(t_n) &= \text{intact volume at time } t_n [m^3] \\
&= V_{if}(t_n) + V_{is}(t_n)
\end{aligned} \tag{4.28}$$

$$\begin{aligned}
V_{if}(t_n) &= \text{intact fluid volume at time } t_n [m^3] \\
&= \theta V_i(t_n)
\end{aligned} \tag{4.29}$$

$$= \theta(1 - d(t_n))V_T \tag{4.30}$$

and

$$\begin{aligned}
V_{is}(t_n) &= \text{intact solid volume at time } t_n [m^3] \\
&= (1 - \theta)V_i(t_n)
\end{aligned} \tag{4.31}$$

$$= (1 - \theta)(1 - d(t_n))V_T. \tag{4.32}$$

This model distributes contaminant masses throughout each sub-volume of the component. Contaminant masses and concentrations can therefore be expressed with notation indicating in which volume they reside, such that

$$C_{df} = \frac{m_{df}}{V_{df}} \quad (4.33)$$

$$C_{ds} = \frac{m_{ds}}{V_{ds}} \quad (4.34)$$

$$C_{if} = \frac{m_{if}}{V_{if}} \quad (4.35)$$

$$C_{is} = \frac{m_{is}}{V_{is}}. \quad (4.36)$$

The contaminant mass in the degraded fluid is the contaminant mass that is treated as “available” to adjacent components.

Sorption The mass in all volumes exists in both sorbed and non-sorbed phases. The relationship between the sorbed mass concentration in the solid phase (e.g. the pore walls),

$$s = \frac{\text{mass of sorbed contaminant}}{\text{mass of total solid phase}} \quad (4.37)$$

and the dissolved liquid concentration,

$$C = \frac{\text{mass of dissolved contaminant}}{\text{volume of total liquid phase}} \quad (4.38)$$

can be characterized by a sorption “isotherm” model. A sorption isotherm describes the equilibrium relationship between the amount of material bound to surfaces and the amount of material in the solution. The MixedCell NuclideModel uses a linear isotherm model.

With the linear isotherm model, the mass of contaminant sorbed into the solid phase

can be found [86], according to the relationship

$$s_p = K_{dp}c_p \quad (4.39)$$

where

s_p = the solid concentration of isotope p [kg/kg]

K_{dp} = the distribution coefficient of isotope p [m^3/kg]

C_p = the liquid concentration of isotope p [kg/m^3].

Thus, from (4.37),

$$\begin{aligned} s_{dsp} &= K_{dp}C_{dfp} \\ &= \frac{K_{dp}m_{dfp}}{V_{df}} \end{aligned}$$

where

s_{dsp} = isotope p concentration in degraded solids [kg/kg]

C_{dfp} = isotope p concentration in degraded fluids [kg/m^3].

In this model, sorption is taken into account throughout the volume. In the intact matrix, the contaminant mass is distributed between the pore walls and the pore fluid by sorption. So too, contaminant mass released from the intact matrix by degradation is distributed between dissolved mass in the free fluid and sorbed mass in the degraded and precipitated solids.

To begin solving for the boundary conditions in this model, the amount of non-sorbed contaminant mass in the degraded fluid volume must be found. Dropping the isotope subscripts and beginning with equations (4.33) and (4.39),

$$m_{df} = C_{df}V_{df} \quad (4.40)$$

and assuming the sorbate is in the degraded solids

$$m_{df} = \frac{s_{ds}V_{df}}{K_d},$$

then applying the definition of s_{ds} and m_{ds}

$$\begin{aligned} m_{df} &= \frac{\frac{m_{ds}}{m_T}V_{df}}{K_d} \\ &= \frac{(dm_T - m_{df})V_{df}}{K_d m_T}. \end{aligned}$$

This can be rearranged to give

$$\begin{aligned} m_{df} &= \frac{dV_{df}}{K_d} \frac{1}{\left(1 + \frac{V_{df}}{K_d m_T}\right)} \\ &= \frac{dV_{df}}{\left(K_d + \frac{V_{df}}{m_T}\right)}. \end{aligned} \quad (4.41)$$

Finally, in terms of total volume,

$$m_{df} = \frac{d^2\theta V_T}{dK_d + \frac{d\theta V_T}{m_T}}. \quad (4.42)$$

Solubility Dissolution of the contaminant into the available fluid volume is constrained by the elemental solubility limit already given in equation (2.5) [41],

$$m_{df,i} \leq V_{df} C_{sol,i} \quad (4.43)$$

where

$m_{df,i}$ = solubility limited mass of isotope i in volume V_{df} [kg]

$C_{sol,i}$ = the maximum dissolved concentration limit of i [kg/m³].

The final available mass is therefore the m_{df} from equation (4.42) constrained by equation (4.43).

4.1.3.3 Lumped Parameter Radionuclide Mass Balance Model

For systems in which the flow is sufficiently slow to be assumed constant over a time step, it is possible to model a system of volumes as a connected lumped parameter models (Figure 4.3). The Lumped Parameter mass balance model implements a response function model based on this lumped parameter interpretation and capable of Piston Flow, Exponential, and Dispersion response functions from Maloszewski and Zuber [65].

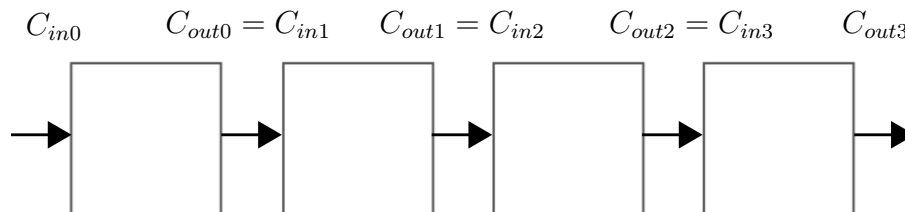


Figure 4.3: A system of volumes can be modeled as lumped parameter models in series.

Each lumped parameter component is modeled according to a relationship between the incoming concentration, $C_{in}(t)$, and the outgoing concentration, $C_{out}(t)$,

$$C_{out}(t) = \int_0^{\infty} C_{in}(t-t')g(t')e^{-\lambda t'} dt' \quad (4.44)$$

where

t' = transit time [s]

$g(t')$ = response function, a.k.a. transit time distribution[-]

λ = radioactive decay constant [s^{-1}].

Selection of the response function is usually based on experimental tracer results in the medium at hand. If such detailed transport data is not available, functions used commonly in chemical engineering applications [65] include the Piston Flow Model (PFM), which approximates pure advection,

$$g_{PFM}(t') = \delta(t' - t_t), \quad (4.45)$$

the Exponential Model (EM) which approximates a well-mixed flow case,

$$g_{EM}(t') = \frac{1}{t_t} e^{-\frac{t'}{t_t}} \quad (4.46)$$

and the so-called Dispersion Model (DM), which actually approximates the solution to

both advective and dispersive transport,

$$g_{DM}(t') = \left(\frac{Pe t_t}{4\pi t'} \right)^{\frac{1}{2}} \frac{1}{t'} e^{-\frac{Pe t_t \left(1 - \frac{t'}{t_t}\right)^2}{4t'}}, \quad (4.47)$$

where

Pe = Peclet number for mass diffusion [-]

t_t = mean tracer age [s]

= t_w if there are no stagnant areas

t_w = mean residence time of water [s]

$$= \frac{V_m}{Q}$$

$$= \frac{z}{v_z}$$

$$= \frac{z\theta_e}{q}$$

in which

V_m = mobile water volume [m^3]

Q = volumetric flow rate [m^3/s]

z = average travel distance in flow direction [m]

v_z = mean water velocity [m/s]

q = Darcy Flux [m/s]

θ_e = effective (connected) porosity [%].

The latter of these, the Dispersion Model satisfies the one dimensional advection-

dispersion equation, and is therefore the most physically relevant for this application. A constant inlet concentration is assumed over the span of a time step such that $C_{in}(t) = C_0$, and the solutions to these for constant concentration at the source boundary are given in Maloszewski and Zuber [65] accordingly,

$$C_{out}(t) = \begin{cases} PFM & C_0 e^{-\lambda t} \\ EM & \frac{C_0}{1+\lambda t} \\ DM & C_0 e^{\frac{Pe}{2} \left(1 - \sqrt{1 + \frac{4\lambda t}{Pe}}\right)}. \end{cases} \quad (4.48)$$

Since CYCLUS handles decay outside of CYDER, the use of these models relies on a reference transit time and decay constant supplied by the user. The behavior of the reference isotope, in this way, fully defines the behavior of all isotopes.

It is important to note that a linear concentration profile is assumed between the inlet and the outlet of a given Component in CYDER,

$$C(z, t) = C_{in}(t) + \frac{C_{out}(t) - C_{in}(t)}{z_{out} - z_{in}}(z - z_{in}). \quad (4.49)$$

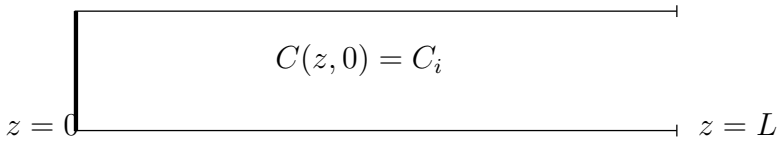
This is an approximation that could be improved by direct use of the response functions themselves, under a change of variables from time to length.

4.1.3.4 One Dimensional Permeable Porous Medium Radionuclide Mass Balance Model

Various solutions to the advection dispersion equation (4.2) have been published for both the first and third types of boundary conditions. The third, Cauchy type, is more

mass conservative, and is the primary kind of boundary condition used at the source for the model implementation in CYDER. Abstraction results informed modifications to the implementation of an analytic solution to the one dimensional advection-dispersion equation with a finite domain and Cauchy and Neumann boundary conditions at the inner and outer boundaries, respectively.

The conceptual model in Figure 4.4 represents solute transport in one dimension with unidirectional flow upward (a conservative assumption) and a finite boundary condition in the positive flow direction. In CYCLUS, radioactive decay is handled external to the components, so there is no need to include production or decay. An approximate solution for these conditions made by Brenner [19] is described below as it is given in van Genuchten et. al, [95],

$$-D \frac{\partial C}{\partial z} \Big|_{z=0} + vC = \begin{cases} vC_0 & t < t_0 \\ 0 & t > t_0 \end{cases} \quad \frac{\partial C}{\partial z} \Big|_L = 0$$


$C(z, 0) = C_i$

$z = 0$ $z = L$

Figure 4.4: A one dimensional, finite, unidirectional flow solution with Cauchy and Neumann boundary conditions

For the boundary conditions,

$$-D \frac{\partial C}{\partial z} \Big|_{z=0} + v_z c = \begin{cases} v_z C_0 & (0 < t < t_0) \\ 0 & (t > t_0) \end{cases} \quad (4.50)$$

and

$$\frac{\partial C}{\partial z} \Big|_{z=L} = 0 \quad (4.51)$$

and the initial condition,

$$C(z, 0) = C_i, \quad (4.52)$$

the solution is given as

$$C(z, t) = \begin{cases} C_i + (C_0 - C_i) A(z, t) & 0 < t \leq t_0 \\ C_i + (C_0 - C_i) A(z, t) - C_0 A(z, t - t_0) & t \geq t_0. \end{cases} \quad (4.53)$$

For the vertical flow coordinate system, A is defined as

$$\begin{aligned} A(z, t) = & \left(\frac{1}{2}\right) \operatorname{erfc} \left[\frac{Rz - vt}{2\sqrt{DRt}} \right] \\ & + \left(\frac{v^2 t}{\pi RD}\right)^{1/2} \exp \left[-\frac{(Rz - vt)^2}{4DRt} \right] \\ & - \frac{1}{2} \left(1 + \frac{vz}{D} + \frac{v^2 t}{DR}\right) \exp \left[\frac{vz}{D} \right] \operatorname{erfc} \left[\frac{Rz + vt}{2\sqrt{DRt}} \right] \\ & + \left(\frac{4v^2 t}{\pi RD}\right)^{1/2} \left[1 + \frac{v}{4D} \left(2L - z + \frac{vt}{R}\right)\right] \exp \left[\frac{vL}{D} - \frac{R}{4Dt} \left(2L - z + \frac{vt}{R}\right)^2 \right] \\ & - \frac{v}{D} \left[2L - z + \frac{3vt}{2R} + \frac{v}{4D} \left(2L - z + \frac{vt}{R}\right)^2\right] \exp \left[\frac{vL}{D} \right] \operatorname{erfc} \left[\frac{R(2L - z) + vt}{2\sqrt{DRt}} \right] \end{aligned} \quad (4.54)$$

where

L =Extent of the solution domain [m]

R =Retardation factor [-].

4.2 Thermal Transport in Cyder

An algorithm and supporting database for rapid thermal repository loading calculation was implemented in CYDER. This algorithm employs a STC method [81, 83] and has resulted from combining a number of resources provided by the UFD campaign. These resources include detailed spent nuclear fuel composition data from Carter [22] and a detailed thermal repository performance analysis tool from Greenberg at LLNL and previously discussed in Section 2.6.2 [35]. Benchmarking was conducted using an additional tool from Bauer at ANL, previously discussed in Section 2.6.1 [46]. By abstraction of and benchmarking against these detailed thermal models, CYDER captures the dominant physics of thermal phenomena affecting repository capacity in various geologic media and as a function of spent fuel composition.

Abstraction based on detailed computational thermal repository performance calculations with the LLNL semi-analytic model has resulted in implementation of the STC estimation algorithm and a supporting reference dataset. This method is capable of rapid estimation of temperature increase near emplacement tunnels as a function of waste composition, limiting radius, r_{lim} , waste package spacing, S , near field thermal conductivity, K_{th} , and near field thermal diffusivity, α_{th} .

4.2.1 Specific Temperature Change Method

Introduced by Radel, Wilson et al., the STC method uses a linear approximation to arrive at the thermal loading density limit [81, 83]. Since the thermal response in a system with a long term transient response is strong function of the transient decay power, it is also a strong function of the isotopic composition of the waste. Thus, the time dependent temperature change, ΔT , at the limiting radius, r_{lim} , can be approximated as proportional to the mass loading density. First, ΔT is determined for a limiting loading density of the

particular material composition then it is normalized to a single kilogram of that material, Δt , the so called STC.

$$\Delta T(r_{lim}) = m \cdot \Delta t(r_{lim}) \quad (4.55)$$

where

ΔT = Temperature change due to m [K]

m = Mass of heat generating material [kg]

Δt = Temperature change due to 1 kg [K]

r_{lim} = Limiting radius [m].

For an arbitrary waste stream composition, scaled curves, Δt_i , calculated in this manner for individual isotopes can be superimposed for each isotope to arrive at an approximate total temperature change.

$$\Delta T(r_{lim}) \sim \sum_i m_i \Delta t_i(r_{lim}) \quad (4.56)$$

where

i = An isotope in the material [-]

m_i = mass of isotope i [kg]

Δt_i = Specific temperature change due to i [K].

4.2.2 Supporting Thermal Response Dataset

To support this calculation in CYDER, a reference data set of temperature change curves was calculated. Repeated runs of a detailed analytic model over the range of values in Table 5.3 determined STC values over a range of thermal heat limit radii, r_{lim} , thermal diffusivity values, α_{th} , thermal conductivity values, K_{th} and waste package spacings, S . Linear interpolation across the discrete parameter space provides a simple thermal reference dataset for use in CYDER.

Thermal Cases			
Parameter	Symbol	Units	Value Range
Diffusivity	α_{th}	$[m^2 \cdot s^{-1}]$	$1.0 \times 10^{-7} - 3.0 \times 10^{-6}$
Conductivity	K_{th}	$[W \cdot m^{-1} \cdot K^{-1}]$	0.1 – 4.5
Spacing	S	$[m]$	2, 5, 10, 15, 20, 25, 50
Radius	r_{lim}	$[m]$	0.1, 0.25, 0.5, 1, 2, 5
Isotope	i	$[-]$	$^{241,243}Am$, $^{242,243,244,245,246}Cm$, $^{238,240,241,242}Pu$, $^{134,135,137}Cs$, ^{90}Sr

Table 4.1: A thermal reference dataset of STC values as a function of each of these parameters was generated by repeated parameterized runs of the LLNL MathCAD model[35, 36].

The analytic model used to populate the reference dataset was created at LLNL for the UFD campaign. In this tool, heat limited thermal response is calculated analytically for each geologic medium, for many waste package loading densities, and for many fuel cycle options [35, 36, 40]. It employs an analytic model from Carslaw and Jaeger and is implemented in MathCAD [21, 79]. The integral solver in the MathCAD toolset is the primary calculation engine for the analytic MathCAD thermal model, which relies on superposition of point, finite-line, and line source integral solutions.

Figure 4.5 demonstrates the scaling of an STC curve according to equation (4.55) to represent the heat from 25.9g of initial ^{242}Cm using the reference data set.

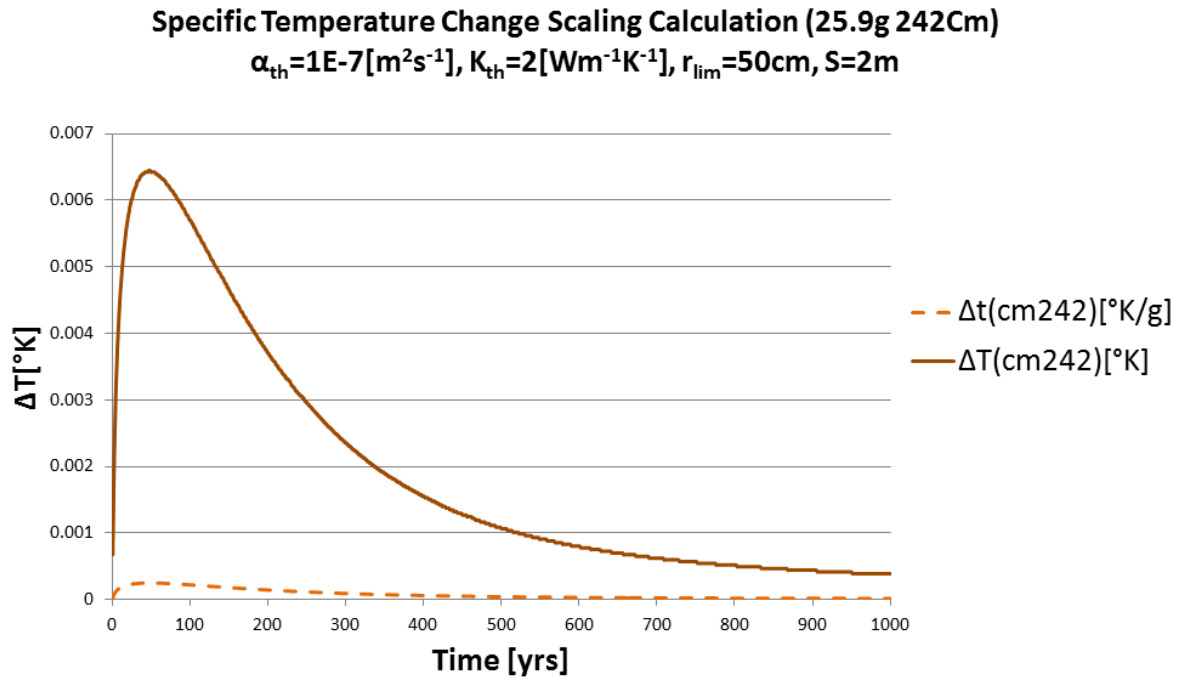


Figure 4.5: As a demonstration of the calculation procedure, the temperature change curve for one initial gram of ^{242}Cm and is scaled to represent 25.9g, approximately the ^{242}Cm inventory per MTHM in 51GWd burnup UOX PWR fuel.

The supporting database was limited to some primary heat contributing isotopes present in traditional spent nuclear fuel, H , such that the superposition in equation (4.56) becomes

$$\Delta T(r_{lim}, S, K_{th}, \alpha_{th}) \sim \sum_{i \in H} m_i \Delta t_i(r_{lim}, S, K_{th}, \alpha_{th}) \quad (4.57)$$

where

$H =$ set of high heat isotopes $[-]$

$S =$ uniform waste package spacing $[m]$

$K_{th} =$ thermal conductivity $[W \cdot m^{-1} \cdot K^{-1}]$

$\alpha_{th} =$ thermal diffusivity $[m^2 \cdot s^{-1}]$

(4.58)

The use of this superposition is demonstrated in Figure 4.6.

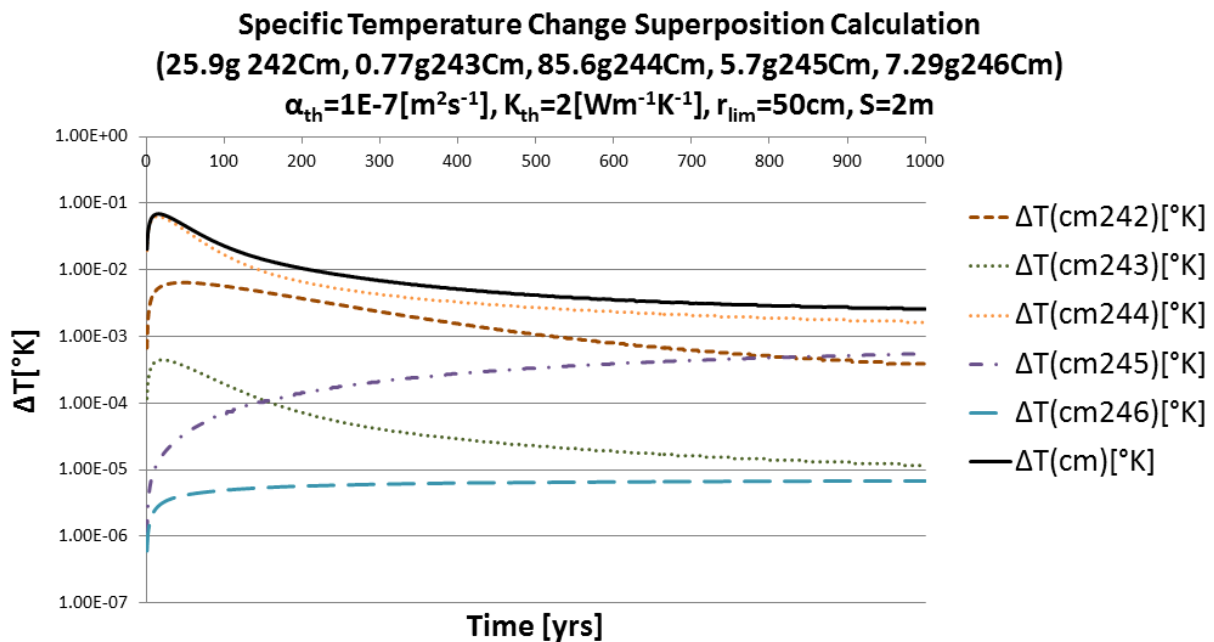


Figure 4.6: As a demonstration of the calculation procedure, scaled temperature change curves for five curium isotopes are superimposed to achieve a total temperature change (note log scale).

The primary outcome of this work is a multidimensional database of repository temper-

ature change per mass of high heat contributing isotopes supporting the implementation of the STC method in CYDER.

A validation effort concerning this tool was performed to assess the validity of the STC method for the purpose of repository thermal response estimation. Comparison of the results of this method with the LLNL model [35] gave results within the accuracy range of the model itself performs against the SINDA code [46] and demonstrated the way in which inaccuracies from neglected low heat contributing nuclides are bounded. Details of that comparison can be found in Appendix B.

Figures 4.7 and 4.8 show the results of one example validation exercise comparing the combined scaling and superposition calculations demonstrated in Figures 4.5 and 4.6 respectively. This particular validation example, containing no neglected nuclides, demonstrates an average error of 1.1% and a maximum error of 4.4%, where percent error is

$$\text{percent error} = 100 \times \frac{|\Delta T_{LLNL} - \Delta T_{STC}|}{\Delta T_{LLNL}}. \quad (4.59)$$

In addition to this validation effort, continual verification of code behavior is enabled by a suite of unit tests packaged with the tool. These tests are provided along with the source code so that they may be performed to evaluate the implemented behavior of units of functionality within the interpolation and specific temperature change algorithms even as the code is improved in the future.

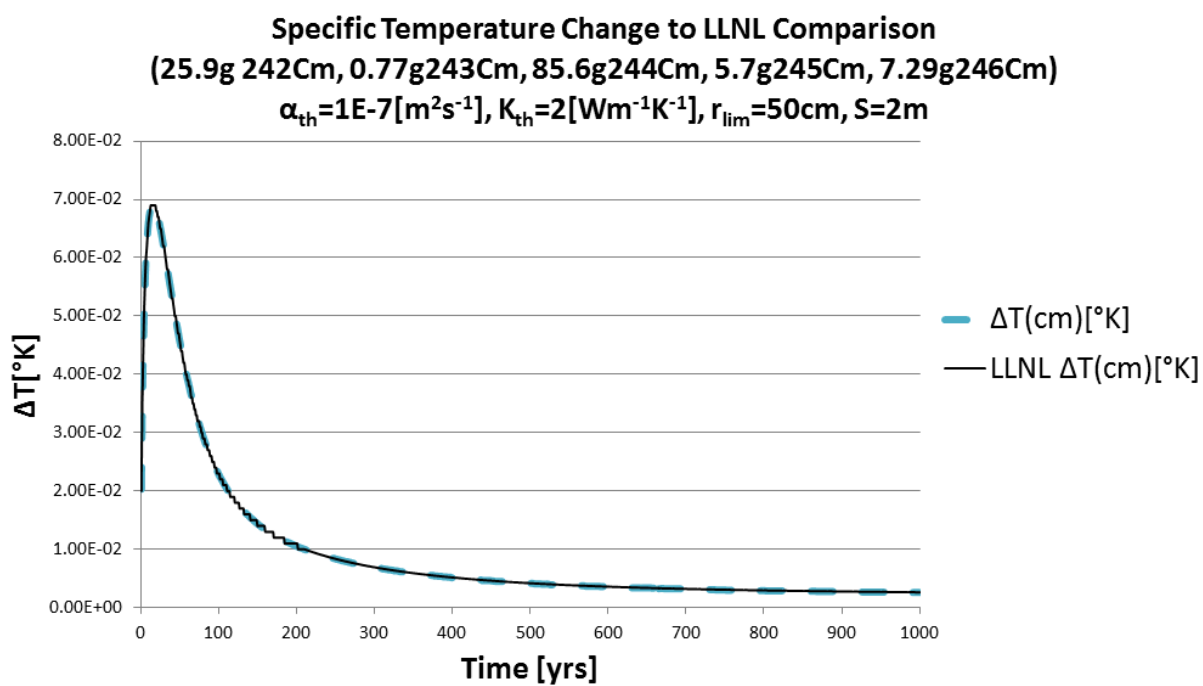


Figure 4.7: This comparison of STC calculated thermal response from Cm inventory per MTHM in 51GWd burnup UOX PWR fuel compares favorably with results from the semi-analytic model from LLNL.

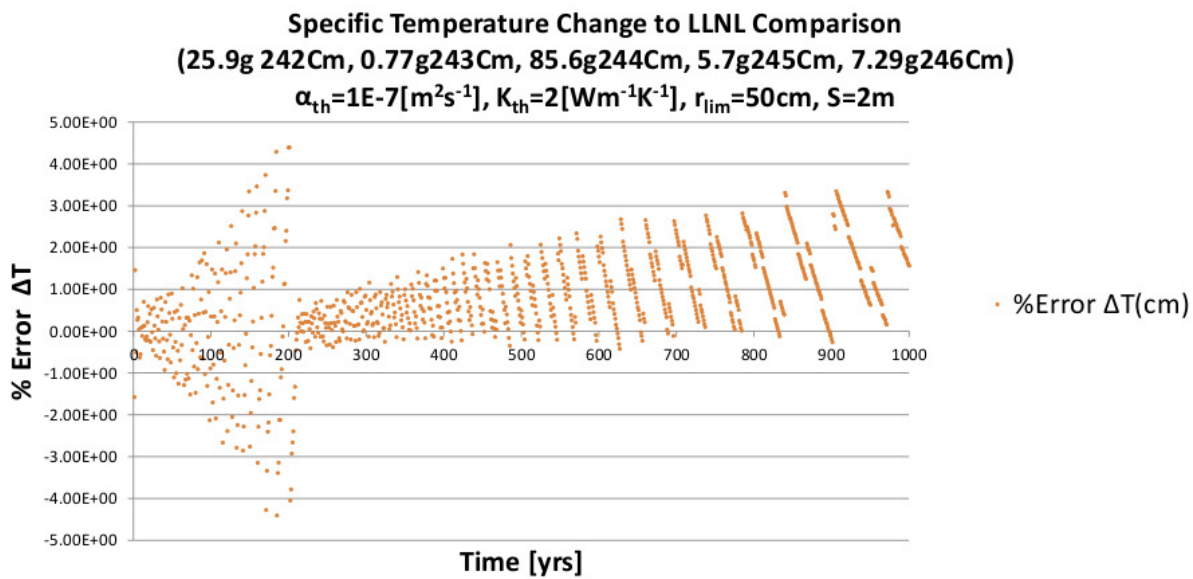


Figure 4.8: Percent error between the semi-analytic model from LLNL and the STC calculated thermal response from Cm inventory per MTHM in 51GWd burnup UOX PWR fuel demonstrates a maximum percent error of 4.4%.

5 DEMONSTRATION CASES AND BENCHMARKING

Basic verification of the integrated behavior of the components in the CYDER model was achieved with a suite of toy base cases and a suite of physics demonstrating validation comparisons.

The toy base cases were simplistic simulations that were intended to verify the fundamental behavior of the mass balance models and mass transfer modes. These aphysical but informative simulations were run to assess the simplistic behavior of an assembly of CYDER components within a simplistic CYCLUS simulation.

The physics demonstrations, on the other hand, sought to demonstrate that the dominant physics of repository performance were captured as intended by the various contaminant and thermal transport models implemented in CYDER.

5.1 Radionuclide Transport Base Cases

In the following base cases, basic transport behavior for aphysical parameterizations demonstrate the successful collective behavior of the modular components in a CYDER repository.

5.1.1 Basic Transport and Containment Problem Specification

Basic transport and containment base cases were conducted to verify the fundamental behavior of all the radionuclide transport models at each component interface. These integration tests neglected thermal transport and capacity estimation to simplify the results.

The problem design includes the following :

- A source facility providing one waste stream per time step
- An initial capacity of five 1 kg waste streams (in most cases)
- Waste form Components each accepting 1 waste stream
- Corresponding waste package Components, one per waste form
- A buffer Component
- A far field Component

5.1.1.1 Degradation Rate Model

The Degradation Rate model should not release contaminants if the degradation rate is 0. If the degradation rate is nonzero, however, and a fixed maximum transport mode is selected, contaminants should become available immediately to the adjacent components, traveling across the interfaces entirely at each time step.

To observe these behaviors, four simulations were run to demonstrate that, for the fixed maximum transfer mode, total containment resulted from a degradation rate of 0 and that congruent release resulted from nonzero degradation rates. In the four following simulations, a waste form with 1 kg is introduced to the repository once per time step for the first five time steps. Those five waste packages are placed into a single buffer component, which is contained by a single far field component. All are represented by the Degradation Rate Model.

Further details of these verification cases can be found in Table 5.1. The 0 degradation rate component was different for each of the four cases. This resulted in total containment at the Waste Form, Waste Package, Buffer, and Far Field interfaces respectively. Results of these base cases can be found in Figures 5.2 through 5.53.

Degradation Rate Model No Release Contaminant Transport

Case ID	Component [Type]	Degradation Rate [yr^{-1}]	Expected Release 100 yrs [%]	Actual Release 100 yrs [%]
DRI	WF	0	100	100
	WP	0.1	0	0
	BUFF	0.1	0	0
	FF	0.1	0	0
DRII	WF	0.1	0	0
	WP	0	100	100
	BUFF	0.1	0	0
	FF	0.1	0	0
DRIII	WF	0.1	0	0
	WP	0.1	0	0
	BUFF	0	100	100
	FF	0.1	0	0
DRIV	WF	0.1	0	0
	WP	0.1	0	0
	BUFF	0.1	0	0
	FF	0	100	100

Table 5.1: Results from demonstration cases for non-release from 0-degradation Degradation Rate modeled Components.

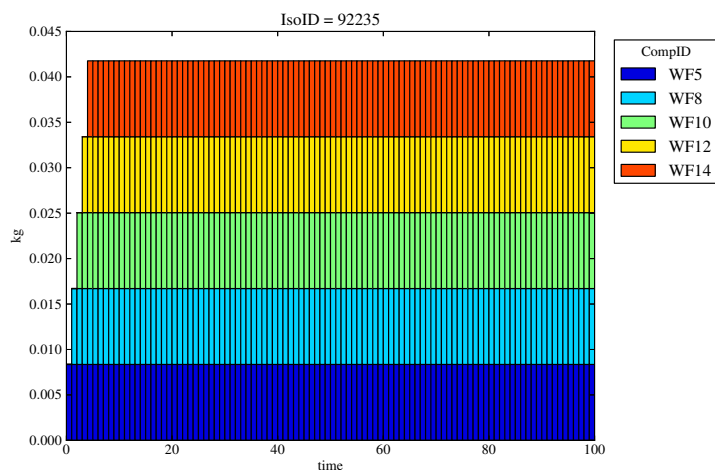


Figure 5.1: For Case DRI, in which total containment in the waste form is assumed ($F_{d,wf} = 0$), ^{235}U takes up permanent residence in the waste form component.

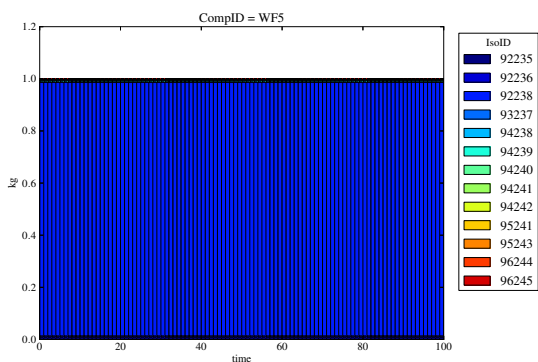


Figure 5.2: Waste Form 5 ($F_d = 0$) never releases material.

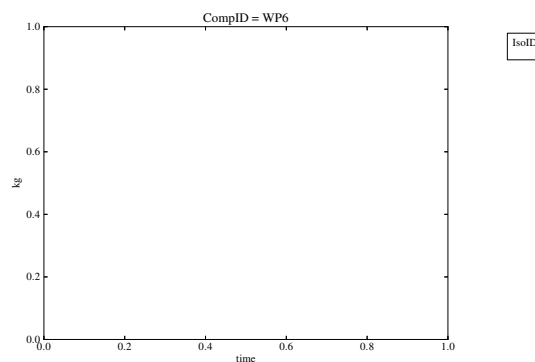


Figure 5.4: Waste Package 6 ($F_d = 0.1$), never receives material.

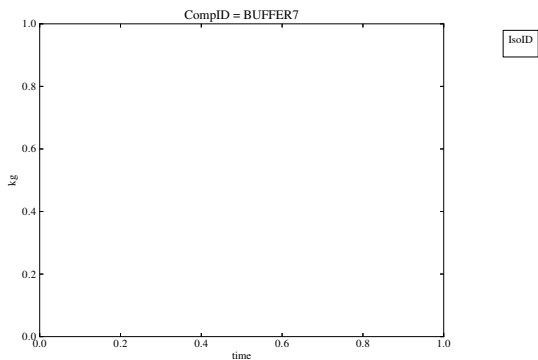


Figure 5.3: The Buffer, component 7 ($F_d = 0.1$), never receives material.

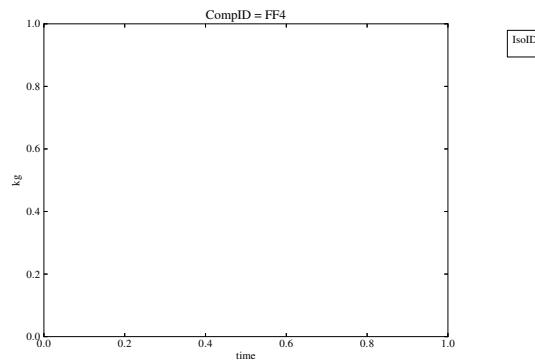


Figure 5.5: The Far Field, component 0 ($F_d = 0.1$), never receives material.

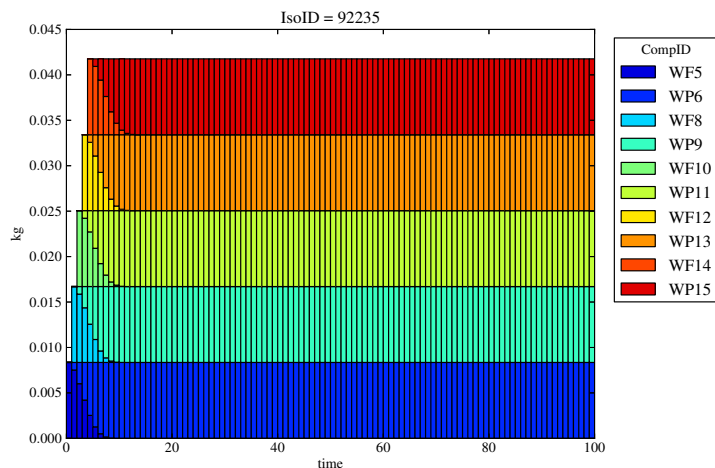


Figure 5.6: For Case DR11, in which total containment in the waste package is assumed ($F_{d,wp} = 0$), ^{235}U travels through waste forms ($F_d = 0.1$) before permanent residence in the waste package components.

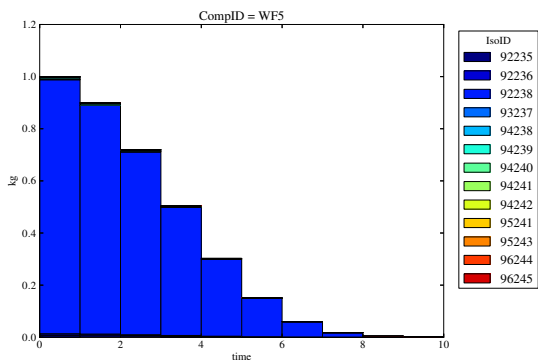


Figure 5.7: Waste Form 5 ($F_d = 0.1$) releases material with degradation.

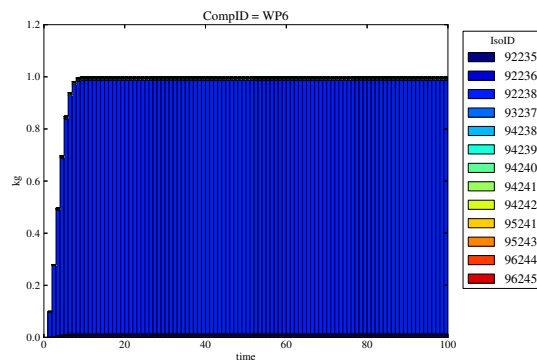


Figure 5.9: Waste Package 6 ($F_d = 0$) achieves total containment.

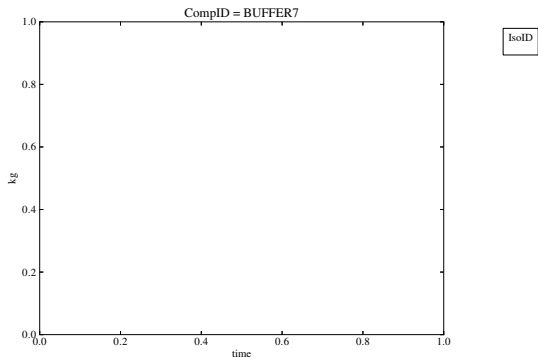


Figure 5.8: The Buffer, component 7 ($F_d = 0.1$), never receives material.

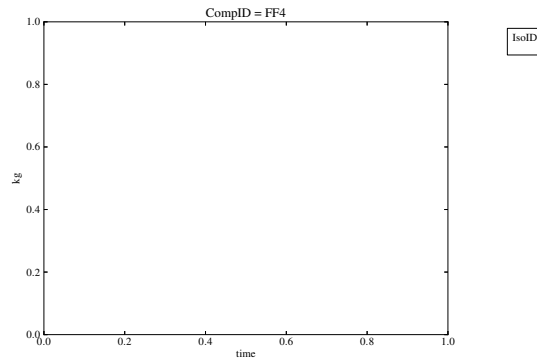


Figure 5.10: The Far Field, component 0 ($F_d = 0.1$), never receives material.

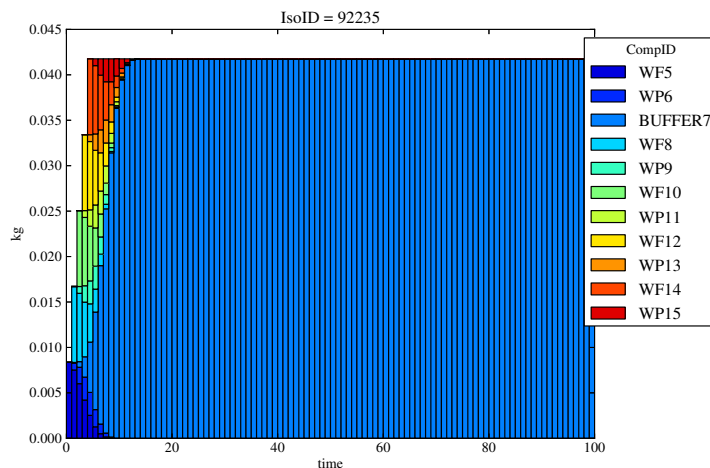


Figure 5.11: For Case DRIII, in which total containment in the buffer is assumed ($F_{d,buffer} = 0$), ^{235}U travels through waste forms and waste package components ($F_d = 0.1$) before permanent residence in the buffer component.

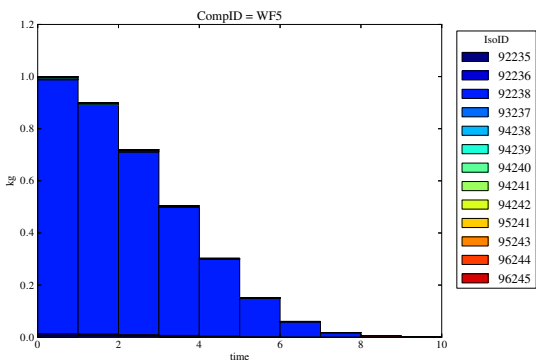


Figure 5.12: Waste Form 5 ($F_d = 0.1$) releases material with degradation.

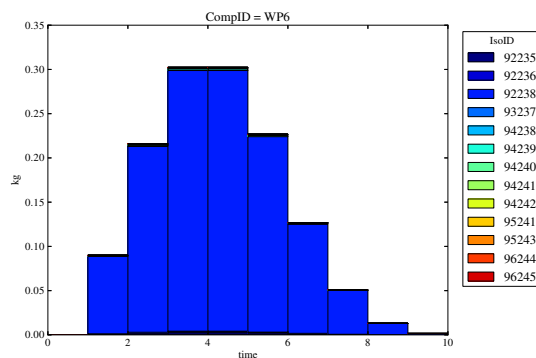


Figure 5.14: Waste Package 6 ($F_d = 0.1$) receives then releases material.

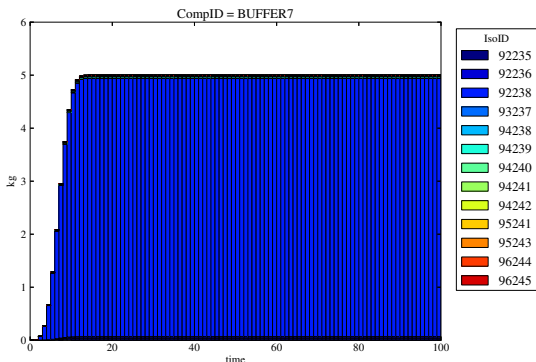


Figure 5.13: The Buffer, component 7 ($F_d = 0$), achieves total containment.

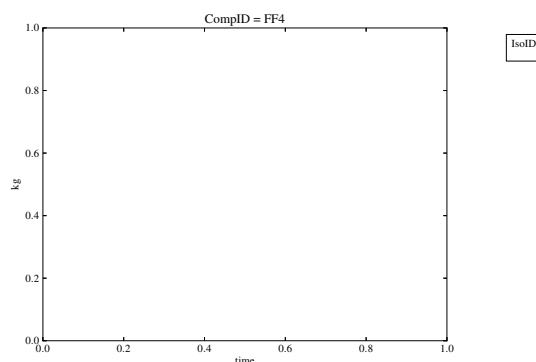


Figure 5.15: The Far Field, component 0 ($F_d = 0.1$), never receives material.

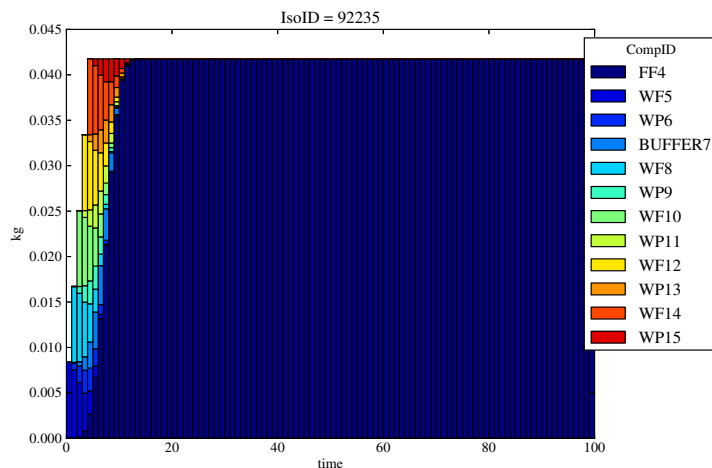


Figure 5.16: For DRIV case in which total containment in the far field is assumed ($F_{d,ff} = 0$), ^{235}U travels through interior components ($F_d = 0.1$) before permanent residence in the far field component.

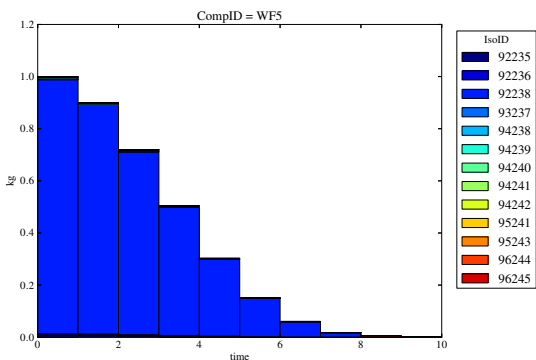


Figure 5.17: Waste Form 5 ($F_d = 0.1$) releases material with degradation.

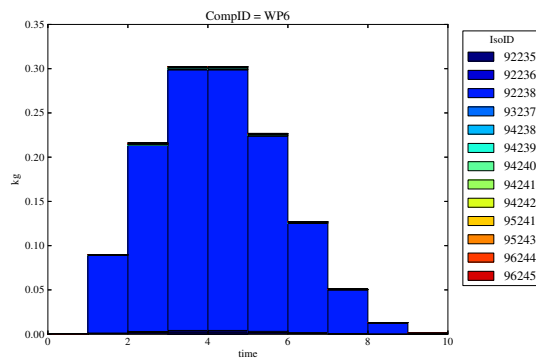


Figure 5.19: Waste Package 6 ($F_d = 0.1$) receives then releases material.

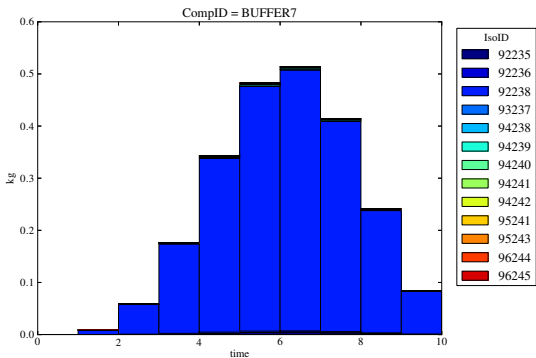


Figure 5.18: The Buffer, component 7 ($F_d = 0.0$), receives and then releases material.

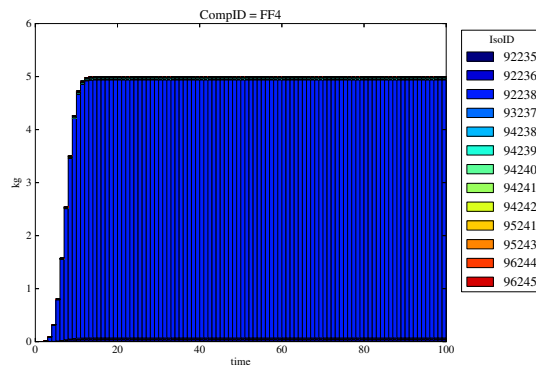


Figure 5.20: All material is released into Far Field, component 0 ($F_D = 0.0$).

5.1.1.2 Mixed Cell Model

The Mixed Cell model behaves similarly to the Degradation Rate model, when sorption and solubility limitation in that model are disabled (as in Figures 5.21 through 5.25). When they are enabled, however, the system is expected to demonstrate sorption limited and solubility limited transport as in Figures 5.26 through 5.30. The extent to which sorption and solubility limitation meet expectations is addressed in this base case.

Dual and single parameter verification cases were run to explore the effects of sorption and solubility limitation both separately and together. Results from two of these base cases can be found in Figures 5.21 through 5.30. The fixed maximum transport mode was used between mixed cell components for speed and clarity of results.

In the two following simulations, a waste form with 1 kg is introduced to the repository once per time step for the first five time steps. Those five waste packages are placed into a single buffer component, which is contained by a single far field component. All are represented by the Mixed Cell Model. Each component except the far field has a degradation rate of 0.1 per time step.

In the first of these two simulations, no sorption or solubility limitation is applied such that the results are, as expected, identical to the identical degradation rate case, DRIV.

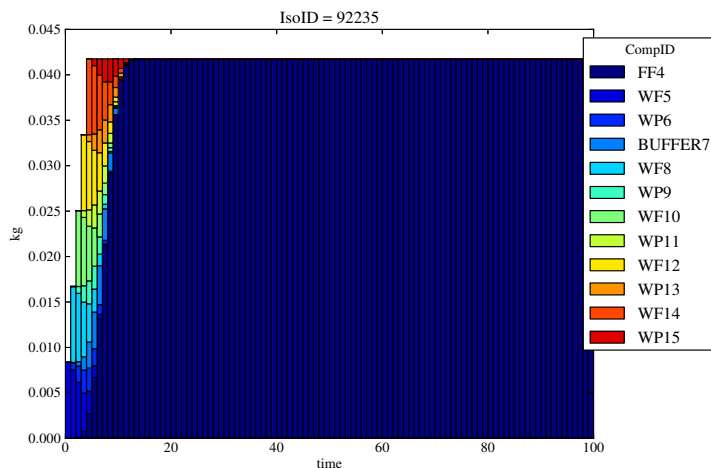


Figure 5.21: For the MCI case in which total containment is only assumed in the far field, but sorption and solubility limitation neglected, demonstrates results identical to DRIV, as expected.

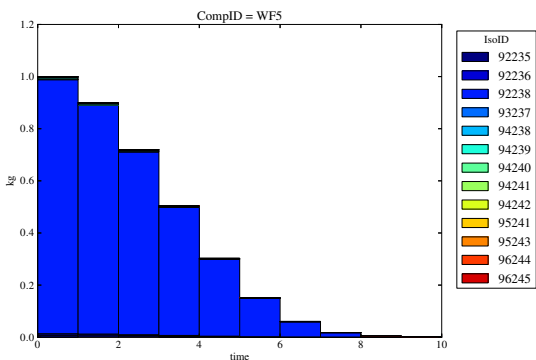


Figure 5.22: Waste Form 5 ($F_d = 0.1$) releases material with degradation.

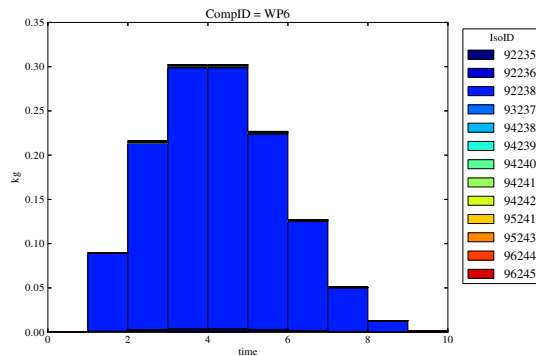


Figure 5.24: Waste Package 6 ($F_d = 0.1$) receives then releases material.

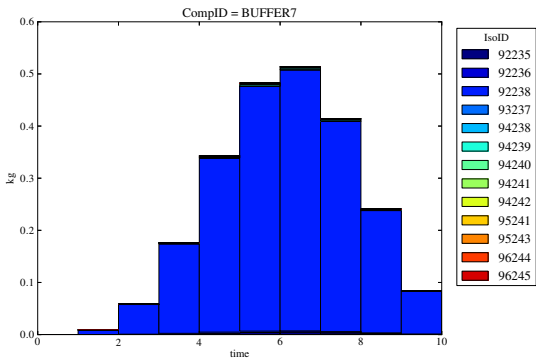


Figure 5.23: The Buffer, component 7 ($F_d = 0.1$), receives then releases material.

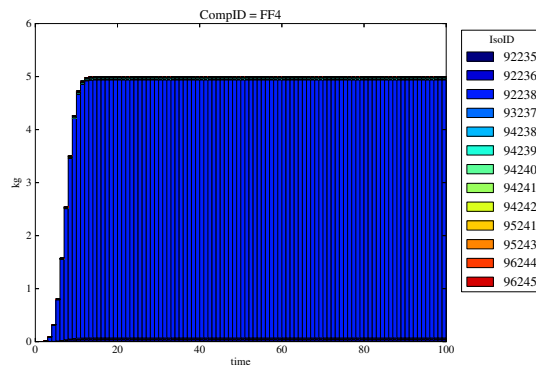


Figure 5.25: All material is released into the Far Field, component 4 ($F_d = 0.0$).

In the second of these two simulations, no sorption is applied, but solubility limitation is set to 0.001 kg/m^3 for all isotopes.

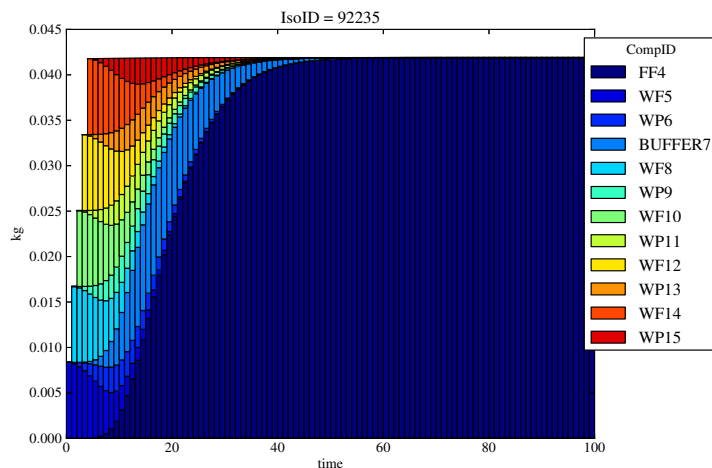


Figure 5.26: For the MCH case in which containment is affected by solubility limitation, ($F_d = 0.1$ for all components), ^{235}U travels more slowly than in the MCI case before permanent residence in the far field component.

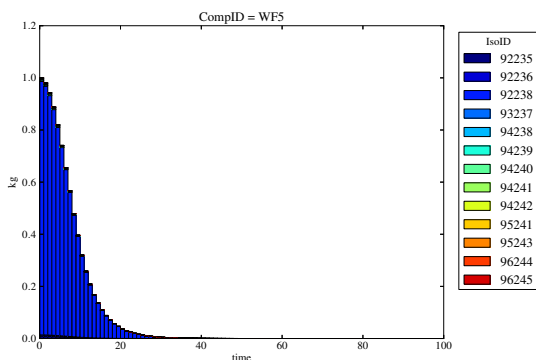


Figure 5.27: Waste Form 5 ($F_d = 0.1$, $S_{ref} = 0.001\text{kg}/\text{m}^3$) releases material with degradation.

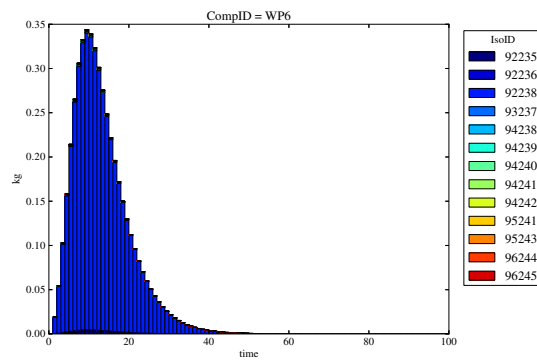


Figure 5.29: Waste Package 6 ($F_d = 0.1$, $S_{ref} = 0.001\text{kg}/\text{m}^3$) receives then releases material.

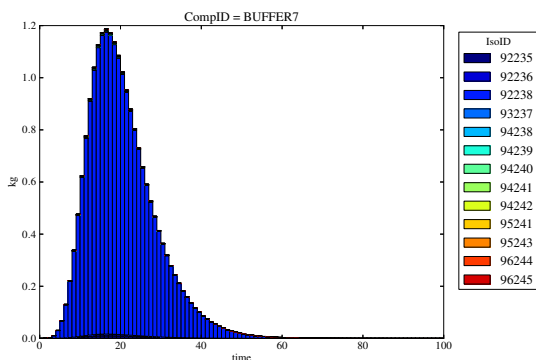


Figure 5.28: The Buffer, component 7 ($F_d = 0.1$, $S_{ref} = 0.001\text{kg}/\text{m}^3$), receives and then releases material.

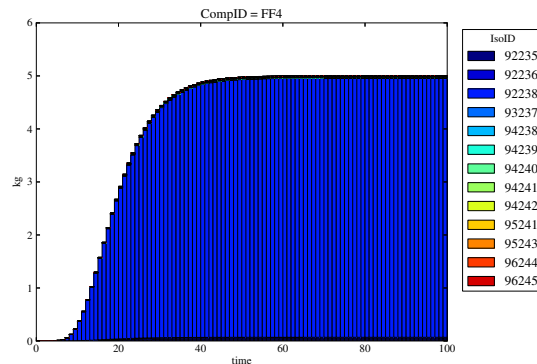


Figure 5.30: All material is released into the Far Field, component 4 ($F_d = 0.0$, $S_{ref} = 0.001\text{kg}/\text{m}^3$).

5.1.1.3 Lumped Parameter Model

The Lumped Parameter model, with its three formulations (Exponential Model, Dispersion Model, and Piston flow Model) is not expected to receive contaminants if the porosity or advective velocity are zero. Otherwise, contaminants are expected to become available to the adjacent components according to the functional forms of the formulations.

To observe the behaviors of each of the three formulations and to demonstrate full containment in cases where it is expected, simulations were run to investigate the impact of using various models. Results of these base cases can be found in Figures 5.36 through 5.35.

In the three following simulations, a waste form with 1 kg is introduced to the repository once per time step for the first five time steps. Those five waste packages are placed into a single buffer component, which is contained by a single far field component. All are represented by the Lumped Parameter Model.

In each of these three simulations, all of the components were represented by the Lumped Parameter model. The transit time was selected to be equal to one time step for each component. For the buffer component, the porosity was selected to be zero to halt flow.

In the first of these simulations, the Piston Flow Model (PFM) was selected from among the three response functions.

In the second of these simulations, the Exponential Model (EM) was selected from among the three response functions.

In the second of these simulations, the Dispersion Model (DM) was selected from among the three response functions.

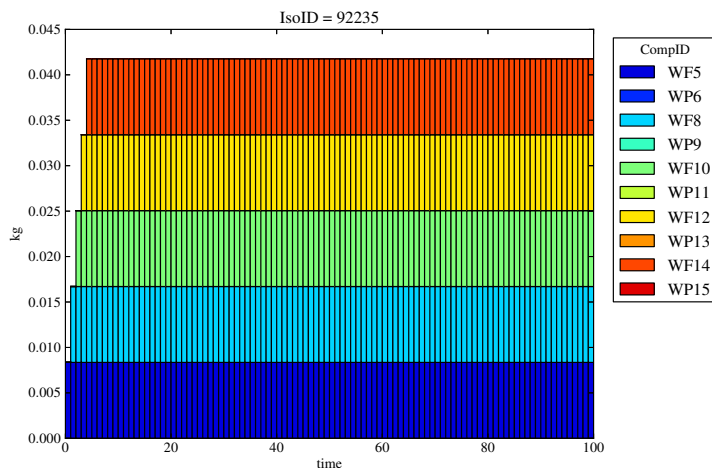


Figure 5.31: For the Piston Flow Model case, LPPFMII, in which total containment in the waste package is expected, ^{235}U travels through the waste form component ($\theta = 0.1$) before permanent residence in the waste package component ($\theta = 0.1$) because the buffer component accepts no material ($\theta = 0.0$).

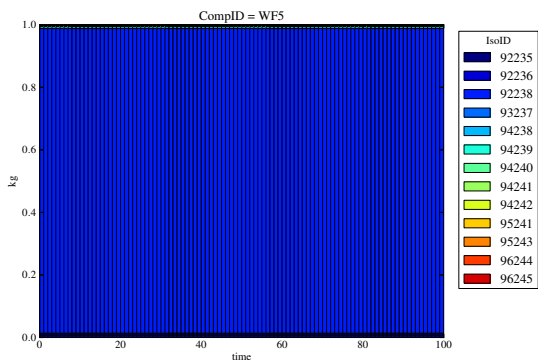


Figure 5.32: Waste Form 5 releases material.

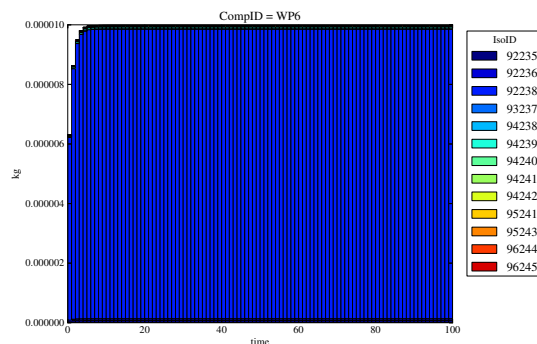


Figure 5.34: Waste Package 6 achieves total containment.

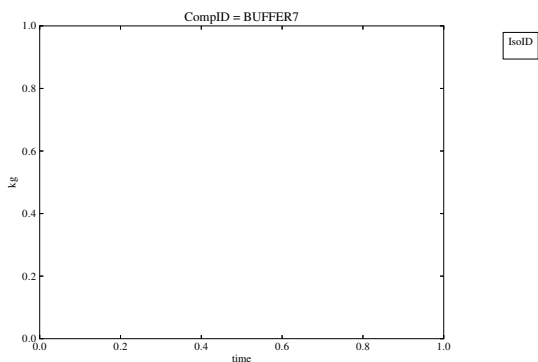


Figure 5.33: The Buffer, component 7, never receives material.

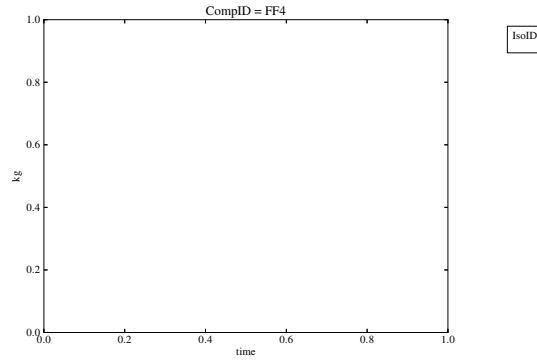


Figure 5.35: The Far Field, component 4, never receives material.

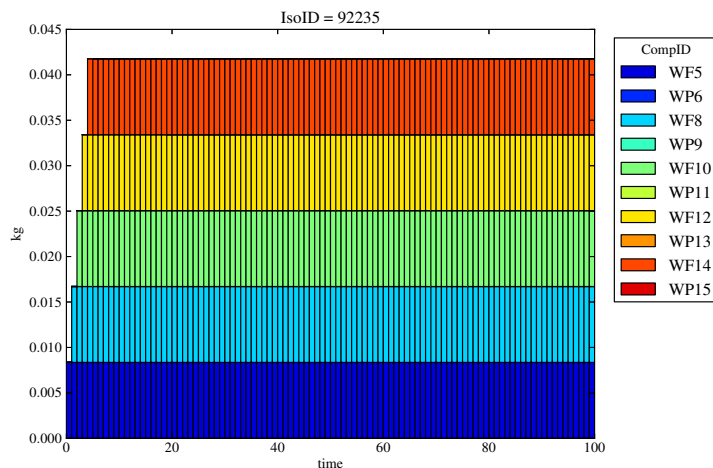


Figure 5.36: For the Exponential Model case, LPEMII, in which total containment in the waste package is expected, ^{235}U travels through the waste form component ($\theta = 0.1$) before permanent residence in the waste package component ($\theta = 0.1$) because the buffer component accepts no material ($\theta = 0.0$).

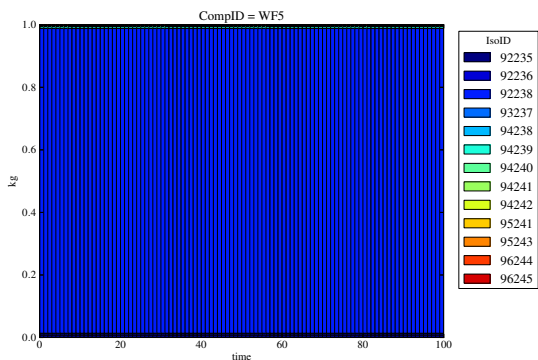


Figure 5.37: Waste Form 5 releases material.

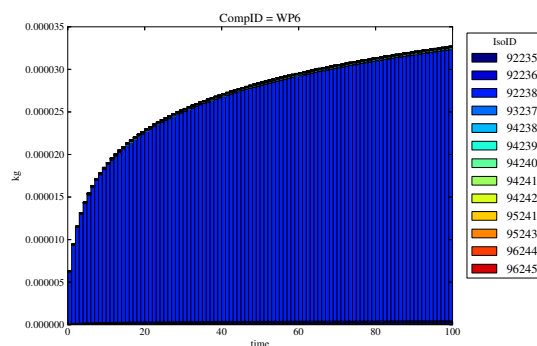


Figure 5.39: Waste Package 6 achieves total containment.

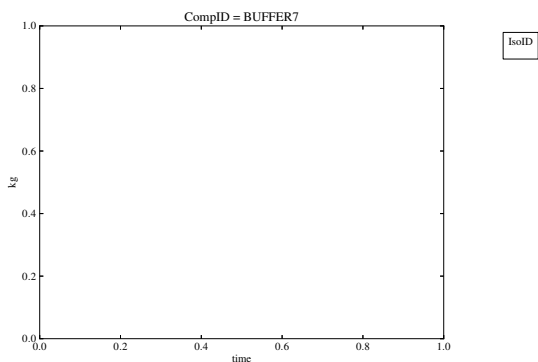


Figure 5.38: The Buffer, component 7, never receives material.

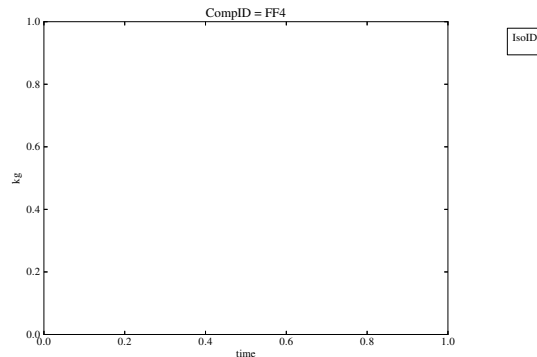


Figure 5.40: The Far Field, component 4, never receives material.

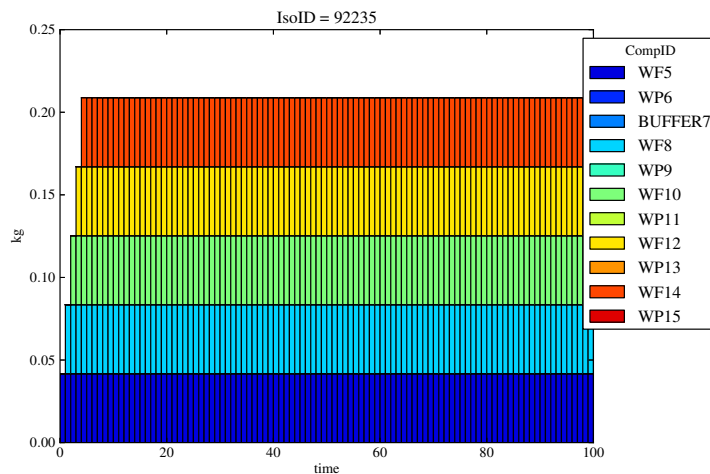


Figure 5.41: For the Dispersion Model case, LPEMII, in which total containment in the waste package is expected, ^{235}U travels through the waste form component ($\theta = 0.1$) before permanent residence in the waste package component ($\theta = 0.1$) because the buffer component accepts no material ($\theta = 0.0$).

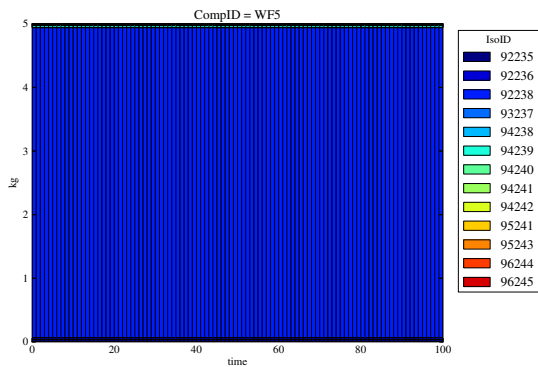


Figure 5.42: Waste Form 5 releases material.

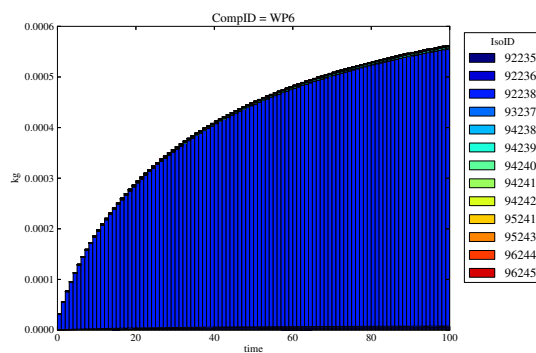


Figure 5.44: Waste Package 6 achieves total containment.

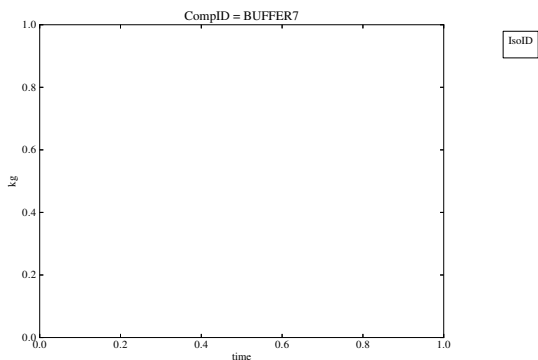


Figure 5.43: The Buffer, component 7, never receives material.

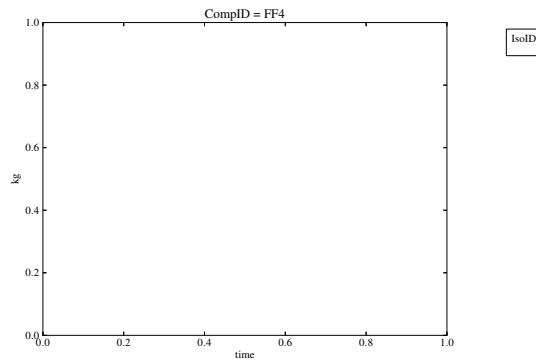


Figure 5.45: The Far Field, component 4, never receives material.

The transit time that parameterizes these models could be based on radioactive tracer experiments in the laboratory. Figures 5.46 and 5.48 demonstrate the dependence of the resulting transport on transit time parameterization. These profiles demonstrate the trends seen in the analytical results demonstrated in Maloszewski and Zuber [65].

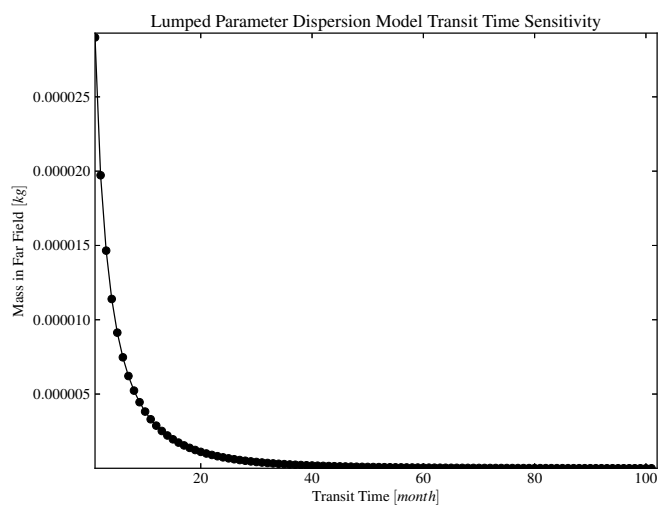


Figure 5.46: The transit time parameterization of the lumped parameter dispersion model of radionuclide transport has a strong effect on the material reaching the far field after 30 years.

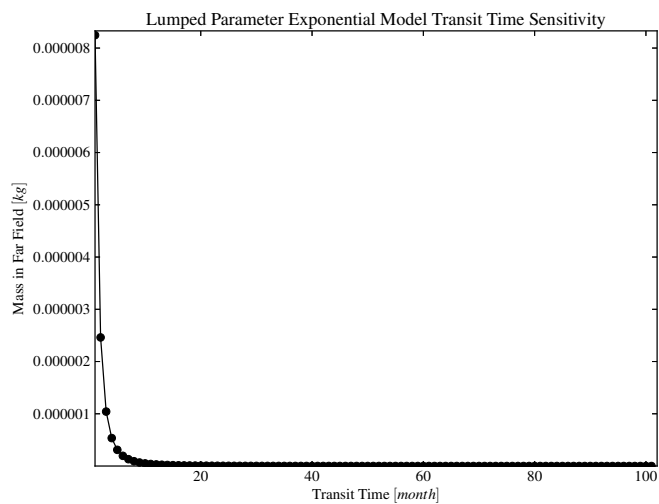


Figure 5.47: The transit time parameterization of the lumped parameter exponential model of radionuclide transport has a strong effect on the material reaching the far field after 30 years.

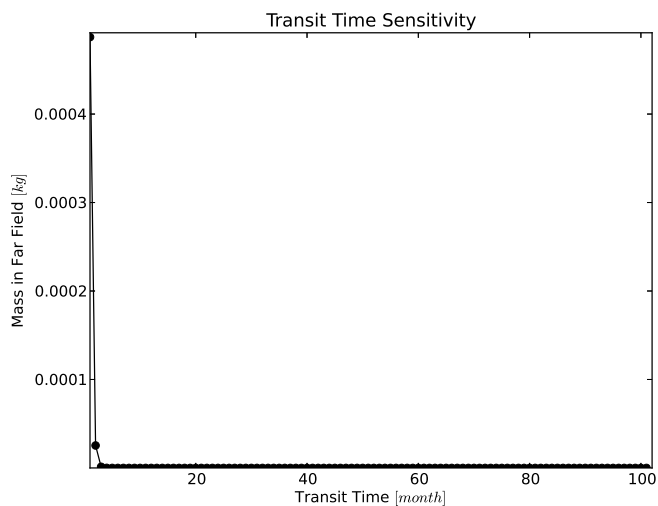


Figure 5.48: The transit time parameterization of the lumped parameter piston flow model of radionuclide transport has a strong effect on the material reaching the far field after 30 years.

5.1.1.4 One Dimensional Permeable Porous Medium Model

The One Dimensional PPM Model does not release contaminants if the porosity is zero or if both the reference diffusivity and advective velocity are zero. Otherwise, however, contaminants are expected to become available to the adjacent components according to the analytical form of the solution. The solution is only valid for advection and dispersion values within a realistic range, and the model accordingly can only be demonstrated for a very slow transport case.

To observe the behavior of the solution and to demonstrate full containment in cases where it is expected, simulations were run with each component represented by a One Dimensional PPM Model, which uses an implicit mass transfer mode. An example simulation, with reference dispersion coefficient at 1×10^{-12} m/s² and advective velocity of 1×10^{-15} m/yr. In this simulation, a waste form with 1000 kg is loaded into a waste package. That waste package is the only package in the buffer and far field components that contain it.

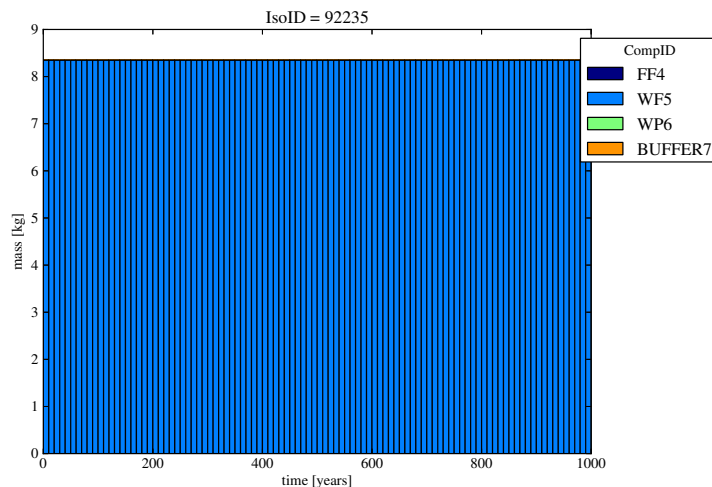


Figure 5.49: For the case in which transport through all components is represented by the 1 Dimensional PPM model, material moves very slowly into the far field.

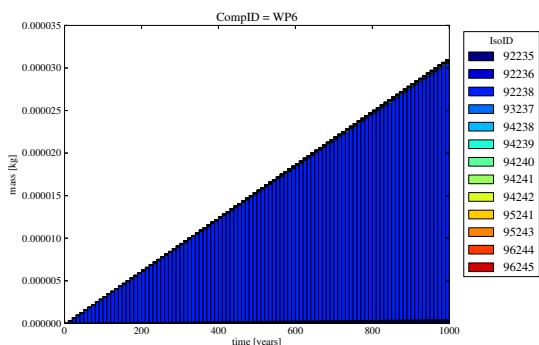


Figure 5.50: Waste Form 5 slowly releases material into Waste Package 6.

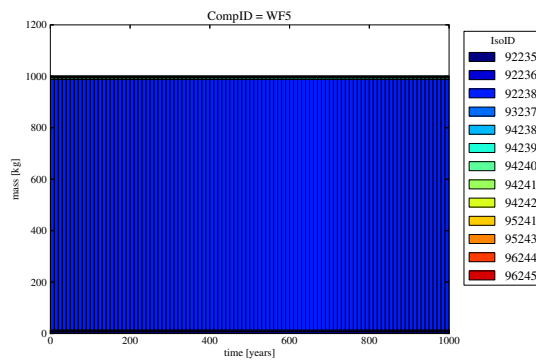


Figure 5.52: Waste Package 6 very slowly receives then releases material.

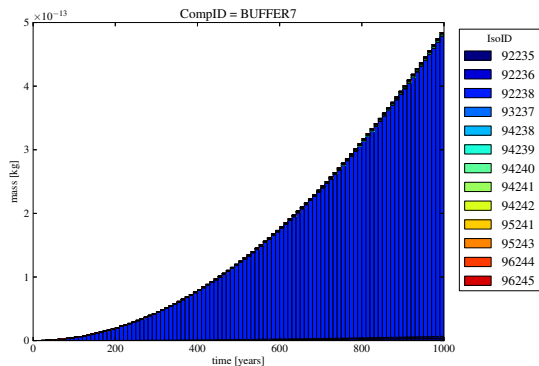


Figure 5.51: The Buffer, component 7 very slowly receives then releases material.

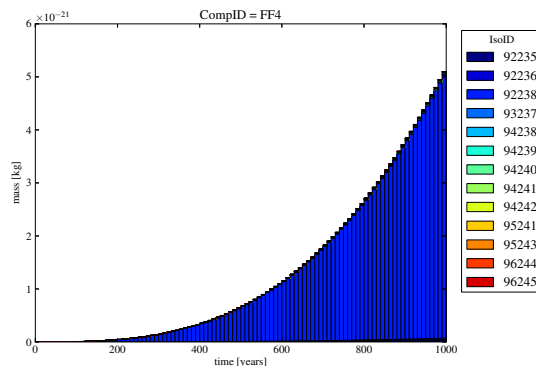


Figure 5.53: All material is released into Far Field, component 4.

is shown in Figure 5.49.

5.2 Radionuclide Transport Validation

As described in Section 4.1, hydrologic contaminant transport in CYDER is implemented with four interchangeable methods in a modular software design. These modeling options alternately optimize speed and fidelity in representations of barrier components within the repository concept (i.e. waste form, waste package, buffer, and geologic medium)[49]. Simplistic models include a congruent release component degradation rate model and a mixed cell control volume model. For systems in which the flow can be assumed constant, a medium fidelity lumped parameter dispersion model is implemented. Also implemented is a Brenner approximation to the Leij et al. solution to the advection dispersion equation for Cauchy boundary condition [19, 60, 95].

Analyses in Table 5.2 were conducted to compare the performance of these radionuclide transport models with more detailed results from the Clay Generic Disposal System Environment (GDSE).

5.2.1 Case I : Vertical Advective Velocity and Diffusion

Coefficient Sensitivity

5.2.1.1 Advection vs. Diffusion Sensitivity GDSM Results

In the parametric sensitivity analysis discussed in section A.4.1, it was shown that for isotopes of interest, higher advective velocity and higher diffusivity lead to higher peak annual doses. However, the relationship between diffusivity and advective velocity adds depth to the notion of a boundary between diffusive and advective regimes.

Radionuclide Transport Benchmark Cases

Parameter	Symbol	Units	Value Range
Hydraulic Reference Diffusivity	$\alpha_{h,ref}$	$[m^2 s]$	$10^{-15} - 10^{-8}$
Hydraulic Conductivity	K_h	$[m \cdot s^{-1}]$	$10^{-13} - 10^{-3}$
Advective Water Velocity	v_{adv}	$[m \cdot s^{-1}]$	$2 \times 10^{-16} - 2 \times 10^{-12}$
Sorption & Behavior	$K_{d,i}$	$[m^3 \cdot kg^{-1}]$	Reducing - Oxidizing
Solubility Limitation	$C_{sol,i}$	$[kg \cdot m^{-3}]$	Reducing - Oxidizing
WF Degradation Rate	f_{wf}	$[month^{-1}]$	0.0001 – 0.9

Table 5.2: The sensitivity analyses conducted in this work covered a range of thermal and hydrologic parameters in the context of canonical fuel cycle choices.

The highly soluble and non-sorbing elements, I and Cl were expected to exhibit behavior that is highly sensitive to advection in the system in the advective regime but less sensitive to advection in the diffusive regime.

In Figures 5.54, 5.55, 5.56, and 5.57, ^{129}I and ^{36}Cl are more sensitive to vertical advective velocity for lower vertical advective velocities. This demonstrates that for vertical advective velocities 6.31×10^{-6} m/yr and above, lower reference diffusivities are ineffective at attenuating the mean of the peak doses for soluble, non-sorbing elements.

The solubility limited and sorbing elements, Tc and Np , in Figures 5.58, 5.59, 5.60, and 5.61 show a very weak influence on peak annual dose rate for low reference diffusivities, but show a direct proportionality between dose and reference diffusivity above a threshold. For ^{99}Tc , for example, that threshold occurs at 1×10^{-11} m²/s.

Dose contribution from ^{99}Tc has a proportional relationship with vertical advective velocity above a regime threshold at 6.31×10^{-5} m/yr, above which the system exhibits sensitivity to advection.

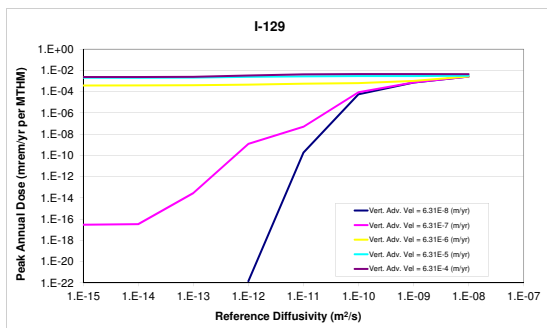


Figure 5.54: ^{129}I reference diffusivity sensitivity.

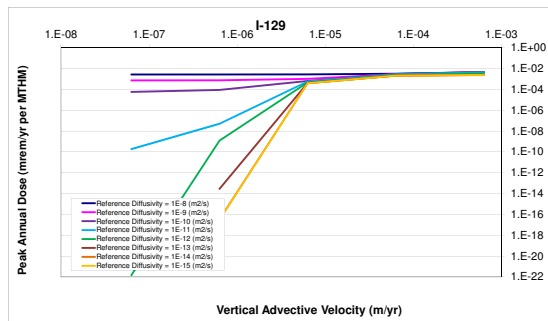


Figure 5.55: ^{129}I vertical advective velocity sensitivity.

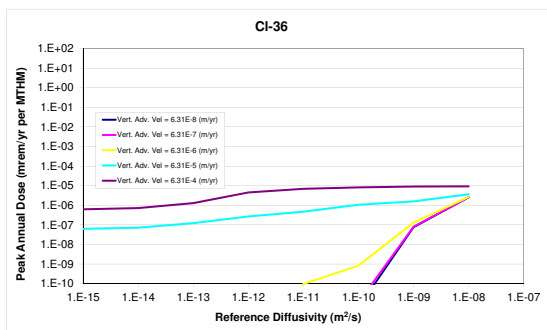


Figure 5.56: ^{36}Cl reference diffusivity sensitivity.

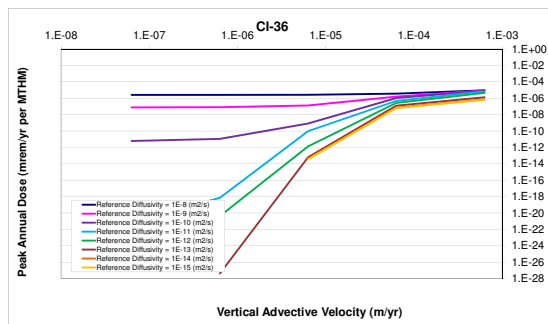


Figure 5.57: ^{36}Cl vertical advective velocity sensitivity.

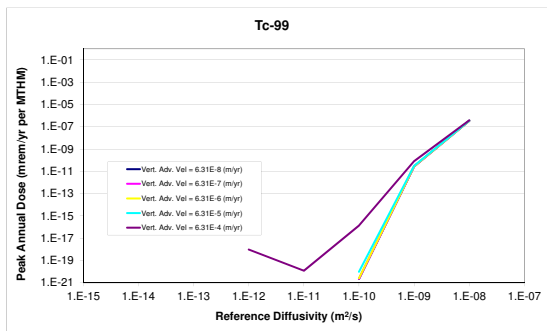


Figure 5.58: ^{99}Tc reference diffusivity sensitivity.

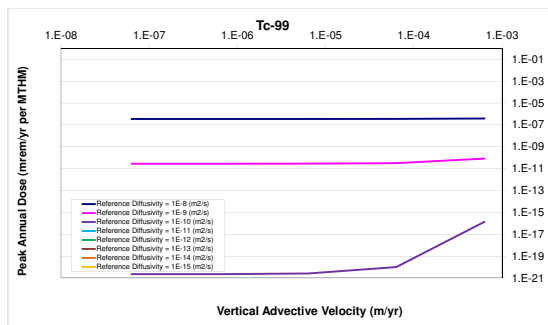


Figure 5.59: ^{99}Tc vertical advective velocity sensitivity.

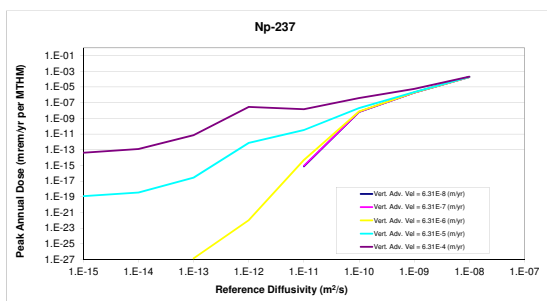


Figure 5.60: ^{237}Np reference diffusivity sensitivity.

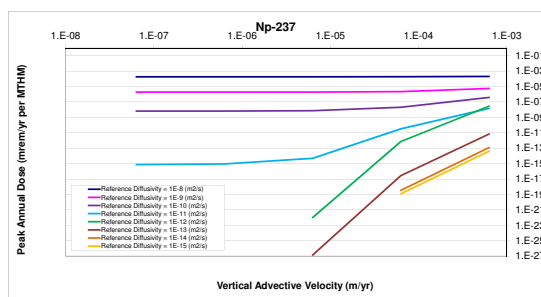


Figure 5.61: ^{237}Np vertical advective velocity sensitivity.

The convergence of the effect of the reference diffusivity and vertical advective velocity for the cases above shows the effect of dissolved concentration (solubility) limits and sorption. Se is non-sorbing, but solubility limited. The results from ^{79}Se in Figure 5.62 and 5.63 show that for low vertical advective velocity, the system is diffusion dominated. However, for high vertical advective velocity, the diffusivity remains important even in the advective regime as spreading facilitates transport in the presence of solubility limited transport.

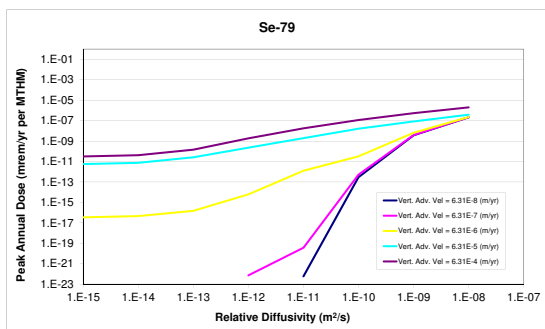


Figure 5.62: ^{79}Se reference diffusivity sensitivity.

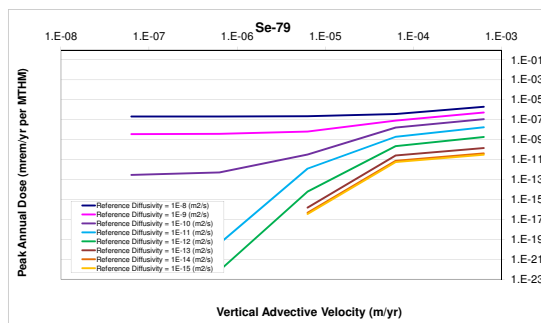


Figure 5.63: ^{79}Se vertical advective velocity sensitivity.

5.2.1.2 Advection vs. Diffusion Sensitivity Cyder Results

Some of the radionuclide transport models in CYDER depend on the advective velocity as well as the diffusion characteristics of the medium. By evaluating the sensitivity to the advective velocity and reference diffusivity of the radionuclide transport in the MixedCell model, trends similar to those found in the GDSM were found with the CYDER tool. Specifically, increased advection and increased diffusion lead to greater release. Also, when both are varied, a boundary between diffusive and advective regimes can be seen. An example of these results are shown in Figure 5.64.

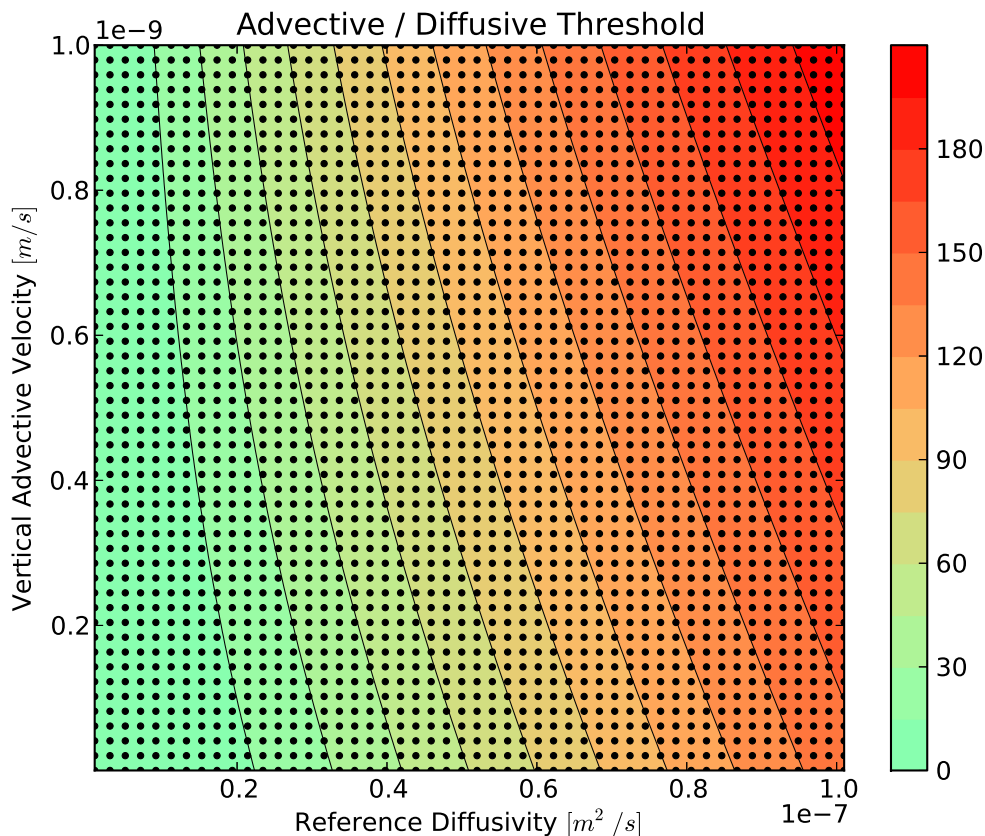


Figure 5.64: Dual advective velocity and reference diffusivity sensitivity for a non-sorbing, infinitely soluble nuclide.

5.2.2 Case II : Solubility Sensitivity

In the parametric sensitivity analysis discussed in section A.4.3, it was shown that for solubility limits below a certain threshold, the dose releases were directly proportional to the solubility limit, indicating that the radionuclide concentration saturated the groundwater up to the solubility limit near the waste form. For solubility limits above the threshold, however, further increase to the limit had no effect on the peak dose. This demonstrates the situation in which the solubility limit is so high that even complete dissolution of the waste inventory into the pore water is insufficient to reach the solubility limit.

In Figures 5.65 and 5.66, it is clear that for solubility constants lower than a threshold, the transport regime is solubility limited and the relationship between peak annual dose and solubility limit is strong. Above the threshold, the transport regime is inventory limited instead.

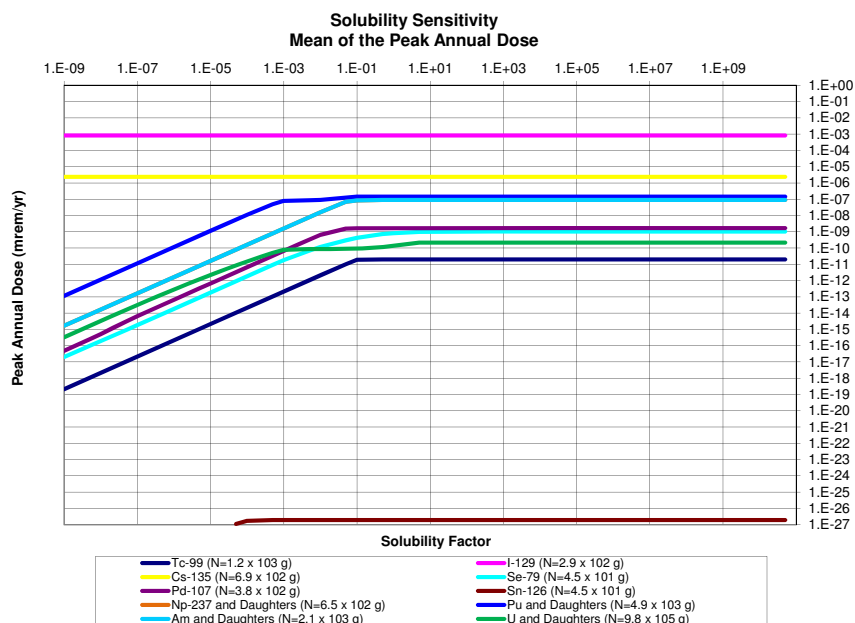


Figure 5.65: Solubility factor sensitivity. The peak annual dose due to an inventory, N , of each isotope.

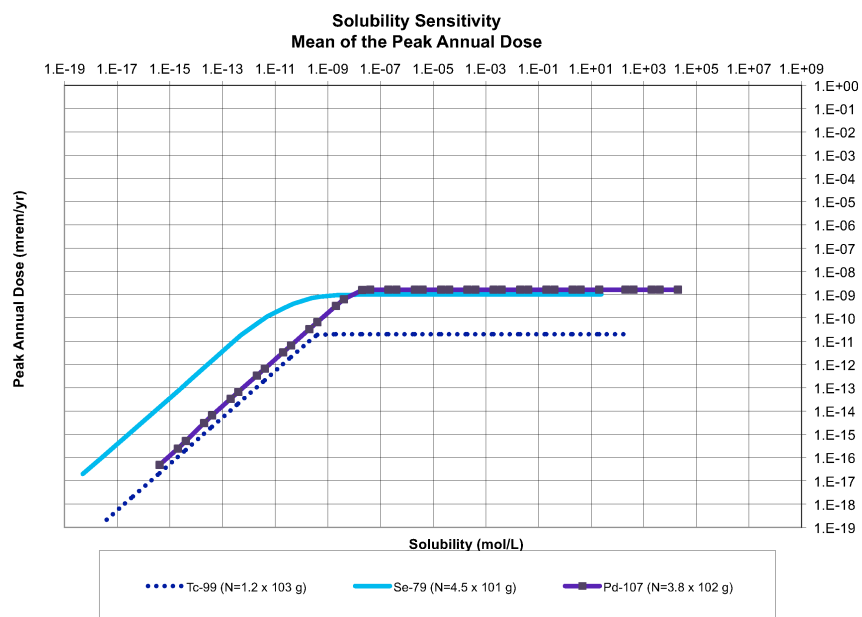


Figure 5.66: Solubility limit sensitivity. The peak annual dose due to an inventory, N , of each isotope.

In the parametric analysis of CYDER performance, it was shown that the solubility sensitivity behavior closely matched that of the GDSM sensitivity behaviors. Specifically, in Figure 5.67, a sharp turnover is seen where the solubility limit exceeds the point at which it limits movement. For increased solubility limits, release remains constant.

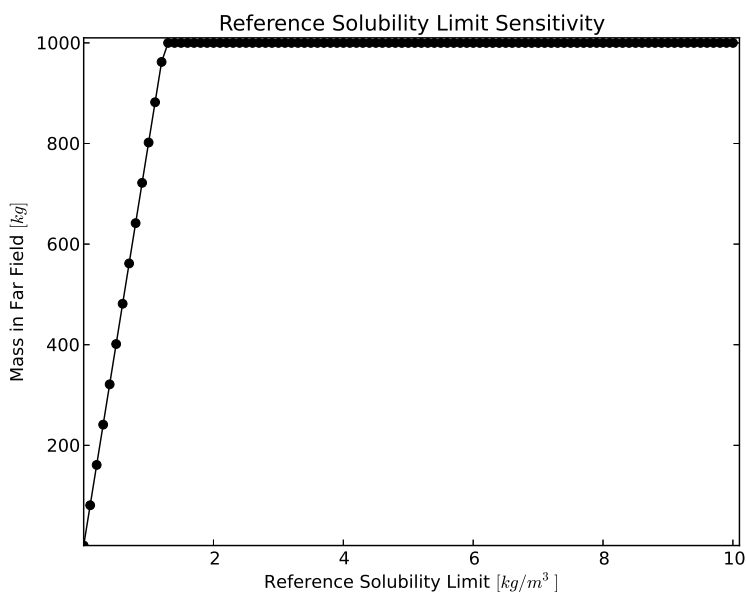


Figure 5.67: Sensitivity demonstration of solubility limitation in CYDER for an arbitrary isotope assigned a variable solubility limit.

5.2.3 Case III : Sorption Sensitivity

5.2.3.1 Reference Distribution Coefficient Sensitivity

As the distribution coefficient K_d , and therefore the retardation coefficient R_f increase, contaminants tend toward the solid phase. An increase in these coefficients, then, has the effect of limiting dissolved concentration.

In the parametric sensitivity analysis discussed in Section A.4.4, the expected inverse relationship between the retardation factor and resulting peak annual dose was found for all elements that were not assumed to be effectively infinitely soluble. In the low retardation coefficient cases, a regime is established in which the peak annual dose is entirely unaffected by changes in retardation coefficient.

For large values of retardation coefficient, the sensitivity to small changes in the

retardation coefficient increases dramatically. In that sensitive regime, the change in peak annual dose is inversely related to the retardation coefficient. Between these two regimes was a transition regime, in which the K_d factor ranges from 1×10^{-5} to 5×10^0 [-].

It is clear from Figures 5.68 and 5.69 that for retardation coefficients greater than a threshold, the relationship between peak annual dose and retardation coefficient is a strong inverse one.

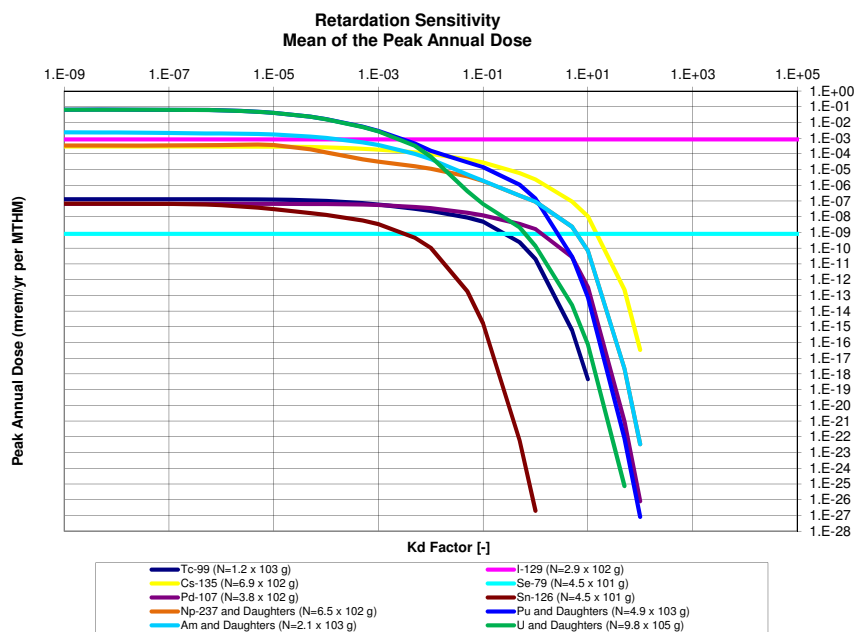


Figure 5.68: K_d factor sensitivity. The peak annual dose due to an inventory, N , of each isotope.

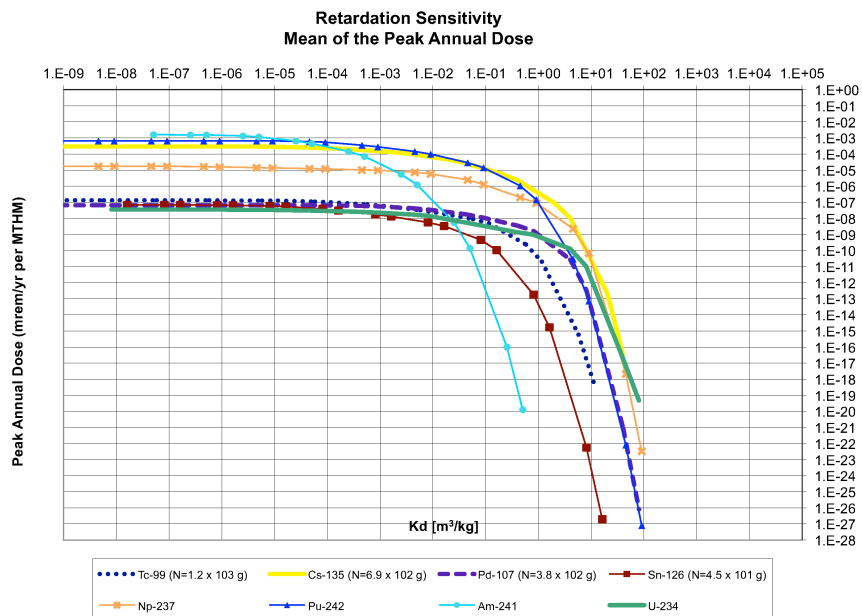


Figure 5.69: K_d sensitivity. The peak annual dose due to an inventory, N , of each isotope.

5.2.3.2 Reference Sorption Coefficient Sensitivity

In the parametric analysis of CYDER performance, it was shown that sorption sensitivity behavior closely matched that of the GDSM sensitivity behaviors. Specifically, in Figure 5.70, increasing the retardation coefficient results in a smooth but dramatic turnover.

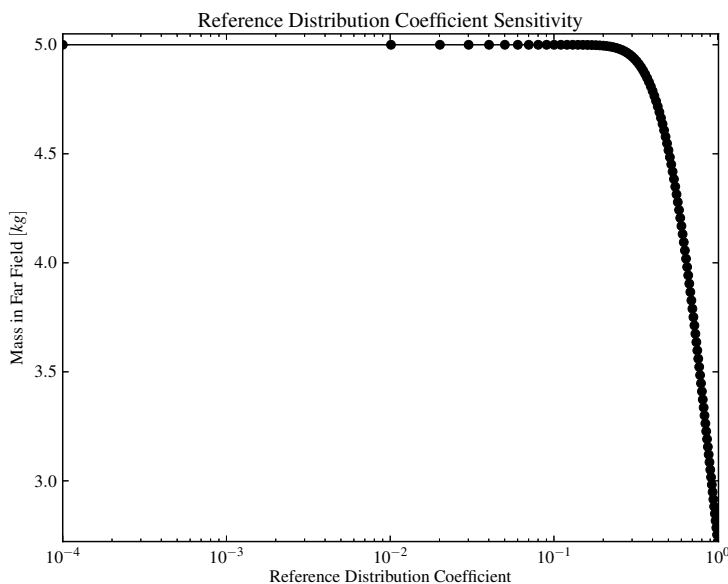


Figure 5.70: K_d sensitivity in the CYDER tool for an arbitrary isotope assigned a variable K_d coefficient.

5.2.4 Case IV : Waste Form Degradation Rate and Inventory Sensitivity

5.2.4.1 Waste Form Degradation Rate and Contaminant Inventory Sensitivity

In the parametric sensitivity analysis discussed in Section A.4.5, the results showed two regimes. In the first regime, the mean of the peak annual dose rates is directly proportional to both the mass factor (an inventory mass multiplier) and the fractional waste form degradation rate. For some radionuclides, attenuation occurs for high values of both parameters as the release of radionuclides is limited by dispersion parameters. This phenomenon can be seen in the figures below in which transition between regimes for higher degradation rates happens at lower mass factors than transition between regimes for lower degradation rates.

The peaks for highly soluble, non-sorbing elements such as I and Cl are directly proportional to mass factor for most values of waste form degradation rates. This effect can be seen in Figures 5.71, 5.72, 5.73, and 5.74.

Highly soluble and non-sorbing ^{129}I demonstrates a direct proportionality between dose rate and fractional degradation rate until a turnover where other natural system parameters dampen transport. Highly soluble and non-sorbing ^{129}I demonstrates a direct proportionality to the mass factor.

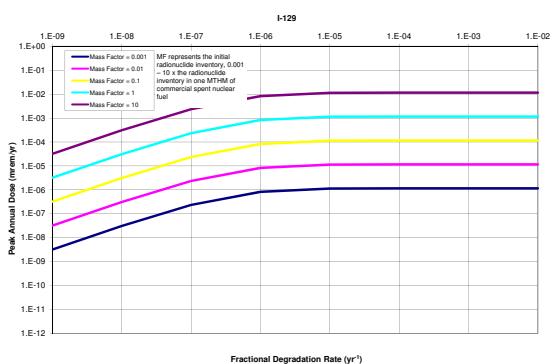


Figure 5.71: ^{129}I waste form degradation rate sensitivity.

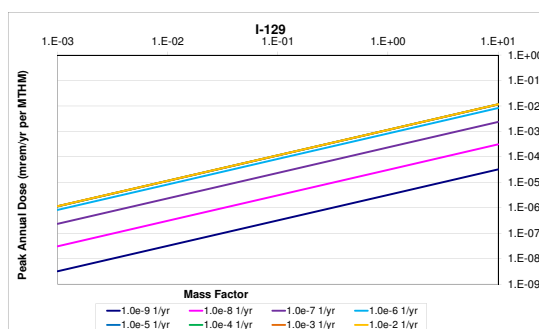


Figure 5.72: ^{129}I mass factor sensitivity.

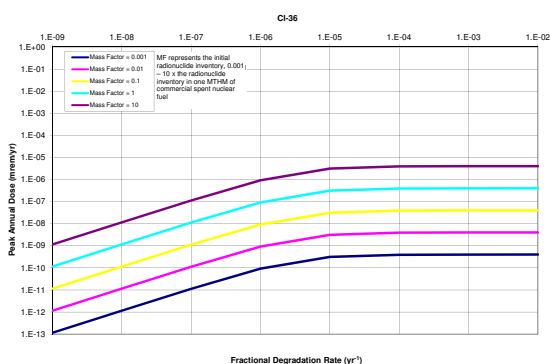


Figure 5.73: ^{36}Cl waste form degradation rate sensitivity.

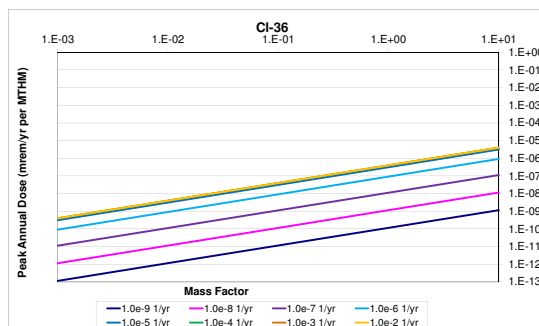


Figure 5.74: ^{36}Cl mass factor sensitivity.

The peaks for solubility limited, sorbing elements such as Tc and Np , on the other hand, have a more dramatic turnover. For very high degradation rates, the dependence on

mass factor starts to round off due to attenuation by solubility limits, as can be seen in Figures 5.75, 5.76 5.77, and 5.78.

Solubility limited and sorbing ^{99}Tc demonstrates a direct proportionality to fractional degradation rate until attuation by its solubility limit and other natural system parameters.

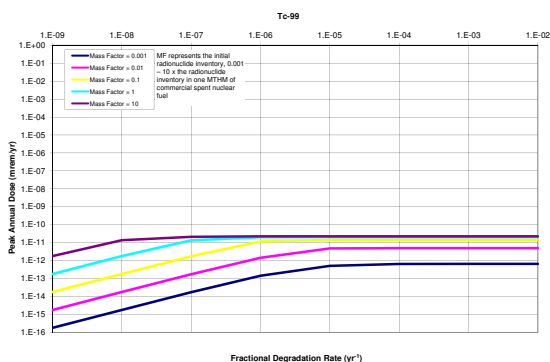


Figure 5.75: ^{99}Tc waste form degradation rate sensitivity.

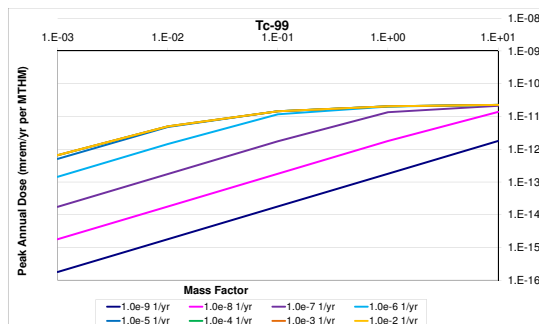


Figure 5.76: ^{99}Tc mass factor sensitivity.

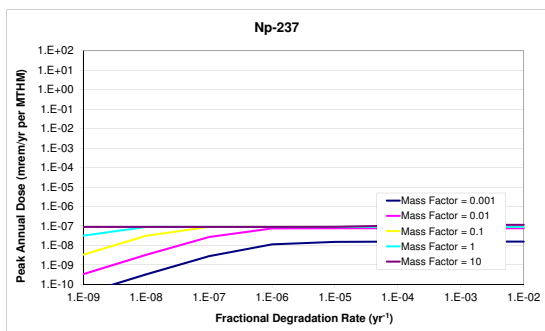


Figure 5.77: ^{237}Np waste form degradation rate sensitivity.

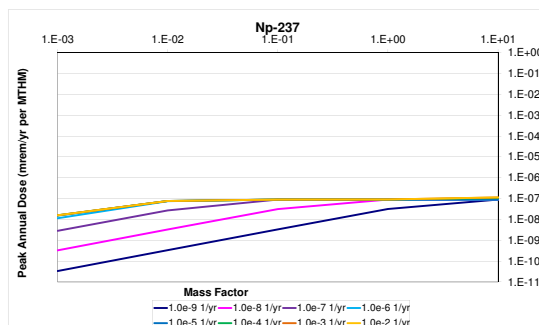


Figure 5.78: ^{237}Np mass factor sensitivity.

In the parametric sensitivity analysis conducted with the CYDER tool, waste form degradation rate sensitivity similarly shows the two regimes noted in the GDSM analysis.

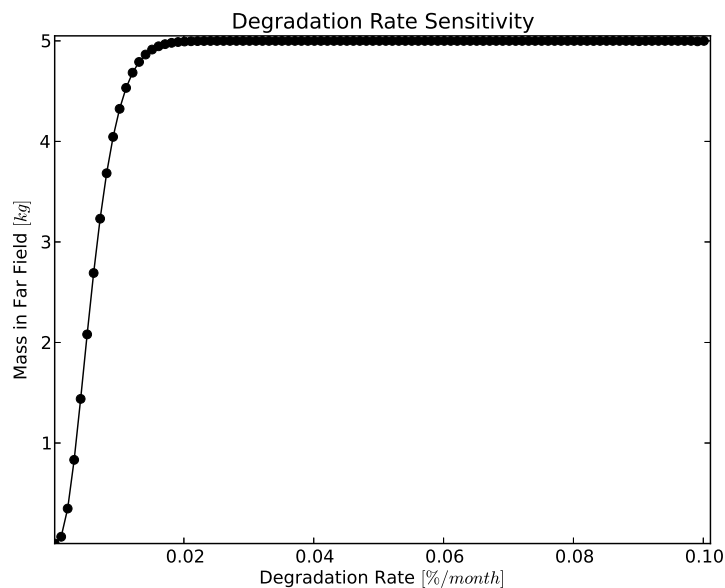


Figure 5.79: Sensitivity demonstration of the degradation rate in CYDER for an arbitrary isotope.

5.3 Thermal Transport Validation

Analyses in this section were conducted to compare the performance of the STC thermal model in CYDER with more detailed results of the LLNL thermal model. The CYDER model captures the trends of the LLNL model for the dominant physics of heat transport in a repository.

The results here provide an overview of the relative importance of thermal parameters that affect the repository capacity of simplified generic disposal concept in various geologic media where conduction is the dominant heat transfer mode. The applicability of this sensitivity analysis is thus restricted to enclosed, backfilled concepts.

5.3.1 Parametric Domain

Sensitivity analyses were conducted which span the parametric range of values generated by the reference specific temperature change database and described in Table 5.3.

Thermal Cases			
Parameter	Symbol	Units	Value Range
Thermal Diffusivity	α_{th}	$[m^2 \cdot s^{-1}]$	1.0×10^{-7} 2.0×10^{-7} 3.0×10^{-7} 4.0×10^{-7} 5.0×10^{-7} 6.0×10^{-7} 7.0×10^{-7} 8.0×10^{-7} 9.0×10^{-7} 1.0×10^{-6} 2.0×10^{-6} 3.0×10^{-6}
Thermal Conductivity	K_{th}	$[W \cdot m^{-1} \cdot K^{-1}]$	0.1, 0.5, 1, 1.5, 2, 2.5, 3, 3.5, 4, 4.5
Spacing	S	$[m]$	2, 5, 10, 15, 20, 25, 50
Radius	r_{lim}	$[m]$	0.1, 0.25, 0.5, 1, 2, 5
Isotope	i	$[-]$	^{241,243} Am, ^{242,243,244,245,246} Cm, ^{238,240,241,242} Pu, ^{134,135,137} Cs, ⁹⁰ Sr

Table 5.3: A thermal reference dataset of STC values as a function of each of these parameters was generated by repeated parameterized runs of the LLNL MathCAD model[35, 36].

These values were selected to provide detail in the near field and at values of α_{th} and K_{th} in the three host media under consideration in this work.

5.3.2 Approach

This analysis utilized the LLNL semi-analytic MathCAD model discussed in Section 2.6.2. It performs detailed calculations of the conductive thermal transport in a generic repository concept with a gridded layout.

It relies on the thermal diffusivity, α_{th} and conductivity K_{th} of the material as well as the waste package spacing, S , and thermally limiting radius, r_{lim} . Finally, it relies on the STC data calculated with the semi-analytic model based on the decay heat profiles of the emplaced wastes, Q . The essential decay heat profiles, Q , were retrieved from a UFD database provided by Carter et al. [22].

5.3.3 Thermal Conductivity Sensitivity Validation

The thermal conductivity, K_{th} of geologic repository host media impacts the speed of transport, and therefore the time evolution of thermal energy deposition, in the medium.

5.3.3.1 LLNL Model Results

In the creation of the STC database, the thermal conductivity was varied across a broad domain for each isotope, i , package spacing, s , limiting radius r_{calc} , and thermal diffusivity α_{th} , considered. By varying the thermal conductivity of the repository model from 0.1 to 4.5 [$W \cdot m^{-1} \cdot K^{-1}$], this sensitivity analysis succeeds in capturing the domain of thermal conductivities witnessed in high thermal conductivity salt deposits as well as low thermal conductivity clays.

Figure 5.80 shows the trend in which increased thermal conductivity of a medium decreases temperature change in the near field. This indicates, then that thermal conductivity is an important parameter for repository geologic medium selection.

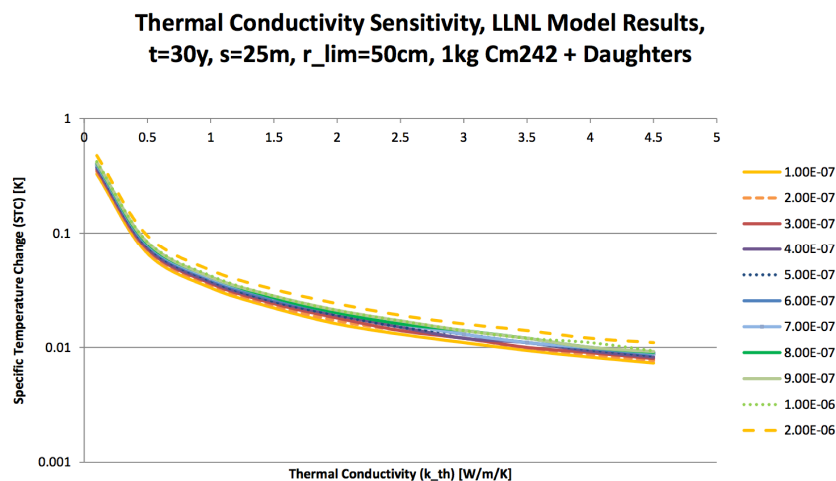


Figure 5.80: Increased thermal conductivity decreases the temperature (here represented by STC) at the limiting radius.

5.3.3.2 Cyder Results

In a similar analysis, the thermal conductivity was investigated. Figure 5.81 shows that the same trend noted for the LLNL model was noted in the CYDER model.

In additional dual parameter studies, the importance of the thermal conductivity was compared both with the spacing between waste packages and the limiting radius. Figures 5.82 and 5.83 validate the trend noted above that increased thermal conductivity of a medium decreases temperature change in the near field. Additionally, analysis with the CYDER STC database demonstrates the way in which the importance of spacing and the importance of the limiting radius decrease with increasing K_{th} .

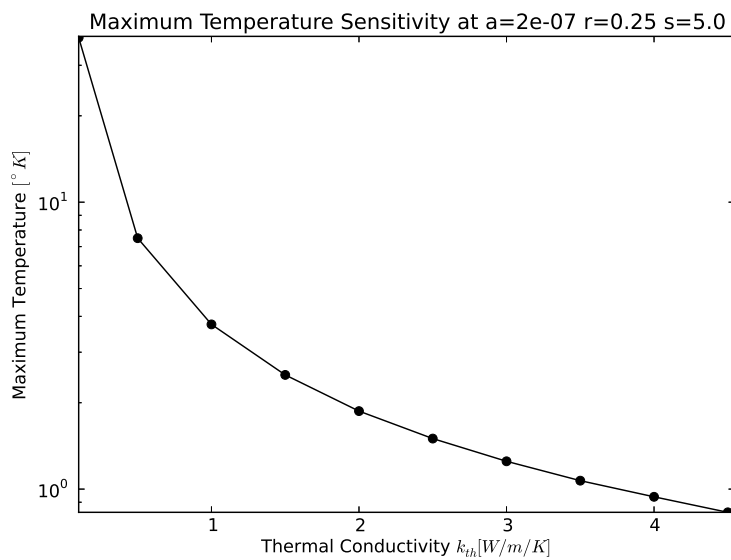


Figure 5.81: Cyder results agree with those of the LLNL model. Increased K_{th} decreases temperature change at the limiting radius. The above example thermal profile results from 10kg of ^{242}Cm , $\alpha_{th} = 2 \times 10^{-7}$, $s = 5m$, and $r_{lim} = 0.25m$.

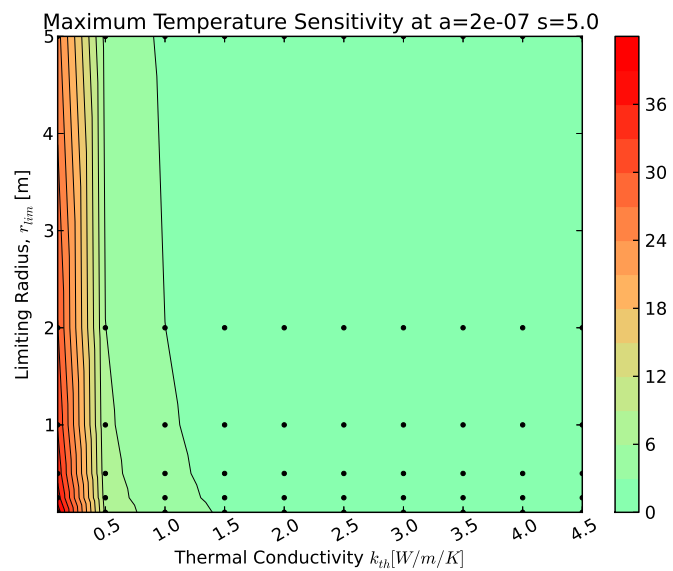


Figure 5.82: CYDER results agree with those of the LLNL model. The importance of the limiting radius decreases with increased K_{th} . The above example thermal profile results from 10kg of ^{242}Cm

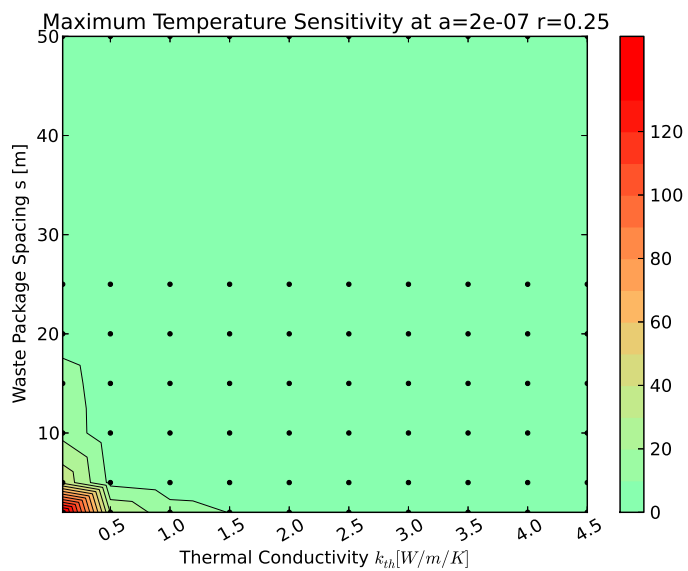


Figure 5.83: Cyder results agree with those of the LLNL model. The importance of the limiting radius decreases with increased K_{th} . The above example thermal profile results from 10kg of ^{242}Cm

5.3.4 Thermal Diffusivity Sensitivity Validation

The thermal diffusivity, α_{th} of geologic repository host media describes the tendency of thermal energy to diffuse through, and therefore be deposited, in the medium. Due to the close relationship between thermal diffusivity and conductivity (as in (2.35)), the results of this section closely related to those in Section 5.3.3.

5.3.4.1 LLNL Model Results

In the creation of the STC database, the thermal diffusivity was varied across a broad domain for each isotope, i , package spacing, s , limiting radius r_{calc} , and thermal conductivity K_{th} , considered. By varying the thermal diffusivity of the disposal system from $0.1 - 3 \times 10^{-6} \text{ m}^2 \cdot \text{s}^{-1}$, this sensitivity analysis succeeds in capturing the domain of thermal diffusivities witnessed in high thermal diffusivity salt deposits as well as low thermal diffusivity clays.

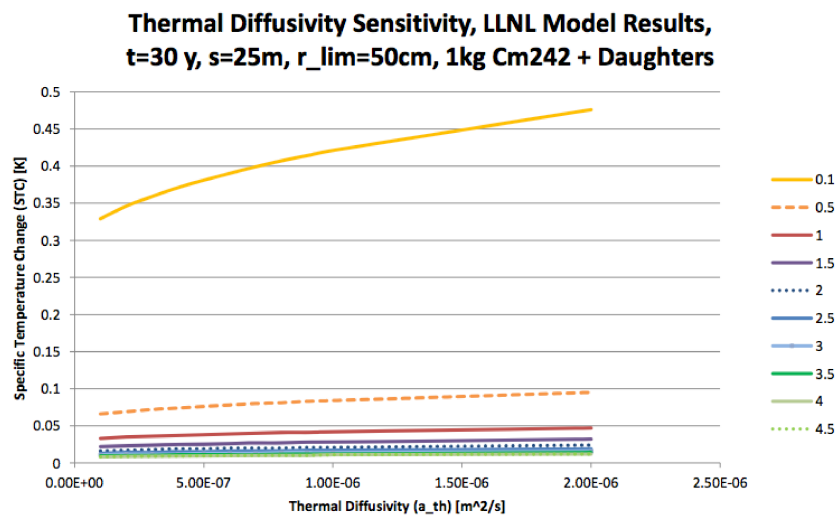


Figure 5.84: Increased thermal diffusivity decreases temperature change (here represented by STC) at the limiting radius (here $r_{calc} = 0.5m$).

Figure 5.84 shows the trend in which increased thermal diffusivity of a medium increases

temperatures in the near field. This indicates, then that thermal diffusivity is an important parameter for repository geologic medium selection.

5.3.4.2 Cyder Results

In a similar analysis, the thermal diffusivity was investigated. Figure 5.85 shows that the same trend noted for the LLNL model was noted in the CYDER model.

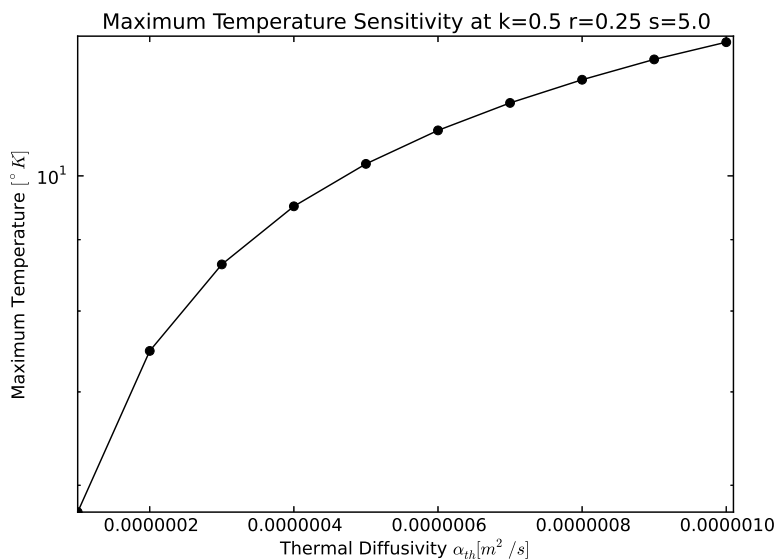


Figure 5.85: Cyder trends agree with those of the LLNL model, in which increased thermal diffusivity results in reduced temperature change at the limiting radius. The above example thermal profile results from 10kg of ^{242}Cm .

Additional dual parameter studies compared thermal diffusivity importance with the spacing between waste packages and the limiting radius.

Figures 5.86 and 5.87 validate the trend noted above that increased thermal diffusivity of a medium decreases temperature change in the near field. Additionally, analysis with the CYDER STC database demonstrates the way in which the importance of K_{th} remains

constant, but the importance of the limiting radius decreases with increasing α_{th} .

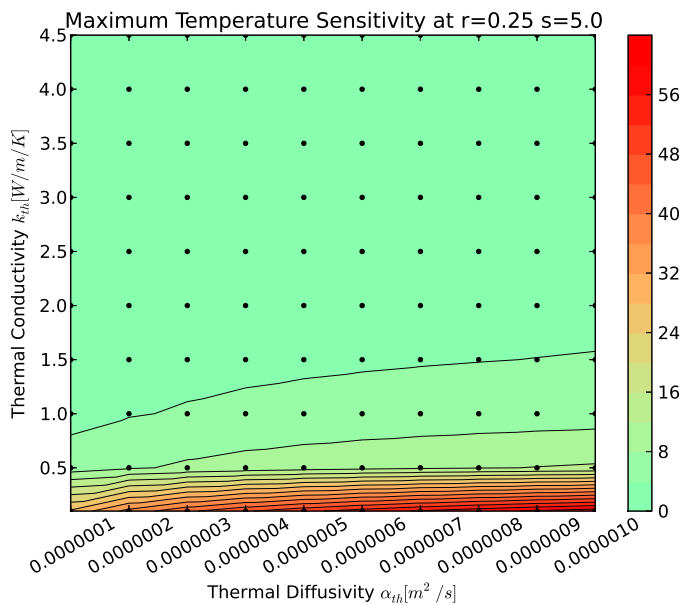


Figure 5.86: Cyder trends agree with those of the LLNL model, in which increased thermal diffusivity results in decreased thermal deposition in the near field. The above example thermal profile results from 10kg of ^{242}Cm .

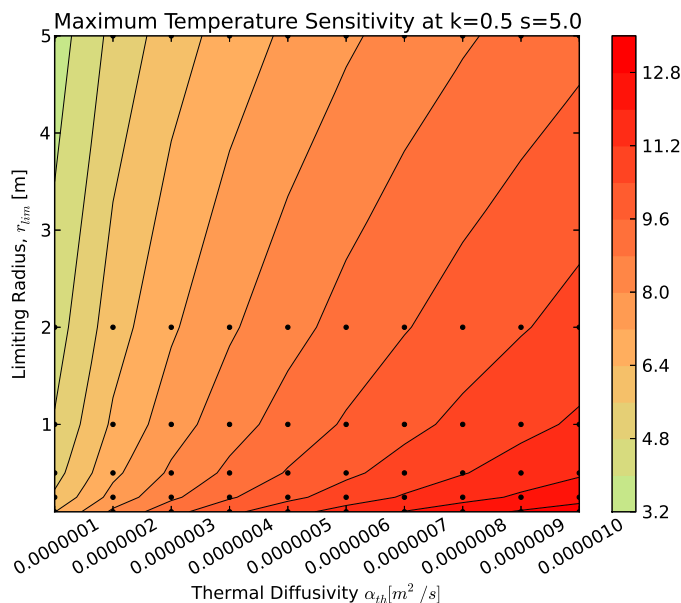


Figure 5.87: CYDER trends agree with those of the LLNL model. The importance of the limiting radius decreases with increased K_{th} . The above example thermal profile results from 10kg of ^{242}Cm

5.3.5 Waste Package Spacing Sensitivity Validation

The waste package spacing s of geologic repository concept affects the areal decay heat burden in the repository and has a strong effect on the thermal energy deposited per unit area in the medium. In the CYDER and LLNL models, the waste packages are placed in a grid, so this spacing represents a change in distance between waste packages on both horizontal axes.

5.3.5.1 LLNL Model Results

In the creation of the STC database, the waste package spacing was varied across a number of values for each isotope, i , limiting radius r_{calc} , thermal diffusivity α_{th} , and thermal conductivity K_{th} , considered. By varying the waste package spacing of the geometric

layout from $0.1 - 5[m]$ this sensitivity analysis succeeds in capturing the domain of waste package spacings present in geologic repository concepts under consideration.

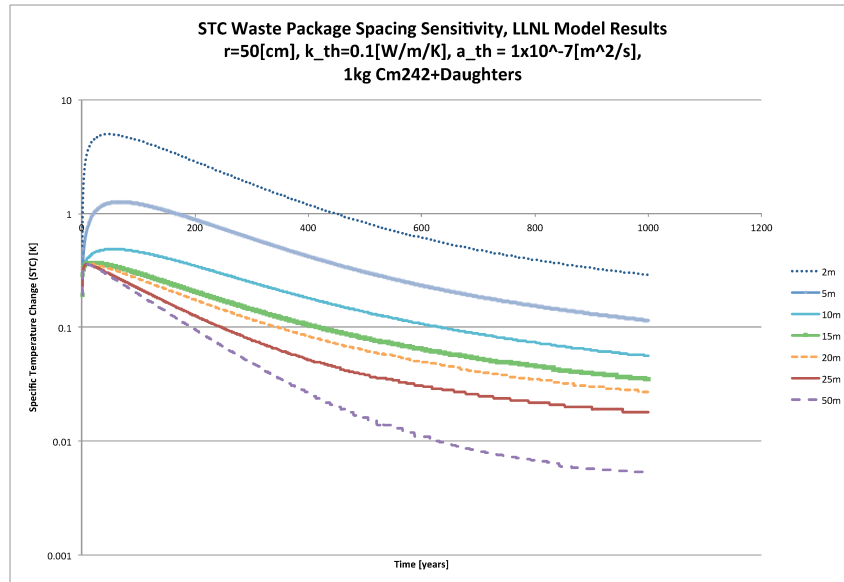


Figure 5.88: Increased waste package spacing decreases temperature change (here represented by STC) in the near field (here $r_{calc} = 0.5$ m).

Figure 5.88 shows the trend in which increased waste package spacing of a medium decreases temperature change in the near field. This indicates that waste package spacing is an important parameter for repository concept design.

Similarly, the location of the limiting radius has a strong effect on the waste package loading limit, for a fixed limiting temperature. In Figure 5.89, the trend is demonstrated in which increased limiting radius (i.e. distance between the waste packages and the limiting radius) decreases the temperature at the limit, as expected.

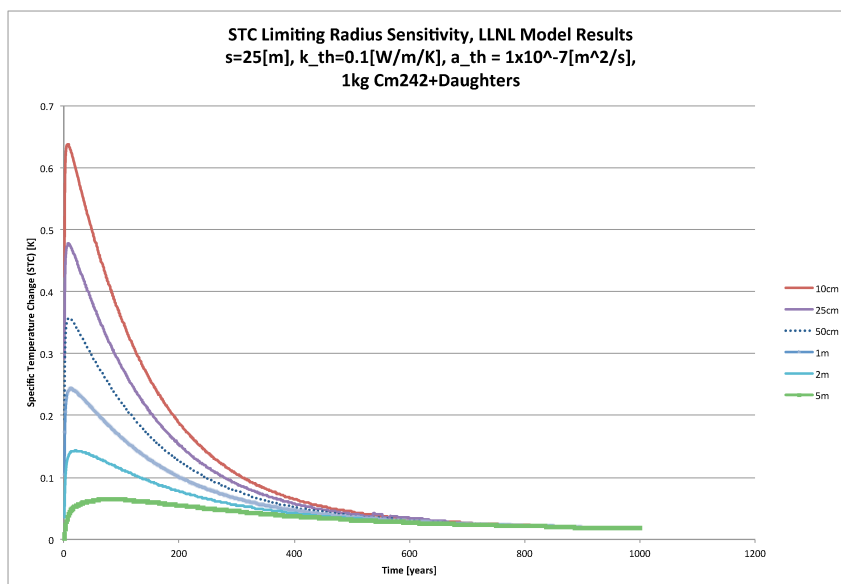


Figure 5.89: Increased limiting radius decreases temperature change contributing to the thermal limit (here represented by STC).

5.3.5.2 Cyder Results

In a similar analysis, spacing and limiting radius were investigated. Figure 5.90 shows that the same spacing trend noted for the LLNL model was noted in the CYDER model.

Similarly, figure 5.91 shows the same trend for r_{lim} in CYDER as seen in the LLNL model.

In a similar analysis, the thermal diffusivity was compared both with the spacing between waste packages and the limiting radius.

Figure 5.92 validates the trend noted above that increased waste package spacing in a repository concept decreases areal thermal energy deposition in the near field. Additionally, analysis with the CYDER STC database demonstrates the way in which the importance of r_{lim} , the limiting radius, impacts the maximum calculated temperature at that radius.

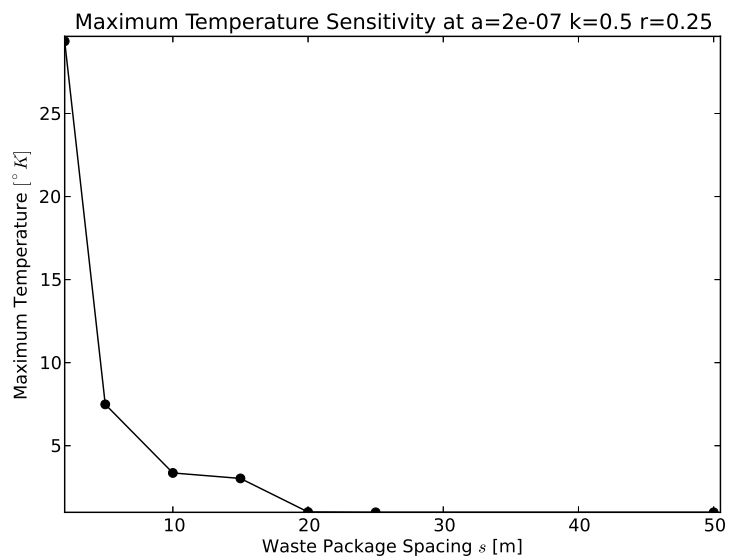


Figure 5.90: Cyder results agree with those of the LLNL model. The spacing between packages is inversely related to the temperature change in the medium at the limiting radius. The above example thermal profile results from 10kg of ^{242}Cm .

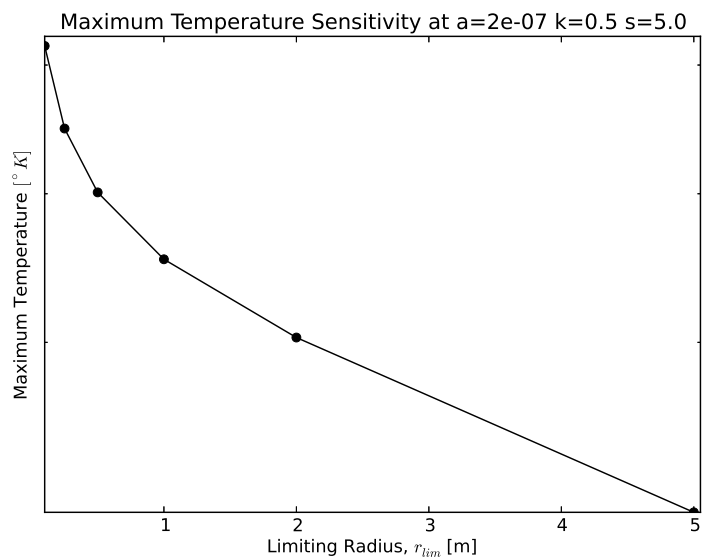


Figure 5.91: Cyder results agree with those of the LLNL model. Increased limiting radius reduces the change in temperature at that radius. The above example thermal profile results from 10kg of ^{242}Cm .

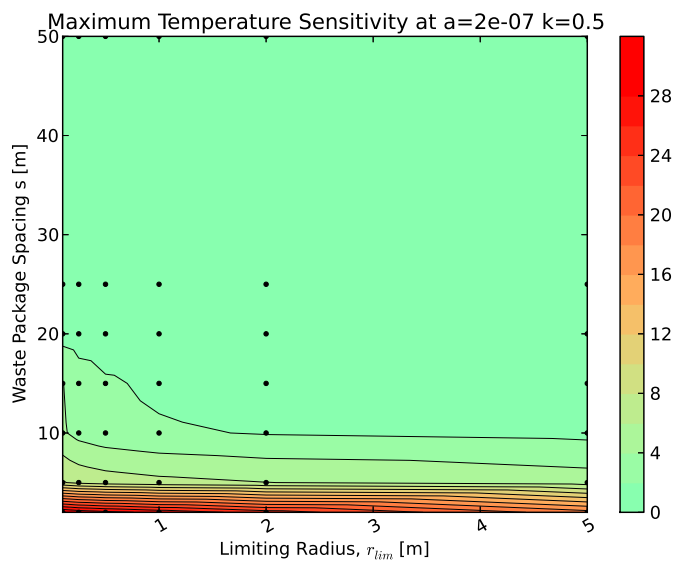


Figure 5.92: Cyder results agree with those of the LLNL model. The importance of the limiting radius decreases with increased s . The above example thermal profile results from 10kg of ^{242}Cm

6 CONCLUSIONS

6.1 Contributions

This work has provided a flexible code for rapid medium fidelity calculation of generic repository performance in the context of fuel cycle analysis. Capable of thermal transport, hydrologic contaminant transport, and integration within a fuel cycle simulation code, CYDER is the first of its kind.

In addition to implementing fundamental modeling capabilities, CYDER has been designed to accommodate the development of advanced capabilities in the future.

In this work, key conceptual components and modeling methods for geologic radioactive waste disposal were identified as part of a literature review, dominant physics of thermal and radionuclide transport were identified by conducting sensitivity analyses with detailed codes. Accordingly, a basic set of abstracted models were developed and implemented within the CYDER code.

A set of basic capabilities within the CYDER library have been developed and validated and an assortment of advanced features, data, testing, and plotting capabilities are functional. The CYDER source code in which these models are implemented is made freely available to interested researchers and potential model developers [48]. In addition to the source code and supporting publications, the CYDER code is well commented and produces clickable, browsable automated documentation with each build. That documentation is also available online.

The application programming interface to this software library is intentionally general, facilitating the incorporation of the models presented here within external software tools in need of a multicomponent disposal system simulator.

Furthermore, this work contributes to an expanding ecosystem of computational models

available for use with the CYCLUS fuel cycle simulator. This hydrologic nuclide transport library, by virtue of its capability to modularly integrate with the CYCLUS fuel cycle simulator has laid the foundation for integrated disposal option analysis in the context of fuel cycle options.

6.2 Suggested Future Work

It is hoped that CYDER will benefit from continued development and use. Future development efforts will likely be led by developer use cases, but are likely to include a number of advanced features that have the potential to extend the capabilities of this tool in significant ways.

Initially, further validation of these models should include full benchmarks against the GDSM results including biosphere conversion of the released source term. Furthermore, thermal benchmarks against recent UFD work for various design concepts would similarly improve the understanding of the range of validity for the thermal model.

Thermal analyses in these results have been used to assess thermal performance of a repository after emplacement. However, dynamic, thermal capacity limited fuel cycle analyses concerning the variation of necessary cooling times among repository concepts and fuel cycles should be conducted using the capacity determination capability arrived at with this model.

Additional advanced capabilities should include the incorporation of fracture enabled transport in a radionuclide transport model. This feature would improve analyses of geologic host media such as granite for which the dominant porosity consists of cracking. Similarly, incorporation of a biosphere model in the far field would substantively benefit the calculation of fuel cycle metrics related to human and environmental effects and will support myriad expected use cases of the tool.

Additional radionuclide transport models, thermal transport models, and supporting data will enrich the capabilities of this code.

REFERENCES

- [1] AB, Svensk karnbranslehantering. 2006. *Long-term safety for KBS-3 repositories at forsmark and laxemar-a first evaluation: Main report of the SR-Can project*. SKB.
- [2] Abkowitz, Mark. 2010. Nuclear waste assessment system for technical evaluation - NUWASTE.
- [3] Ahn, Joonhong. 1988. Mass transfer and transport of radionuclides in fractured porous rock. Tech. Rep., California Univ., Berkeley, CA.
- [4] ———. 2004. An environmental impact measure for nuclear fuel cycle evaluation. *Journal of Nuclear Science and Technology* 41(3):296 – 306.
- [5] ———. 2007. Environmental impact of yucca mountain repository in the case of canister failure. *Nuclear technology* 157(1):87 – 105.
- [6] Ahn, Joonhong, D. Kawasaki, and P. L. Chambre. 2002. Relationship among performance of geologic repositories, canister-array configuration, and radionuclide mass in waste. *Nuclear Technology* 140(1).
- [7] Anderson, Mary P., and William W. Woessner. 1992. *Applied groundwater modeling: simulation of flow and advective transport*. Academic Press.
- [8] ANDRA. 2005. Argile: Evaluation de la faisabilite du stockage geologique en formation argileuse. Tech. Rep., Agence Nationale Pour la Gestion des Dechets Radioactifs, Paris.
- [9] ———. 2005. Granite: Evaluation de la faisabilite du stockage geologique en formation granite. Tech. Rep., Agence Nationale Pour la Gestion des Dechets Radioactifs, Paris.

- [10] Avila, R., J. Cervantes, and C. Estrada-Gasca. 2000. Transient thermal response in nuclear waste repositories. *Nuclear Engineering and Design* 198(3):307–316.
- [11] Bateman, Harry. 1908. 1910. the solution of a system of differential equations occurring in the theory of radio-active transformations. In *Proc. cambridge philosophical soc*, vol. 15, 423.
- [12] Bauer, T.H., and R.A. Wigeland. 2007. Geologic repository design and disposal: GNEP spent fuel processing-waste volume. In *Proceedings of GLOBAL*, 5.
- [13] Berkowitz, Brian, Jacob Bear, and Carol Braester. 1988. Continuum models for contaminant transport in fractured porous formations. *Water Resources Research* 24(8):PP. 1225 – 1236.
- [14] Blink, James, T. A. Buscheck, William G. Halsey, and T. Wolery. 2010. Disposal systems evaluations and tool development-engineered barrier system evaluation. Tech. Rep., Lawrence Livermore National Laboratory LLNL, Livermore, CA.
- [15] Boucher, Lionel. 2010. International comparison for transition scenario codes involving COSI, DESAE, EVOLCODE, FAMILY and VISION. CEA France.
- [16] Bouvier, E., Joonhong Ahn, and T. Ikegami. 2007. *Comparison of environmental impacts for PWR-UO₂, PWR-MOX and FBR*. LaGrange Park, IL: American Nuclear Society.
- [17] Bracke, G., T. Beuth, K. Fischer-Appelt, J. Larue, and M. Navarro. 2008. Safety functions derived from geochemistry for safety analysis of final disposal of high-level radioactive waste. *Uranium, Mining and Hydrogeology* 771—778.

- [18] Brady, P. V., B. W. Arnold, G. A. Freeze, P. N. Swift, S. J. Bauer, J. L. Kanney, R. P. Rechard, and J. S. Stein. 2009. Deep borehole disposal of high-level radioactive waste. *SAND2009-4401, Sandia National Laboratories*.
- [19] Brenner, Howard. 1962. The diffusion model of longitudinal mixing in beds of finite length. numerical values. *Chemical Engineering Science* 17(4):229–243.
- [20] Brewitz, Wernt, and Ulrich Noseck. 2002. Long-term performance of spent fuel in geological repositories. *Comptes Rendus Physique* 3(7-8):879–889.
- [21] Carslaw, H. S., and J. C. Jaeger. 1959. Conduction of heat in solids. *Oxford: Clarendon Press, 1959, 2nd ed.* 1.
- [22] Carter, J. T., A. J. Luptak, J. Gastelum, C. Stockman, and A. Miller. 2011. Fuel cycle potential waste inventory for disposition. Tech. Rep., FCR&D-USED-2010-000031, Rev. 3.
- [23] Carter, Joe, F. Hansen, R. Kehrman, and T. Hayes. 2011. A generic salt repository for disposal of waste from a spent nuclear fuel recycle facility. Tech. Rep., SRNL-RP-2011-00149 Rev. 0. Aiken, SC: Savannah River National Laboratory.
- [24] Clayton, Daniel, Geoff Freeze, Ernest Hardin, W. Mark Nutt, Jens Birkholzer, H.H. Liu, and Shaoping Chu. 2011. Generic disposal system modeling - fiscal year 2011 progress report. Tech. Rep. FCRD-USED-2011-000184, U.S. Department of Energy, Sandia, NM.
- [25] Diodato, D. M. 1994. A compendium of fracture flow models. *Work sponsored by US Department of Defense, United States Army, Europe, Combat Maneuver Training Center, Hohenfels, Germany*.

- [26] DOE. 2002. Yucca mountain science and engineering report. *US Department of Energy, Las Vegas, NV DOE/RW-0539-1, Rev 1.*
- [27] ———. 2008. The report to the president and the congress by the secretary of energy on the need for a second repository. Office of Civilian Radioactive Waste Management DOE/RW-0595, Department of Energy, Washington D.C.
- [28] ———. 2010. Nuclear energy research & development roadmap: Report to congress.
- [29] ———. 2013. Strategy for the management and disposal of used nuclear fuel and high-level radioactive waste. Tech. Rep., United States Department of Energy, Washington D.C., United States.
- [30] Durham, W. B., V. V. Mirkovich, and H. C. Heard. 1987. Thermal diffusivity of igneous rocks at elevated pressure and temperature. *Journal of Geophysical Research: Solid Earth* 92(B11):11615—11634.
- [31] El-Wakil, Mohamed Mohamed. 1981. *Nuclear heat transport*. American Nuclear Society.
- [32] Gaski, J. 1987. SINDA system improved numerical differencing analyzer.
- [33] Golder Associates. 2010. *GoldSim contaminant transport module*. Version 6.0 ed. GoldSim Technology Group.
- [34] ———. 2010. *GoldSim graphical simulation environment user's guide*. Version 5.1 ed. GoldSim Technology Group.
- [35] Greenberg, Harris, James Blink, Massimiliano Fratoni, Mark Sutton, and Amber Ross. 2012. Application of analytical heat transfer models of multi-layered natural

- and engineered barriers in potential high-level nuclear waste repositories. In *WM2012*. Phoenix, AZ. LLNL-CONF-511672.
- [36] Greenberg, Harris, Montu Sharma, and Mark Sutton. 2012. Investigations on repository near-field thermal modeling. Tech. Rep., Lawrence Livermore National Laboratory.
- [37] Gregg, Robert. 2011. ORION v3.12 results.
- [38] Guerin, L., and M. Kazimi. 2009. Impact of alternative nuclear fuel cycle options on infrastructure and fuel requirements, actinide and waste inventories, and economics. Technical Report MIT-NFC-TR-111, Massachusetts Institute of Technology, Cambridge, MA, United States.
- [39] Guerin, Laurent. 2009. A benchmark study of computer codes for system analysis of the nuclear fuel cycle. Tech. Rep., Massachusetts Institute of Technology. Center for Advanced Nuclear Energy Systems. Nuclear Fuel Cycle Program.
- [40] Hardin, Ernest, James Blink, Harris Greenberg, Mark Sutton, Massimo Fratoni, Joe Carter, Mark Dupont, and Rob Howard. 2011. Generic repository design concepts and thermal analysis - 8.8.2011 draft. Tech. Rep. FCRD-USED-2011-000143, Department of Energy Office of Used Fuel Disposition, Sandia.
- [41] Hedin, A. 2002. Integrated analytic radionuclide transport model for a spent nuclear fuel repository in saturated fractured rock. *Nuclear Technology* 138(2).
- [42] Higgs, J.J.W. 1987. Clay as a barrier to radionuclide migration. *Progress in Nuclear Energy* 19(2):173–207.
- [43] Ho, C. K. 2000. Dual porosity vs. dual permeability models of matrix diffusion in fractured rock. Tech. Rep., Sandia National Laboratories.

- [44] Huff, Kathryn. 2013. Cyclus fuel cycle simulation capabilities with the cyder disposal system model (in press). In *Proceedings of GLOBAL 2013*. Salt Lake City, UT, United States.
- [45] Huff, Kathryn, and Theodore H. Bauer. 2012. Benchmarking a new closed-form thermal analysis technique against a traditional lumped parameter, finite-difference method. Technical Report FCRD-UFD-000142, Argonne National Laboratory, Argonne, IL, United States.
- [46] ———. 2012. Numerical calibration of an analytical generic nuclear repository heat transfer model. In *Transactions of the american nuclear society*, vol. 106 of *Modeling and Simulation in the Fuel Cycle*, 260—263. Chicago, IL, United States: American Nuclear Society, La Grange Park, IL 60526, United States.
- [47] Huff, Kathryn, and Mark Nutt. 2012. Key processes and parameters in a generic clay disposal system model. In *Transactions of the american nuclear society*, vol. 107 of *Environmental Sciences – General*, 208—211. San Diego, CA: the American Nuclear Society.
- [48] Huff, Kathryn D. 2013. Cyder : A generic geology repository performance library.
- [49] ———. 2013. Hydrologic nuclide transport models in cyder, a geologic disposal software library. In *WM2013*. Phoenix, AZ: Waste Management Symposium.
- [50] Huff, Kathryn D., and Alexander T. Bara. 2013. Dynamic determination of thermal repository capacity for fuel cycle analysis. In *Transactions of the american nuclear society*, vol. 108, 123–126. Atlanta, GA, United States.
- [51] Incropera, Frank. 2006. *Fundamentals of heat and mass transfer*. 6th ed. Hoboken N.J.: Wiley.

- [52] International Atomic Energy Agency. 1996. International basic safety standards for protection against ionizing radiation and for the safety of radiation sources. *International Atomic Energy Agency, Vienna* No 115.
- [53] Johnson, L., C. Ferry, C. Poinssot, and P. Lovera. 2005. Spent fuel radionuclide source-term model for assessing spent fuel performance in geological disposal. part i: Assessment of the instant release fraction. *Journal of Nuclear Materials* 346(1): 56—65.
- [54] Johnson, L., B. Kunz, C. Frei, Nagra, and Projekt Opalinuston. 2002. *Project opalinus clay: Safety report: Demonstration of disposal feasibility for spent fuel, vitrified high-level waste and long-lived intermediate-level waste (entsorgungsnachweis)*. Nagra, National cooperative for the Disposal of Radioactive Waste.
- [55] Johnson, L. H. 2002. *Calculations of the temperature evolution of a repository for spent fuel, vitrified high-level waste and intermediate level waste in opalinus clay*. Nagra.
- [56] Kawasaki, D., Joonhong Ahn, P. L. Chambre, and William G. Halsey. 2004. Congruent release of long-lived radionuclides from multiple canister arrays. *Nuclear technology* 148(2):181 – 193.
- [57] Kessler, J. H., J. Kemeny, F. King, A. M. Ross, and B. Ross. 2006. Room at the mountain: Estimated maximum amounts of commercial spent nuclear fuel capable of disposal in a yucca mountain repository. Tech. Rep., The ASME Foundation, Inc., New York.
- [58] Kim, J., Y. Lee, and M. Koo. 2007. Thermal properties of granite from korea. *AGU Fall Meeting Abstracts* 11:0576.

- [59] Lee, Joon H., Daniel Clayton, Carlos Jove-Colon, and Yifeng Wang. 2012. A preliminary performance assessment for salt disposal of high-level nuclear waste-12173. In *Proceedings of the waste management symposium*. SAND2012-0158C, Phoenix, AZ: WMSym.
- [60] Leij, Feike J., Todd H. Skaggs, and Martinus Th. Van Genuchten. 1991. Analytical solutions for solute transport in three-dimensional semi-infinite porous media. *Water resources research* 27(10):2719—2733.
- [61] von Lensa, W., R. Nabbi, and M. Rossbach. 2008. *RED-IMPACT impact of partitioning, transmutation and waste reduction technologies on the final nuclear waste disposal*. Forschungszentrum Julich.
- [62] Li, J., M. Nicholson, W. C Proctor, M. S Yim, and D. McNelis. 2007. Examining repository loading options to expand yucca mountain repository capacity. In *Proceedings of GLOBAL*, 519 — 525.
- [63] Li, Jun. 2006. A methodology to evaluate nuclear waste transmutation/fuel cycle systems. PhD dissertation, North Carolina State University, Raleigh, N.C.
- [64] Li, Jun, M. S Yim, and D. McNelis. 2008. The specific temperature increase method for repository thermal analysis. *Transactions of the American Nuclear Society* 99: 216 — 218.
- [65] Maloszewski, Piotr, and Andrzej Zuber. 1996. Lumped parameter models for the interpretation of environmental tracer data. *Manual on mathematical models in isotope hydrology*. IAEA-TECDOC-910 9—59.

- [66] Miron, A., J. Valentine, J. Christenson, M. Hawwari, S. Bhatt, M. L. Dunzik-Gougar, and M. Lineberry. 2009. Identification and analysis of critical gaps in nuclear fuel cycle codes required by the SINEMA program. Tech. Rep., University of Cincinnati.
- [67] Murthy, D.N. Prabhakar, Michael Bulmer, and John A. Eccleston. 2004. Weibull model selection for reliability modelling. *Reliability Engineering & System Safety* 86(3):257—267.
- [68] Nicholson, M. A. 2007. *Thermal loading and uncertainty analysis of high level waste in yucca mountain*. North Carolina State University.
- [69] Nieland, J. D., K. D. Mellegard, Roger S. Schalge, and Hugh D. Kaiser. 2001. Storage of chilled natural gas in bedded salt storage caverns: Economic and technical feasibility. Topical Report RSI-1354 DE-AC26-97FT34350, United States Department of Energy National Energy Technology Laboratory 626 Cochrans Mill Road Pittsburgh, Pennsylvania 15236.
- [70] Nutt, Mark. 2011. Personal communication.
- [71] Nutt, W. M. 2010. Used fuel disposition research and development roadmap-FY10 status. Tech. Rep., Argonne National Laboratory.
- [72] Nutt, W. Mark, Edgar E. Morris, Yifeng Wang, Joon H. Lee, Carlos Jove-Colon, and Shaoping Chu. 2009. Generic repository concept analyses to support the establishment of waste form performance requirements – generic tuff and salt model development and results. Tech. Rep. GNEP-WAST-PMO-MI-DV-2008-000146, US–DOE–NE Separations and Waste Form Campaign.

- [73] NWTRB. 2011. NWTRB workshop on evaluation of waste streams associated with LWR fuel cycle options. Tech. Rep., Nuclear Waste Technical Review Board, Arlington, VA, United States.
- [74] OECD Nuclear Energy Agency. 2006. *Advanced nuclear fuel cycles and radioactive waste management*. OECD Publishing.
- [75] ONDRAF-NIRAS. 2001. Technical overview of the SAFIR 2 report. Tech. Rep. Nirond 2001-05 E, ONDRAF-NIRAS, Belgium.
- [76] Papoulis, A., and S. U. Pillai. 2002. *Probability, random variables, and stochastic processes*. 4th ed. Series in Electrical and Computer Engineering, McGraw-Hill.
- [77] Piet, S., T. Bjornard, B. Dixon, D. Gombert, C. Laws, and G. Matthern. 2007. Which elements should be recycled for a comprehensive fuel cycle? *Proc. Global 2007* 1595.
- [78] Posiva. 2010. *Interim summary report of the safety case 2009*. POSIVA.
- [79] ptc. 2010. MathCAD engineering calculations software.
- [80] Pusch, Roland, Lennart Borgesson, and Mikael Erlstrom. 1987. *Alteration of isolating properties of dense smectite clay in repository environment as exemplified by seven pre-quaternary clays*. Swedish Nuclear Fuel and Waste Management Co.
- [81] Radel, T. E. 2007. *Repository modeling for fuel cycle scenario analysis*. University of Wisconsin – Madison.
- [82] Radel, Tracy E., and Paul P. H. Wilson. 2007. Determination of repository loading values in fuel cycle scenario analysis codes. In *2007 annual meeting on american*

- nuclear society, jun 24 - 28 2007*, vol. 96 of *Transactions of the American Nuclear Society*, 205–206. Boston, MA, United states: American Nuclear Society.
- [83] Radel, Tracy E., Paul P.H. Wilson, R. M. Grady, and Theodore H. Bauer. 2007. Effect of separation efficiency on repository loading values in fuel cycle scenario analysis codes. In *American nuclear society transactions*. LaGrange Park, IL: American Nuclear Society.
- [84] Savoye, S., F. Goutelard, C. Beaucaire, Y. Charles, A. Fayette, M. Herbette, Y. Larabi, and D. Coelho. 2011. Effect of temperature on the containment properties of argillaceous rocks: The case study of callovo-oxfordian claystones. *Journal of Contaminant Hydrology*.
- [85] Schneider, E., M. Knebel, and W. Schwenk-Ferrero. 2004. NFCSim scenario studies of german and european reactor fleets. Tech. Rep., LA-UR-04-4911, Los Alamos National Laboratory.
- [86] Schwartz, F. W., and H. Zhang. 2004. Fundamentals of ground water. *Environmental Geology* 45:1037—1038.
- [87] Soelberg, N., S. Priebe, D. Gombert, and T. Bauer. 2009. Heat management strategy trade study. *Advanced Fuel Cycle Initiative, AFCI-SYSA-PMO-MI-DV-2009-000169, INL/EXT-09-16708*.
- [88] Surma, Fabrice, and Yves Geraud. 2003. Porosity and thermal conductivity of the soultz-sous-forets granite. In *Thermo-hydro-mechanical coupling in fractured rock*, ed. Hans-Joachim Kämpel, 1125—1136. Pageoph Topical Volumes, Birkhauser Basel.

- [89] Swift, Peter, and Mark Nutt. 2010. Applying insights from repository safety assessments. In *Proceedings of 11th information exchange meeting on partitioning and transmutation*. San Francisco, CA: OECD-NEA.
- [90] Tikhonravova, P. I. 2007. Effect of the water content on the thermal diffusivity of clay loams with different degrees of salinization in the transvolga region. *Eurasian Soil Science* 40(1):47—50.
- [91] Turner, Stephen L. 2010. Discrete modeling: OCRWM total system model DRAFT. Fuel Cycle Technologies FCR&D-XXXX-2009-XXXXXX, Argonne National Laboratory, Argonne, IL, United States.
- [92] Uleberg, K., and J. Kleppe. 1996. Dual porosity, dual permeability formulation for fractured reservoir simulation. In *Norwegian university of science and technology, trondheim RUTH seminar, stavanger*.
- [93] Van Den Durpel, L., D. C. Wade, and Abdellatif Yacout. 2006. DANESS: a system dynamics code for the holistic assessment of nuclear energy system strategies. *Proceedings of the 2006 System Dynamics Conference*.
- [94] Van Genuchten, Martinus Th. 1981. Analytical solutions for chemical transport with simultaneous adsorption, zero-order production and first-order decay. *Journal of Hydrology* 49(3-4):213—233.
- [95] Van Genuchten, Martinus Th., and W. J. Alves. 1982. Analytical solutions of the one-dimensional convective-dispersive solute transport equation. *Technical Bulletin* 9(1661).
- [96] Wang, Herbert Fan, and Mary P. Anderson. 1982. *Introduction to groundwater modeling*. Academic Press.

- [97] Wigeland, Roald A., Theodore H. Bauer, Thomas H. Fanning, and Edgar E. Morris. 2006. Separations and transmutation criteria to improve utilization of a geologic repository. *Nuclear Technology* 154:95–106.
- [98] Wigeland, Roald A., Edgar E. Morris, and Theodore H. Bauer. 2006. Criteria derived for geologic disposal concepts. In *Ninth information exchange meeting on actinide and fission product partitioning & transmutation*. Nimes, France.
- [99] Williams, N. H. 2001. Total system performance assessment – analyses for disposal of commercial and DOE waste inventories at yucca mountain – input to final environmental impact statement and site suitability evaluation REV 00 ICN 02. Tech. Rep., Bechtel SAIC Company, LLC.
- [100] Wilson, P. 2009. The adoption of advanced fuel cycle technology under a single repository policy. Tech. Rep., University of Wisconsin-Madison.
- [101] Wilson, Paul P. H. 2011. Comparing nuclear fuel cycle options. *A report for the Reactor & Fuel Cycle Technology Subcommittee of the Blue Ribbon Commission on America's Nuclear Future*.
- [102] Wilson, Paul P. H., Kathryn D. Huff, Matthew Gidden, and Robert Carlsen. 2012. Cyclus: A nuclear fuel cycle code from the university of wisconsin madison.
- [103] Yacout, A. M., J. J. Jacobson, G. E. Matthern, S. J. Piet, D. E. Shropshire, and C. Laws. 2006. VISION – verifiable fuel cycle simulation of nuclear fuel cycle dynamics. In *Waste management symposium*.

A RADIONUCLIDE TRANSPORT SENSITIVITY ANALYSIS

The four GDSMss developed by the UFD campaign facilitate sensitivity analysis of the long-term post-closure performance of geologic repositories in generic media with respect to various key processes and parameters [24]. Processes and parameters expected to be influential to repository performance include the rate of waste form degradation, timing of waste package failure, and various coupled geochemical and hydrologic characteristics of the natural system including diffusion, solubility, and advection.

The results here provide an overview of the relative importance of processes that affect the repository performance of simplified generic disposal concept in clay. This work is not intended to give an assessment of the performance of a disposal system. Rather, it is intended to generically identify properties and parameters expected to influence repository performance in a saturated, homogeneous geologic environment.

A.1 Approach

This analysis utilized the GDSM developed by the UFD campaign to represent a clay repository concept. The GDSM performs detailed calculations of radionuclide transport within a clay repository concept [24].

The radionuclide transport calculations are performed within the GoldSim simulation platform. GoldSim is a commercial simulation environment [33, 34]. Probabilistic elements of the GoldSim modeling framework enable the models to incorporate simple probabilistic FEPs that affect repository performance including waste package failure, waste form dissolution, and an optional vertical advective fast pathway [24].

The GoldSim framework and its contaminant transport module provide a simulation framework and radionuclide transport toolset that the GDSMs have utilized to simulate

chemical and physical attenuation processes including radionuclide solubility, dispersion phenomena, and reversible sorption [33, 34].

A.2 Mean of the Peak Annual Dose

In this analysis, repository performance is quantified by radiation dose to a hypothetical receptor. Specifically, this sensitivity analysis focuses on parameters that affect the mean of the peak annual dose. The mean of the peak annual dose,

$$D_{MoP,i} = \frac{\sum_{r=1}^N \max [D_{r,i}(t)|_{\forall t}]}{N} \quad (\text{A.1})$$

where

$D_{MoP,i}$ = mean of the peak annual dose due to isotope i [*mrem/yr*]

$D_i(t)$ = annual dose in realization r at time t due to isotope i [*mrem/yr*]

N = Number of realizations,

is a conservative metric of repository performance. The mean of the peak annual dose should not be confused with the peak of the mean annual dose,

$$D_{PoM,i} = \max \left[\frac{\sum_{r=1}^N D_{r,i}(t)|_{\forall t}}{N} \right] \quad (\text{A.2})$$

= peak of the mean annual dose due to isotope i [*mrem/yr*].

The mean of the peak annual dose rate given in equation (A.1) captures trends as well

as the peak of the mean annual dose rate given in equation (A.2). However, the mean of the peaks metric, $D_{MoP,i}$, was chosen in this analysis because it is more conservative since it is able to capture temporally local dose maxima and consistently reports higher dose values than the peak of the means, $D_{PoM,i}$.

A.3 Sampling Scheme

The multiple barrier system modeled in the clay GDSM calls for a multi-faceted sensitivity analysis. The importance of any single component or environmental parameter must be analyzed in the context of the full system of barrier components and environmental parameters. Thus, this analysis has undertaken an analysis strategy to develop a many dimensional overview of the key factors in modeled repository performance.

To address this, both individual and dual parametric studies were performed. Individual parameter studies varied a single parameter of interest in detail over a broad range of values. Dual parameter sensitivity studies were performed for pairs of parameters expected to exhibit some covariance. For each parameter or pair of parameters, forty simulation groups varied the parameter or parameters within the range considered. Example tables of the resulting forty simulation groups for individual and dual parametric study configurations appear in Tables A.1 and A.2 respectively.

P	P_1	Group 1
	P_2	Group 2
	P_3	Group 3
	\cdot	\cdot
	\cdot	\cdot
	\cdot	\cdot
	P_{40}	Group 40

Table A.1: For an individual one group of 100 realizations was run for each discrete value, P_i , within the range considered for P .

Dual Parameter Study

		Q				
		Q_1	Q_2	Q_3	Q_4	Q_5
P	P_1	Group 1	Group 2	Group 3	Group 4	Group 5
	P_2	Group 6	Group 7	Group 8	Group 9	Group 10
	P_3	Group 11	Group 12	Group 13	Group 14	Group 15
	P_4	Group 16	Group 17	Group 18	Group 19	Group 20
	P_5	Group 21	Group 22	Group 23	Group 24	Group 25
	P_6	Group 26	Group 27	Group 28	Group 29	Group 30
	P_7	Group 31	Group 32	Group 33	Group 34	Group 35
	P_8	Group 36	Group 37	Group 38	Group 39	Group 40

Table A.2: The simulation groups for a dual simulation sample each parameter within the range over which it was considered.

For each simulation group, a 100 realization simulation was completed. Each realization held the parameters being analyzed as constant and sampled stochastic values for uncertain parameters not being studied. A sampling scheme developed in previous generic disposal media modeling was implemented in this model in order to ensure that the each 100 realization simulation sampled identical values for uncertain parameters [24, 72].

In order to independently analyze the dose contributions from radioisotope groups, four cases,

- Americium and its daughters,
- Plutonium and its daughters,
- Uranium and its daughters,
- Neptunium, its daughters, and fission products

were run independently. This allowed an evaluation of the importance of daughter production from distinct actinide chains.

A.4 Parametric Analyses With The Clay GDSM

These analyses were performed using the Clay GDSM developed by the UFD campaign[24]. The Clay GDSM is built on the GoldSim software and tracks the movement of key radionuclides through the natural system and engineered barriers [33, 34].

The disposal concept modeled by the Clay GDSM includes an EBS which can undergo rate based dissolution and barrier failure. Releases from the EBS enter near field and subsequently far field host rock regions in which diffusive and advective transport take place, attenuated by solubility limits as well as sorption and dispersion phenomena.

The Clay GDSM models a single waste form, a waste package, additional EBSs, an EDZ, and a far field zone using a batch reactor mixing cell framework. This waste unit cell is modeled with boundary conditions such that it may be repeated assuming an infinite repository configuration. The waste form and engineered barrier system are modeled as well-mixed volumes and radial transport away from the cylindrical base case unit cell is modeled as one dimensional. Two radionuclide release pathways are considered. One is the nominal, undisturbed case, while the other is a fast pathway capable of simulating a hypothetical disturbed case [24].

A.4.1 Vertical Advective Velocity and Reference Diffusivity

Transport out of the EBS and through the permeable, porous geosphere involves advection, diffusion, and hydraulic dispersion phenomena. Advection is transport driven by bulk water velocity, while diffusion is the result of Brownian motion across concentration gradients. The method by which the dominant solute transport mode (diffusive or advective) is determined for a particular porous medium is by use of the dimensionless Peclet number,

$$\begin{aligned}
Pe &= \frac{nvL}{\alpha\theta v + D_{eff}}, \\
&= \frac{\text{advective rate}}{\text{diffusive rate}}
\end{aligned}
\tag{A.3}$$

where

θ = solute accessible porosity [%]

v = advective velocity [$m \cdot s^{-1}$]

L = transport distance [m]

α = dispersivity [m]

D_{eff} = effective diffusion coefficient [$m^2 \cdot s^{-1}$].

For a high Pe number, advection is the dominant transport mode, while diffusive or dispersive transport dominates for a low Pe number [86].

In this analysis, the threshold between primarily diffusive and primarily advective transport was investigated by varying the vertical advective velocity in conjunction with the diffusion coefficient. It was expected that for the low diffusion coefficients and low advective velocities usually found in clay media, the model should behave entirely in the diffusive regime, but as the vertical advective velocity grows, system behavior should increasingly approach the advective regime.

A.4.1.1 Parametric Range

The diffusion coefficient was altered as in Section A.4.2 and the vertical advective velocity of the far field was altered as well.

From Table 5.5-1 of the Argile Safety Evaluation by ANDRA, the vertical hydraulic gradient is 0.4, while the hydraulic conductivity is 5.0×10^{14} m/s. The resulting vertical advective velocity is then 2.0×10^{-14} m/s, which is 6.31×10^{-7} m/yr [8].

As in Section A.4.2, in order to isolate the effect of the far field behavior, the waste form degradation rate was set to be very high as were the solubility and advective flow rate through the EBS. This guaranteed that in the first few time steps, the far field was the primary barrier to release.

The forty runs are a combination of the five values of the vertical advective velocity and eight magnitudes of relative diffusivity (see Table A.3).

		Vertical Advective Velocity [m/yr]				
		6.31E-08	6.31E-07	6.31E-06	6.31E-05	6.31E-04
Reference Diffusivity (m ² /s)	Groupings					
	1.E-08	1	2	3	4	5
	1.E-09	6	7	8	9	10
	1.E-10	11	12	13	14	15
	1.E-11	16	17	18	19	20
	1.E-12	21	22	23	24	25
	1.E-13	26	27	28	29	30
	1.E-14	31	32	33	34	35
1.E-15	36	37	38	39	40	

Table A.3: Vertical advective velocity and diffusion coefficient simulation groupings.

To capture the importance of the vertical advective velocity, a range was chosen to span a number of orders of magnitude between 6.31×10^{-8} and 6.31×10^{-4} m/yr. The relative diffusivity was simultaneously varied over the eight magnitudes between 10^{-8} and 10^{-15} m²/s. It is worth noting that both the relative diffusivity and the vertical advective velocity are functions of porosity in the host rock and are therefore expected to vary together.

A.4.2 Diffusion Coefficient of Far Field

In clay media, diffusion dominates far field hydrogeologic transport due to characteristically low hydraulic head gradients and permeability. Thus, the effective diffusion coefficient is a parameter to which repository performance in clay media is expected to be very sensitive.

The sensitivity of the peak dose to the reference diffusivity of the host rock was analyzed. In this model, the reference diffusivity of the medium was the input parameter used to vary the effective diffusivity in a controlled manner. In GoldSim's transport module, the effective diffusion coefficient is defined as

$$D_{eff} = n\tau D_{ref} D_{rel} \quad (A.4)$$

$$D_{eff} = \text{effective diffusion coefficient } [m^2/s],$$

$$D_{rel} = \text{relative diffusivity for each isotope in water } [\%],$$

$$D_{ref} = \text{reference diffusivity in water } [m^2/s],$$

$$\tau = \text{tortuosity}[\%],$$

$$n = \text{porosity}[\%].$$

(A.5)

The reference diffusivity was altered while the porosity and the tortuosity were both set to 1. Thus, the simulation rendered the effective diffusivity equal to the product of the reference diffusivity and the relative diffusivity (set to 1 for all isotopes). This allowed the diffusivity to be controlled directly for all isotopes.

The waste inventory total mass was also altered for each value of the reference diffusivity. That is, the radionuclide inventory in a reference MTHM of commercial spent nuclear fuel was multiplied by a scalar mass factor. It was expected that changing these two parameters

in tandem would capture the importance of diffusivity in the far field to the repository performance as well as a threshold at which the effect of waste inventory dissolution is attenuated by solubility limits.

Finally, in order to isolate the effect of the far field behavior, the waste form degradation rate was set to be very high as were the solubility and advective flow rate through the EBS. This guaranteed that contaminant flowthrough in the near field was unhindered, leaving the far field as the dominant barrier to release.

A.4.2.1 Parametric Range

The forty runs corresponded to eight values of relative diffusivity and five values of inventory mass multiplier. That is, the reference diffusivity was varied over the eight magnitudes between 10^{-8} and 10^{-15} m^2/s . The Mass Factor, the unitless inventory multiplier, was simultaneously varied over the five magnitudes between 10^{-4} and 10^1 . That is, the radionuclide inventory was varied between 10^{-4} and 10^1 of that in one MTHM of SNF, which is expected to cover the full range of inventories in current wasteforms.

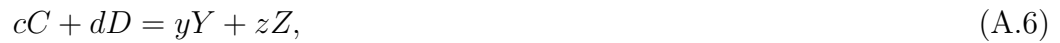
		Mass Factor				
		0.001	0.01	0.1	1	10
		Groupings				
Reference Diffusivity (m^2/s)	1.E-08	1	2	3	4	5
	1.E-09	6	7	8	9	10
	1.E-10	11	12	13	14	15
	1.E-11	16	17	18	19	20
	1.E-12	21	22	23	24	25
	1.E-13	26	27	28	29	30
	1.E-14	31	32	33	34	35
	1.E-15	36	37	38	39	40

Table A.4: Diffusion coefficient and mass factor simulation groupings.

A.4.3 Solubility Limitation

This study varied the solubility coefficients for each isotope in the simulation to help inform the effect of reprocessing on repository benefit for the clay repository scenario. The importance of the actinide contribution relative to the contribution from ^{129}I , ^{79}Se , and ^{99}Tc was of particular interest.

The dissolution behavior of a solute in an aqueous solutions is called its solubility. This behavior is limited by the solute's solubility limit, described by an equilibrium constant that depends upon temperature, water chemistry, and the properties of the element. The solubility constant for ordinary solutes, K_s gives units of concentration, kg/m^3 , and can be determined algebraically by the law of mass action which gives the partitioning at equilibrium between reactants and products. For a reaction



where

$c, d, y, z =$ amount of respective constituent [mol]

$C, D =$ reactants $[-]$

$Y, Z =$ products $[-]$,

the law of mass action gives

$$K = \frac{(Y)^y(Z)^z}{(C)^c(D)^d} \quad (A.7)$$

where

(X) = the equilibrium molal concentration of X [mol/m^3]

K = the equilibrium constant [-].

The equilibrium constant for many reactions are known, and can be found in chemical tables. Thereafter, the solubility constraints of a solution at equilibrium can be found algebraically. In cases of salts that dissociate in aqueous solutions, this equilibrium constant is called the salt's solubility product K_{sp} .

This equilibrium model, however, is only appropriate for dilute situations, and nondilute solutions at partial equilibrium must be treated with an activity model by substituting the activities of the constituents for their molal concentrations,

$$[X] = \gamma_x(X) \tag{A.8}$$

where

$[X]$ = activity of X [-]

γ_x = activity coefficient of X[-]

(X) = molal concentration of X [mol/m^3]

such that

$$\begin{aligned}
 IAP &= \text{Ion Activity Product } [-]. \\
 &= \frac{[Y]^y[Z]^z}{[C]^c[D]^d}
 \end{aligned}
 \tag{A.9}$$

(A.10)

The ratio between the IAP and the equilibrium constant (IAP/K) quantifies the departure from equilibrium of a solution. This information is useful during the transient stage in which a solute is first introduced to a solution. When $IAP/K < 1$, the solution is undersaturated with respect to the products. When, conversely, $IAP/K > 1$, the solution is oversaturated and precipitation of solids in the volume will occur.

A.4.3.1 Parametric Range

The solubility coefficients were varied in this simulation using a multiplier. The reference solubilities for each element were multiplied by the multiplier for each simulation group. This technique preserved relative solubility among elements. Forty values of solubility coefficient multiplier were used to change the far field solubility. This did not alter any of the solubility in the EDZ, WF, or Fast Path solubilities.

The values of the solubility multiplier were deliberately varied over many magnitudes, from 1^{-9} through 5×10^{10} . This multiplier multiplied the most likely values of solubility for each element, so the relative solubility between elements was preserved.

A.4.4 The Partition Coefficient

This analysis investigated the peak dose rate contribution from various radionuclides to the partition coefficient of those radionuclides.

The partition or distribution coefficient, K_d , relates the amount of contaminant adsorbed into the solid phase of the host medium to the amount of contaminant adsorbed into the aqueous phase of the host medium. It is a common empirical coefficient used to capture the effects of a number of retardation mechanisms. The coefficient K_d , in units of $\text{m}^3 \cdot \text{kg}^{-1}$, is the ratio of the mass of contaminant in the solid to the mass of contaminant in the solution.

The retardation factor, R_f , which is the ratio between velocity of water through a volume and the velocity of a contaminant through that volume, can be expressed in terms of the partition coefficient,

$$R_f = 1 + \frac{\rho_b}{n_e} K_d \quad (\text{A.11})$$

where

$$\rho_b = \text{bulk density}[\text{kg} \cdot \text{m}^{-3}]$$

and

$$n_e = \text{effective porosity of the medium}[\%].$$

A.4.4.1 Parametric Range

The parameters in this model were all set to the default values except a multiplier applied to the partitioning K_d coefficients.

The multiplier took the forty values $1 \times 10^{-9}, 5 \times 10^{-8}, \dots, 5 \times 10^{10}$ Only the far field

partition coefficients were altered by this factor. Partition coefficients effecting the EDZ and fast pathway were not changed.

A.4.5 Waste Form Degradation Rate

The sensitivity of peak dose rate to the waste form degradation rate was determined with respect to varying inventories of waste.

The sensitivity of repository performance to waste form degradation rate was expected to vary according to the waste inventory. For cases in which the dominant dose contributing radionuclides have half-lives much shorter than the expected waste form lifetime, the waste form degradation rate is not expected to have an effect. So too, for cases in which the primary barrier to release, the slow diffusive pathway, dominates overall repository performance, the waste form engineered barrier was expected to have a negligible effect on repository performance in comparison.

In the case of a clay repository, the effect of the long time scale of the diffusive release pathway was to dampen the potential effect of high waste form degradation rates.

A.4.5.1 Parametric Range

These runs varied the waste form degradation rate and the waste inventory mass factor. There were forty runs corresponding to eight values of the waste form degradation rate and five values of the mass factor.

The waste form degradation rate was varied over the eight magnitudes between 10^{-9} and 10^{-2} 1/yr. The inventory mass factor was varied over the five magnitudes between 0.001 and 10.0.

A.4.5.2 Safety Indicators

Safety indicators for post closure repository performance have been developed by the UFD campaign which utilize the inventory multiplier that was varied in this study [72]. These indicators are normalized by a normalization factor (100 mrem/yr) recommended by the International Atomic Energy Agency (IAEA) as the limit to “relevant critical members of the public” [52]. The functional form for this safety indicator for a single waste category, HLW, is just

$$SI_G = \left(\frac{\sum_{i=1}^N D_{G,i}(I_i, F_d)}{100mrem/yr} \right) [GWe/yr]. \quad (A.12)$$

where

SI_G = Safety indicator for disposal in media type G[GWe/yr]

N = Number of key radionuclides considered in this indicator

$D_{G,i}$ = Peak dose rate from isotope i in media type G[mrem/yr]

F_d = Fractional waste form degradation rate[1/yr].

Tables A.5, A.6, and A.7 report the safety indicators for various independent isotopes and, where applicable, their daughters.

		Inventory Factor				
		0.001	0.01	0.1	1	10
		I-129 (N=2.9 × 10² g)				
Degradation Rate	1.E-09	3.E-11	3.E-10	3.E-09	3.E-08	3.E-07
	1.E-08	3.E-10	3.E-09	3.E-08	3.E-07	3.E-06
	1.E-07	2.E-09	2.E-08	2.E-07	2.E-06	2.E-05
	1.E-06	8.E-09	8.E-08	8.E-07	8.E-06	8.E-05
	1.E-05	1.E-08	1.E-07	1.E-06	1.E-05	1.E-04
	1.E-04	1.E-08	1.E-07	1.E-06	1.E-05	1.E-04
	1.E-03	1.E-08	1.E-07	1.E-06	1.E-05	1.E-04
1.E-02	1.E-08	1.E-07	1.E-06	1.E-05	1.E-04	
		Cl-36 (N=1 g)				
Degradation Rate	1.E-09	1.E-15	1.E-14	1.E-13	1.E-12	1.E-11
	1.E-08	1.E-14	1.E-13	1.E-12	1.E-11	1.E-10
	1.E-07	1.E-13	1.E-12	1.E-11	1.E-10	1.E-09
	1.E-06	9.E-13	9.E-12	9.E-11	9.E-10	9.E-09
	1.E-05	3.E-12	3.E-11	3.E-10	3.E-09	3.E-08
	1.E-04	4.E-12	4.E-11	4.E-10	4.E-09	4.E-08
	1.E-03	4.E-12	4.E-11	4.E-10	4.E-09	4.E-08
1.E-02	4.E-12	4.E-11	4.E-10	4.E-09	4.E-08	

Table A.5: Safety indicators for soluble, non-sorbing nuclides.

		Inventory Factor				
		0.001	0.01	0.1	1	10
		Pd-107 (N=3.8 x 10² g)				
Degradation Rate	1.E-09	2.E-16	2.E-15	2.E-14	2.E-13	2.E-12
	1.E-08	2.E-15	2.E-14	2.E-13	2.E-12	1.E-11
	1.E-07	2.E-14	2.E-13	2.E-12	8.E-12	3.E-11
	1.E-06	5.E-14	5.E-13	3.E-12	2.E-11	3.E-11
	1.E-05	5.E-14	5.E-13	4.E-12	2.E-11	3.E-11
	1.E-04	5.E-14	5.E-13	4.E-12	2.E-11	3.E-11
	1.E-03	5.E-14	5.E-13	4.E-12	2.E-11	3.E-11
	1.E-02	5.E-14	5.E-13	4.E-12	2.E-11	3.E-11
		Sn-126 (N=4.5 x 10¹ g)				
Degradation Rate	1.E-09	0.E+00	0.E+00	0.E+00	0.E+00	0.E+00
	1.E-08	0.E+00	0.E+00	0.E+00	0.E+00	0.E+00
	1.E-07	0.E+00	0.E+00	0.E+00	0.E+00	2.E-29
	1.E-06	0.E+00	0.E+00	0.E+00	2.E-29	5.E-29
	1.E-05	0.E+00	0.E+00	1.E-29	3.E-29	5.E-29
	1.E-04	0.E+00	0.E+00	1.E-29	3.E-29	5.E-29
	1.E-03	0.E+00	0.E+00	1.E-29	3.E-29	5.E-29
	1.E-02	0.E+00	0.E+00	1.E-29	3.E-29	5.E-29
		Zr-93 & Nb-93				
Degradation Rate	1.E-09	1.E-17	1.E-16	1.E-15	1.E-14	1.E-13
	1.E-08	1.E-16	1.E-15	1.E-14	1.E-13	7.E-13
	1.E-07	1.E-15	1.E-14	1.E-13	6.E-13	3.E-12
	1.E-06	4.E-15	4.E-14	3.E-13	1.E-12	4.E-12
	1.E-05	6.E-15	6.E-14	4.E-13	2.E-12	4.E-12
	1.E-04	6.E-15	6.E-14	4.E-13	2.E-12	4.E-12
	1.E-03	7.E-15	6.E-14	4.E-13	2.E-12	4.E-12
	1.E-02	7.E-15	6.E-14	4.E-13	2.E-12	4.E-12
		Tc-99 (N=1.2 x 10³ g)				
Degradation Rate	1.E-09	2.E-18	2.E-17	2.E-16	2.E-15	2.E-14
	1.E-08	2.E-17	2.E-16	2.E-15	2.E-14	1.E-13
	1.E-07	2.E-16	2.E-15	2.E-14	1.E-13	2.E-13
	1.E-06	1.E-15	1.E-14	1.E-13	2.E-13	2.E-13
	1.E-05	5.E-15	5.E-14	1.E-13	2.E-13	2.E-13
	1.E-04	7.E-15	5.E-14	1.E-13	2.E-13	2.E-13
	1.E-03	7.E-15	5.E-14	1.E-13	2.E-13	2.E-13
	1.E-02	7.E-15	5.E-14	1.E-13	2.E-13	2.E-13
		Cs-135 (N=6.9 x 10² g)				
Degradation Rate	1.E-09	6.E-14	6.E-13	6.E-12	6.E-11	6.E-10
	1.E-08	6.E-13	6.E-12	6.E-11	6.E-10	6.E-09
	1.E-07	5.E-12	5.E-11	5.E-10	5.E-09	5.E-08
	1.E-06	2.E-11	2.E-10	2.E-09	2.E-08	2.E-07
	1.E-05	3.E-11	3.E-10	3.E-09	3.E-08	3.E-07
	1.E-04	4.E-11	4.E-10	4.E-09	4.E-08	4.E-07
	1.E-03	4.E-11	4.E-10	4.E-09	4.E-08	4.E-07
	1.E-02	4.E-11	4.E-10	4.E-09	4.E-08	4.E-07
		Se-79 (N=4.5 x 10¹ g)				
Degradation Rate	1.E-09	2.E-14	2.E-13	2.E-12	5.E-12	8.E-12
	1.E-08	2.E-13	2.E-12	5.E-12	8.E-12	8.E-12
	1.E-07	2.E-12	5.E-12	8.E-12	8.E-12	8.E-12
	1.E-06	5.E-12	8.E-12	8.E-12	8.E-12	8.E-12
	1.E-05	6.E-12	8.E-12	8.E-12	8.E-12	8.E-12
	1.E-04	6.E-12	8.E-12	8.E-12	8.E-12	8.E-12
	1.E-03	6.E-12	8.E-12	8.E-12	8.E-12	8.E-12
	1.E-02	6.E-12	8.E-12	8.E-12	8.E-12	8.E-12

Table A.6: Safety indicators for solubility limited and sorbing nuclides.

		Inventory Factor				
		0.001	0.01	0.1	1	10
		Np-237 and Daughters (N=6.5 × 10² g)				
Degradation Rate	1.E-09	3.E-13	3.E-12	3.E-11	3.E-10	9.E-10
	1.E-08	3.E-12	3.E-11	3.E-10	9.E-10	9.E-10
	1.E-07	3.E-11	3.E-10	9.E-10	9.E-10	9.E-10
	1.E-06	1.E-10	8.E-10	9.E-10	9.E-10	9.E-10
	1.E-05	2.E-10	8.E-10	9.E-10	9.E-10	9.E-10
	1.E-04	2.E-10	8.E-10	9.E-10	9.E-10	1.E-09
	1.E-03	2.E-10	8.E-10	9.E-10	9.E-10	1.E-09
	1.E-02	2.E-10	8.E-10	9.E-10	9.E-10	1.E-09
		Pu and Daughters (N=4.9 × 10³ g)				
Degradation Rate	1.E-09	4.E-15	4.E-14	4.E-13	3.E-12	2.E-11
	1.E-08	4.E-14	3.E-13	3.E-12	2.E-11	2.E-10
	1.E-07	3.E-13	2.E-12	2.E-11	2.E-10	2.E-09
	1.E-06	2.E-12	2.E-11	2.E-10	1.E-09	9.E-09
	1.E-05	4.E-12	4.E-11	4.E-10	3.E-09	1.E-08
	1.E-04	5.E-12	5.E-11	5.E-10	3.E-09	1.E-08
	1.E-03	5.E-12	5.E-11	5.E-10	3.E-09	1.E-08
	1.E-02	5.E-12	5.E-11	5.E-10	3.E-09	1.E-08
		Am and Daughters (N=2.1 × 10³ g)				
Degradation Rate	1.E-09	3.E-13	3.E-12	3.E-11	3.E-10	9.E-10
	1.E-08	3.E-12	3.E-11	3.E-10	9.E-10	9.E-10
	1.E-07	3.E-11	3.E-10	9.E-10	9.E-10	9.E-10
	1.E-06	1.E-10	8.E-10	9.E-10	9.E-10	9.E-10
	1.E-05	2.E-10	8.E-10	9.E-10	9.E-10	9.E-10
	1.E-04	2.E-10	8.E-10	9.E-10	9.E-10	1.E-09
	1.E-03	2.E-10	8.E-10	9.E-10	9.E-10	1.E-09
	1.E-02	2.E-10	8.E-10	9.E-10	9.E-10	1.E-09
		U and Daughters (N=9.8 × 10⁵ g)				
Degradation Rate	1.E-09	2.E-15	2.E-14	1.E-13	5.E-13	6.E-13
	1.E-08	2.E-14	1.E-13	5.E-13	6.E-13	7.E-13
	1.E-07	1.E-13	4.E-13	6.E-13	7.E-13	2.E-12
	1.E-06	3.E-13	6.E-13	7.E-13	1.E-12	7.E-12
	1.E-05	4.E-13	7.E-13	8.E-13	2.E-12	9.E-12
	1.E-04	4.E-13	7.E-13	9.E-13	3.E-12	9.E-12
	1.E-03	4.E-13	7.E-13	9.E-13	3.E-12	9.E-12
	1.E-02	4.E-13	7.E-13	9.E-13	3.E-12	9.E-12

Table A.7: Safety indicators for the actinides and their daughters.

A.4.6 Waste Package Failure Time

The time of waste package failure was not expected to greatly affect the magnitude of the mean of the peak doses except for cases in which waste package failure times exceeded the half lives of dominant dose-contributing nuclides. That is, since the dominant dose-contributing radionuclides for the reference case are quite long lived (^{129}I , etc.), all but the longest reasonable waste package containment lifetime is overwhelmed by the half life of the dominant radionuclides. The long time scales of radionuclide release was expected to render the the waste package lifetime irrelevant if it was shorter than a million years.

Though the model contains a unit cell-type model, it is possible to determine, in post processing, the results of a simulation with temporally heterogeneous failures among waste packages. That is, by a weighted sum of the time histories of the no-fail case and the all-fail case, it is possible to mimic a time-varying failure among the many waste packages.

A.4.6.1 Parametric Range

To investigate the effect of the waste package failure time, it was varied over five magnitudes from one thousand to ten million years. Simultaneously, the reference diffusivity was varied over the eight magnitudes between 1×10^{-8} and 1×10^{-15} in order to determine the correlation between increased radionuclide mobility and the waste package lifetime.

B THERMAL CALCULATION ACCURACY DETERMINATION

A benchmarking effort was conducted to determine the accuracy of the semi-analytic generic geologic medium thermal repository model developed at LLNL[35, 36, 40] relative to the more traditional, numerical, lumped parameter technique in the SINDA\G model from ANL.

The fast-running semi-analytic thermal transport model assumes uniform thermal properties throughout a homogenous storage medium. Arrays of time-dependent heat sources are included geometrically as arrays of line segments and points. The solver uses a source-based linear superposition of closed form analytical functions from each contributing point or line to arrive at an estimate of the thermal evolution of a generic geologic repository. Temperature rise throughout the storage medium is computed as a linear superposition of temperature rises. It is modeled using the MathCAD mathematical engine and is parameterized to allow myriad gridded repository geometries and geologic characteristics [79].

It was anticipated that the accuracy and utility of the temperature field calculated with the LLNL semi-analytic model would provide an accurate “birds-eye” view in regions that are many tunnel radii away from actual storage units; i.e., at distances where tunnels and individual storage units could realistically be approximated as physical lines or points. However, geometrically explicit storage units, waste packages, tunnel walls and close-in rock are not included in the MathCad model. The present benchmarking effort therefore focuses on the ability of the semi-analytic model to accurately represent the close-in temperature field.

Specifically, close-in temperatures computed with the LLNL MathCAD model were benchmarked against temperatures computed using geometrically-explicit lumped-parameter, repository thermal modeling technique developed over several years at ANL using the

SINDA\G thermal modeling code [32]. Application of this numerical modeling technique to underground storage of heat generating nuclear waste streams within the proposed YMR Site has been widely reported [97]. New SINDA\G thermal models presented here share this same basic modeling approach.

B.1 Description of the Comparisons

The two models were compared for a single tunnel case with UOX spent fuel and a 0.35 meter tunnel radius. Shared assumptions of the model benchmarks include a single UOX assembly fuel loading per 5m of tunnel, calculation radii, numbers of adjacent tunnels, and geologic thermal parameters. The benchmarking cases run in this validation effort for the simplified single tunnel case are listed in Table B.1.

B.2 Results

The benchmarking effort between the semi-analytic MathCAD model and the SINDA\G numerical model showed that the semi-analytic model was sufficiently in agreement with the numerical model for its purpose, rapid evaluation of generic repository configurations. The semi-analytic model gave peak temperatures for all cases run which agreed with the numerical numerical model within $4^{\circ}C$ and, for calculation radii less than 5 meters, consistently reported peak temperature timing within 11 years of the SINDA\G numerical model. In light of the magnitude of uncertainties involved in generically modeling a non-site-specific geologic repository, this sufficiently validated the semi-analytic model with respect to its goals.

Peak times agreed well for close radii, though peak values were consistently underestimated by the semi-analytic model. However, the time of peak heat arrived consistently

Benchmarking Results for Single Drift Scenario

Material	Clay $K_{th} = 2.5$ $\alpha = 1.13 \times 10^{-6}$			Salt $K_{th} = 4.2$ $\alpha = 2.07 \times 10^{-6}$		
	Peak Temperature Discrepancy $T_{peak,numeric} - T_{peak,analytic} [^{\circ}C]$					
Years Cooling	10	25	50	10	25	50
R=0.35m	3.0	2.3	1.6	2.0	1.7	1.2
R=0.69m	3.1	2.4	1.6	2.2	1.8	1.3
R=3.46m	2.1	1.9	1.5	2.2	1.7	1.3
R=7.04m	3.1	2.4	1.8	2.5	2.1	2.2
R=14.32m	3.6	2.9	2.1	2.8	2.6	3.7
	Peak Heat Timing Discrepancy $t_{peak,numeric} - t_{peak,analytic} [yr]$					
Material	Clay $K_{th} = 2.5$ $\alpha = 1.13 \times 10^{-6}$			Salt $K_{th} = 4.2$ $\alpha = 2.07 \times 10^{-6}$		
Years Cooling	10	25	50	10	25	50
R=0.35m	1	1	1	1	1	3
R=0.69m	2	2	1	2	3	4
R=3.46m	9	7	6	4	2	11
R=7.04m	4	13	10	11	10	288
R=14.32m	16	14	21	17	285	282

Table B.1: Benchmarking in the single tunnel case showed that the peak heat was calculated to be lower and arrived consistently sooner in the semi-analytic model.

sooner and the peak temperature value was consistently lower in the homogeneous medium semi-analytic model than in the SINDA\G model.

The results from the single and multiple drift scenarios are summarized in Tables B.1 and B.2, respectively.

Benchmarking Results for 101 Drift Scenario

Material	Clay $K_{th} = 2.5$ $\alpha = 1.13 \times 10^{-6}$		
	Peak Temperature Discrepancy $T_{peak,numeric} - T_{peak,analytic} [^{\circ}C]$		
Years Cooling	10	25	50
R=0.35m	7	4.6	2.1
	Peak Heat Timing Discrepancy $t_{peak,numeric} - t_{peak,analytic} [yr]$		
R=0.35m	-13.5	2	-6

Table B.2: Benchmarking in the multiple tunnel case showed that the peak heat was calculated to be consistently lower in the semi-analytic model and deviated further from the numerical model than did the single tunnel case.